



POLITECNICO
MILANO 1863

SCUOLA DI INGEGNERIA INDUSTRIALE
E DELL'INFORMAZIONE

Control of transition phases in rigid-wing airborne wind energy system

TESI DI LAUREA MAGISTRALE IN
AUTOMATION AND CONTROL ENGINEERING - INGEGNERIA
DELL'AUTOMAZIONE

Author: **Pedro Pablo Mitidieri**

Student ID: 938781

Advisor: Prof. Lorenzo Mario Fagiano

Co-advisors:

Academic Year: 2021-22

Abstract

The present thesis tackles the study of an Airborne Wind Energy system, device designed to harness the wind's energy and transform it into electricity, with the aim of proposing a methodological approach to design the transition between one cycle of electricity production and the next.

In order to achieve this objective, a realistic model of the system is developed. The system under study is composed of three main elements, the drone, the tether and the generator. The system is highly nonlinear and open-loop unstable. Once a proper model of it is developed, the mission is divided in different stages based on their characteristics. Each of these parts is studied separately and a unique control strategy, and its set of references, developed. The decision of the stage changes and how to change the control system's structure is delegated to a State Machine, which is also planned and presented. Once the system has finished one generation round, the tether has been reeled out to a maximum, there is a transition phase to start the next generation round. During this retraction phase the drone glides back towards some predefined points and manoeuvre towards a correct attitude to start the generation phase again. All of these is possible thanks to the usage of the control surfaces and a loose tether. The retraction phases divided in four parts, each of them distinct from the other. This division is done to simplify the understanding strategy and to tackle different problems with specific solutions.

To produce a methodological approach, it is necessary to look for key parameters, those that will allow the transition to be done effectively. Several of them are tried and dependencies among them are found. Finally 4 parameters remained, and a complete mission using them is presented. In addition, the explanation of their particular effects is added, along with a graphic representation of the transition modification when each one of them is changed.

Keywords: AWE system, retraction phase, methodological approach, transition phase

Abstract in lingua italiana

La presente tesi affronta lo studio di un sistema Airborne Wind Energy, dispositivo progettato per sfruttare l'energia del vento e trasformarla in energia elettrica, con l'obiettivo di proporre un approccio metodologico per progettare la transizione tra un ciclo di produzione d'energia elettrica e l'altro.

Per raggiungere questo obiettivo, viene sviluppato un modello realistico del sistema. Le tipologie di sistemi oggetto di studio sono composte da tre elementi principali, il drone, il cavo e il generatore. Con un verace e proprio modello del sistema, la missione è suddivisa in diverse fasi in base alle loro caratteristiche. Ognuna di queste parti viene studiata separatamente e viene sviluppata una strategia di controllo univoca e il relativo insieme di riferimenti. La decisione dei cambi di fase e di come modificare la struttura del sistema di controllo è delegata a una Macchina a Stati, anch'essa progettata e presentata.

Una volta che il sistema ha terminato un round di generazione, il cavo è stato srotolato al massimo, c'è una fase di transizione per iniziare il round di generazione successiva. Durante questa fase di retrazione il drone scivola indietro verso alcuni punti predefiniti e manovra verso un assetto corretto per ricominciare la fase di generazione. Tutto ciò è possibile grazie all'utilizzo delle superfici di controllo e di un laccio allentato. Le fasi di retrazione suddivise in quattro parti, ciascuna distinta dall'altra. Questa divisione viene fatta per semplificare la strategia di comprensione e per affrontare diversi problemi con soluzioni specifiche.

Per produrre un approccio metodologico, è necessario cercare parametri chiave, quelli che consentiranno di effettuare efficacemente la transizione. Molti di loro vengono provati e vengono trovate dipendenze tra di loro. Alla fine sono rimasti 4 parametri e viene presentata una missione completa che li utilizza. Inoltre, viene aggiunta la spiegazione dei loro particolari effetti, insieme a una rappresentazione grafica della modifica della transizione quando ciascuno di essi viene modificato.

Parole chiave: Sistema AWE, fase di retrazione, approccio metodologico, fase di transizione

Contents

Abstract	i
Abstract in lingua italiana	iii
Contents	v
1 Introduction	1
1.1 Current situation and context	1
1.2 Renewable energy sources	3
1.3 Wind energy systems	4
1.3.1 Wind turbines	4
1.3.2 Airborne wind energy (AWE)	6
2 System description and operating strategies	11
2.1 System description	11
2.2 Operation scheme	12
2.3 Reentry strategies	13
2.4 Coordinate systems	14
2.5 Tether properties	17
3 Mathematical models	19
3.1 Tether model	19
3.1.1 Tether Forces	19
3.1.2 Length of the tether	20
3.1.3 Matlab solver	20
3.2 Hybrid drone model	20
3.2.1 Aerodynamic data	21
3.2.2 Aerodynamic forces and moments	21
3.2.3 Motors' effect	22

3.2.4	Dynamic equations	23
3.2.5	Quaternion update	25
4	Control System	27
4.1	Control layout	27
4.2	State machine	28
4.2.1	Representative values	28
4.2.2	Possible Phases	28
4.3	Hovering control	37
4.3.1	Altitude controller	38
4.3.2	Taut tether control	38
4.3.3	Loose tether control	39
4.3.4	Control allocation - Hovering	41
4.4	Airplane mode control	42
4.4.1	Inner layer - attitude controller	42
4.4.2	Outer layer	44
4.4.3	Signal selector	49
5	Results	53
5.1	Hovering controllers synthesis	53
5.1.1	Hovering's cascade control decoupling	53
5.1.2	Altitude controller - Hovering	54
5.1.3	Inner layer controller - Hovering	55
5.1.4	Middle layer controller - Hovering	56
5.1.5	Velocity controller - Hovering	62
5.1.6	Position controller - Hovering	65
5.2	Airplane controllers synthesis	66
5.2.1	Generation Inner layer - Airplane	66
5.2.2	Retraction and Transition Inner layer - Airplane	69
5.2.3	Generation Outer layer - Airplane	71
5.2.4	Retraction and transition Outer layer - Airplane	74
5.3	References	75
5.3.1	Hovering - Phase 1	75
5.3.2	Tether engaging - Phase 2	76
5.3.3	Climbing - Phase 3	76
5.3.4	Generation - Phase 4 and 5	77
5.3.5	Transition - Phase 6	79
5.4	Strategy outline	82

5.5	Simulation	85
5.5.1	Hover up to the sphere limits	85
5.5.2	Climbing and stabilization phases	85
5.5.3	Generation phase	87
5.5.4	Transition	89
6	Conclusions and future developments	99
	Bibliography	101
	List of Algorithms	103
	List of Figures	105
	List of Tables	107
	List of Acronyms	109
	List of Symbols	111
	Acknowledgements	115

1 | Introduction

1.1. Current situation and context

The world population is increasing non-stop. Nowadays, the population amount to approximately 7 billions and by 2050 is expected to be around 8.7 billions, in the more conservative scenario [5]. A similar process is expected to occur to the energy consumption. The COVID-19 produced a sharp decrease in this metric in 2020, which fell 3.5%, and also in both the economy, 3.3% fall, and in the CO2 emissions, 5.2% fall [6]. However, it is expected that in 2021 all the metrics have come back to the pre-pandemic behaviour, i.e. increasing tendency. This bounce is expected to put the economy at a level which is a little bit higher than the pre-pandemic one. On the other hand, both energy consumption and CO2 emissions are not expected to regain the levels of the pre-pandemic situation [6]. Also, It is important to remark that while coal, oil and gas usage decreased during the pandemic, both the usage and the installation of renewable energies increased [6]. This is a good piece of news when facing global warming.

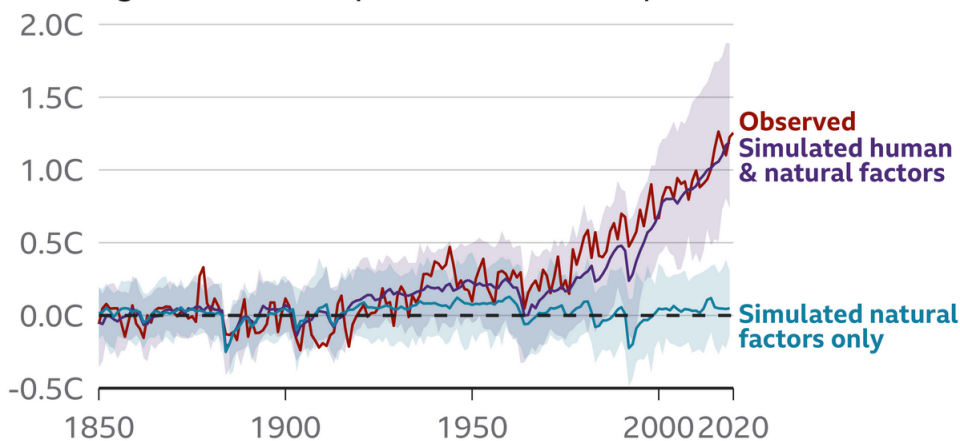
Nonetheless, in 2010 fossil fuels represented a 79% of the primary energy mix. In 2050, the best scenario shows a reduction up to 59% while the worst portrays a small decrease of 2% until reaching 77%. When combining these figures with the expected increase of the energy consumption for these 2 scenarios of 27% and 61% respectively [5], it is easy to see that in the worst case scenario the percentage was decreased but the absolute amount is highly increased. To illustrate this calculus, I am proposing the following example, given that the 2010's consumptions amounts to 100, leaving the units aside for simplicity, the total energy produced based on fossil fuels is 79. In 2050, we are experiencing an increase of 61% in the consumption to reach 161. The portion of this amount that is produced based on fossil fuels is 0.77, which gives as a result an absolute amount of almost 124, which compared to the previous 79 represents a sharp increase in the total amount of fossil fuels used. In the best possible scenario, although the remarkable reduction in the fossil fuels usage, there is also the increase in power generation and consumption. Using the same example as before, given a total of 100 in 2010 and 79 for fossil fuels, in 2050 the amount would be of almost 75. In this case, we hopefully see that the total amount is less

than in 2010. However, this is the best possible scenario and this is currently generating environmental problems and will keep generating them if appropriate measures are not taken.

The Intergovernmental Panel on Climate Change (IPCC) has released a new report this year in which they state the current situation of the climate change on Earth. By the words of Prof Ed Hawkins, "It is a statement of fact, we cannot be any more certain; it is unequivocal and indisputable that humans are warming the planet.", who is one of the report's authors [2]. In this new report, it is stated that our influence on the climate is decisive and has shaped our current experience. The findings in this report are so categorical that a rapid, immediate and large-scale reductions on green-house gas emissions must be applied if we are hoping to see only an average increase in between 1.5 and 2 Celsius degrees in the long-term, as they explain that the effects on the temperature needs between 20 and 30 years to stabilize in the final value. In addition, new technology along with more and better data have allowed them to produce better climatological models. The new findings are crystal-clear, as can be seen in figure 1.1.

Human influence has warmed the climate

Change in average global temperature relative to 1850-1900, showing observed temperatures and computer simulations



Note: Shaded areas show possible range for simulated scenarios

Source: IPCC, 2021: Summary for Policymakers



Figure 1.1: Human effect on climate

The effect of our development can be seen clearly in this image. Since the industrial revolution, humanity has been emitting green-house gases and has yet to cease. The observations show an obvious change in the tendency, where the average temperature has increased non-stop since 1900 more or less. Based on this information and many more,

the experts belonging to the IPCC have produced a model, shown in purple, that can make use of metrics which take into account our effect on the planet to effectively track the climate change we are experiencing. With that comparison to prove the accuracy of their model, they have removed our contribution from the model to produce the light-blue line. It can be easily seen how this line follows the behaviour of pre-industrial-revolution planet. The comparison of the two is an evident proof of our huge impact on the climate and how we have the power to change it in a fairly small amount of time.

Thankfully, this warning is not being taken lightly. The European Union is making great efforts to become a neutral Continent, with its objective set in 2050 [15]. For instance, one of the several milestones is to reduce 55% the car emissions by 2030, another is that by 2035 all new cars should be 0 emissions. These are great news for all, however, this new regulations are forcing a massive burden on the European's electric system, from the generation to the transportation. Having seen the figures presented before, with the current energy mix the transitions presented above will not have a huge impact. The renewable sources should be improved and become massively widespread. The good news are that during the pandemic the increase in the production facilities deployed continued, as stated before, and it has been several years that the amount of finished ones is increasing. In addition, there are several options that are being exploited which allows for their implementation in a wide variety of climates and geographic situations.

1.2. Renewable energy sources

Renewable energy may come from very diverse sources. Some of them are more developed and widespread than others. They can be classified as follows [11]:

- Solar energy systems: the idea behind this type of energy is to use the sunlight energy to generate useful energy. There are several variants [14], with the most common being the solar cells which are based in a selection of materials which directly converts sunlight in electricity. Another option is the Solar water heating systems, whose name is very descriptive and it is used to heat up water and it is applicable for heating the water needed at home or for swimming pools. A different option are solar power plants, which may have different layouts but they share the same principle, heat a fluid so that it moves a generator to produce electricity. They are usually comprised by reflective surfaces that focus the sun energy into the fluid reservoir. A different option for harnessing the solar energy is Passive solar heating, which relays on a clever design and the proper selection of materials for using daylight in a desired way. For instance, given a sensible choice of materials

and the design of a building, it is possible to store the energy provided by the sun during the day and use it to keep it warm during night, thus reducing the amount of energy required for its normal use [4].

- Wind energy systems: the wind energy is harnessed by different means to transform it in a more useful type of energy, always defined by the desired outcome. This concept has been around for a long time, one of the most common uses is the old windmills, structures designed for leveraging the wind energy for pumping water or grinding grains, for instance. Another very common is the usage of wind to move boats in the sea. Nowadays, one important application is the production of electricity from the wind. Wind turbines are placed both on-shore and off-shore. Another option is the one studied in this thesis, an airborne wind energy (AWE) systems. Which differs from the previous one in that AWE systems are comprised of three main elements. The wing or blade, the ground station and the tether. The latter is used for coupling the first two. The first one transforms the wind energy into a mechanical force which is used by the second one to produce electricity.
- Hydroelectric energy systems: the concept in which this one is based is also antique. Nowadays, the idea still is to use fast-moving water in a large river or rapidly descending water from a high point but the objective is to convert all that energy into electricity through the spinning of generator's blades.
- Geothermal power systems: this system is based on the high temperatures present way below the Earth's surface level. They are used as the source of energy to heat up some masses of water, that will later move steam-based generators.
- Ocean energy systems: from the oceans there are two main sources of energy. The one based on the tides and the other based on the waves. Using different systems, the idea is to harness these movements to generate electricity.

1.3. Wind energy systems

As it was already said above, the scope of this thesis is encompassed in the category of wind energy systems, particularly for the AWE systems. Thus, a more detailed explanation about this kind of systems is presented.

1.3.1. Wind turbines

All the energy produced by leveraging the wind is obtained thanks to the wind turbines. This complex system features several key components, namely the blades, the tower, the

generator, the control unit and several subsystems. In the figure 1.2 it is possible to see one simple scheme with several parts of the system in a simplified view.

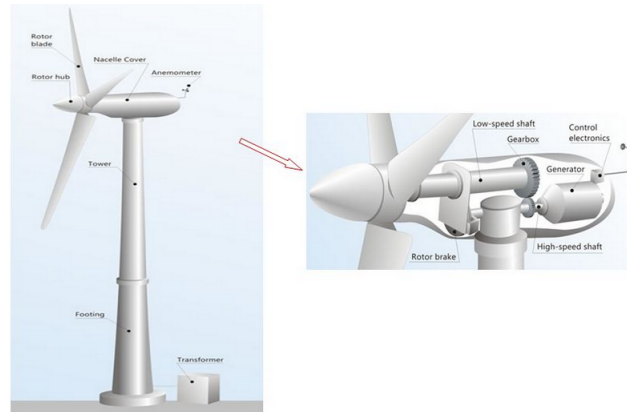


Figure 1.2: Wind turbine scheme

The wind turbines face a significant problem. There exist a theoretical limit for the maximum amount of kinematic energy that they can convert into spinning, thus a limit for their efficiency, called Betz limit that amounts to 59.3% of the kinematic energy. In practice, the limit is set in between 35 to 45%. As a result, designers have taken another path to increase the power generation capacity, which is increasing the size of the wind turbines, as portrayed in figure 1.3.

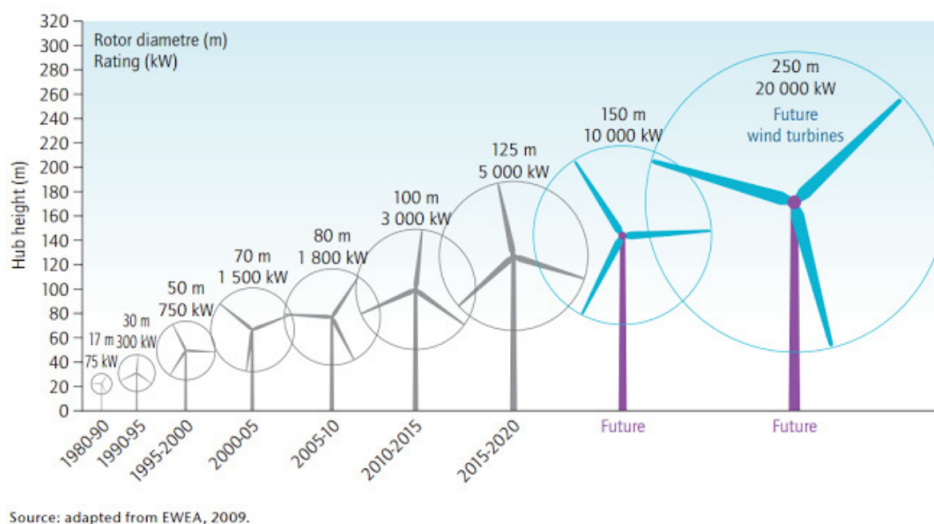


Figure 1.3: Wind turbine development through years [9]

This increase in size is well theoretically founded. As the tower becomes higher, the winds that affects them are becoming stronger too. This advantage can be accounted

by the simple rule of doubling the height of the tower produces 12% more energy. In addition, the longer the blades, the more energy is able to produce. This relation can be summarized as doubling the blades' length will yield an almost four time increase in the power generation. Based on these numbers, it is easy to realize why the wind turbines are increasing non-stop. There is also another consideration to make, the distance between wind turbines is directly proportional to the blade length. Given a length D , the next wind turbine should be placed at a distance of $7D$ along the prevalent wind direction and when placing the wind turbine perpendicularly to that direction the distance amounts to $4D$. These two rules are applied so that the aerodynamic interference is minimum. As a result, as the wind turbines become bigger, the space needed for a wind farm sharply increases.

1.3.2. Airborne wind energy (AWE)

In contrast with the previously stated situation, AWE systems hold a clear advantage. They can fly at different altitudes to minimize the aerodynamic interference in a much smaller area. This is accomplished thanks to the system's inherent advantages. At first, this system has the capability of working at different altitudes by just adjusting some parameters without any change in the hardware. It gives the possibility to minimize the aerodynamic coupling even with the production stations closer than with the wind turbines. The main restriction is having a safe distance to avoid collisions with other AWE systems working at the same time.

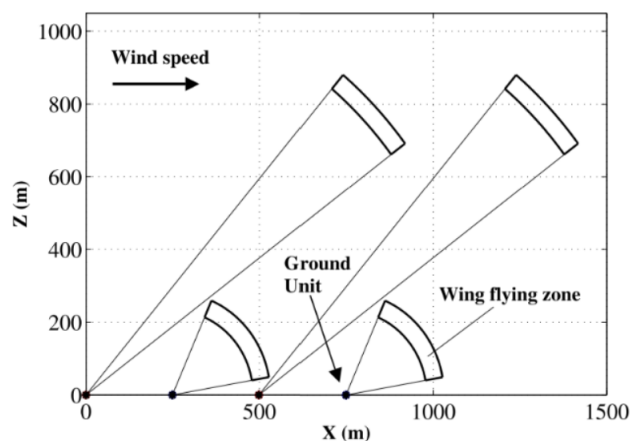


Figure 1.4: AWE systems working closely thanks to different altitudes for each of them. [7]

Another important advantage to highlight is the capacity of this systems to fly at higher

altitudes, which provides a clear advantage in terms of the wind quality, as it is less turbulent and of higher velocity. The power density at 500-1000 meters above sea level is on average 4 times higher than at 50-100 meters [7].

In addition, the AWE system, considered from the point of view of manufacturing, are potentially much less costly. This assumption is based on the following ideas, the amount of material to be used are less, the logistic to set up one of this systems appears to be a fraction of the required for setting up a wind turbine and the sum of the production cost of all the different parts could possibly be less for the AWE system.

The potential reduction in manufacturing cost and the capability of the system to work at higher altitudes, with its benefits, are some of the best advantages of the system. It is also worth to compare the Capacity Factor(CF) of this systems with the ones for wind turbines. The CF is the average power generated by a wind generator over a year with respect to the rated power. As it can be seen, it is an excellent measurement of how well the system is harnessing the available wind energy at a given location. The figure 1.5 shows the comparison of this coefficient for AWEs systems and wind turbines. It is possible to see different location where the coefficient was estimated and for each of these two range of altitudes, where the wind was averaged. Finally, on the right the CFs are shown and it is clear how the closer the wind turbines can get is only half of the CF achieved by the AWEs. This is a promising piece of information, as it shows how much energy the system would be able to extract from the wind, with its direct implications from the economic point of view.

Nevertheless, not everything are advantages for the AWE systems. One of the most important complications of these kind of systems is the control design. Controllers for wind turbines have been studied for a long time and nowadays they are very robust and reliable, added to the fact that the wind turbines are less sensitive to wind changes from a stability point of view. On the other hand, the AWE systems are from the starting point an unstable system and also are more affected by the wind changes. If these is added to the recent interest in this system, when compared to the wind turbines, the result is a field in which there is a lot of room for improvement. This development is crucial for this technology to take off and compete in the energy sector and provide its benefits to us all.

Site	Average wind speed		Estimated CF	
	50-150m	200-800m	Wind tower	AWE-GLG
Buenos Aires (Argentina)	5.7 m/s	9.1 m/s	0.18	0.63
Melbourne (Australia)	5.2 m/s	8.7 m/s	0.15	0.56
Porto Alegre (Brazil)	4.9 m/s	7.5 m/s	0.13	0.52
Nenjiang (China)	2.7 m/s	5.2 m/s	0.04	0.3
Taipei (China-Taiwan)	1.5 m/s	5.6 m/s	0.02	0.32
St. Cristobal (Ecuador)	6 m/s	6.5 m/s	0.15	0.44
Nice (France)	4.5 m/s	5.8 m/s	0.09	0.33
Calcutta (India)	2.8 m/s	5.6 m/s	0.02	0.31
Brindisi (Italy)	7.2 m/s	8.5 m/s	0.31	0.6
Linate (Italy)	0.7 m/s	5.9 m/s	0.006	0.33
Bandar Abbas (Iran)	1.5 m/s	5.6 m/s	0.02	0.32
Misawa (Japan)	4.4 m/s	7.8 m/s	0.11	0.5
Casablanca (Morocco)	2.4 m/s	7 m/s	0.03	0.45
De Bilt (The Netherlands)	8 m/s	10.7 m/s	0.36	0.71
Bodø (Norway)	6.9 m/s	8.7 m/s	0.28	0.56
Leba (Poland)	8.1 m/s	10.1 m/s	0.38	0.71
St. Petersburg (Russian Federation)	4.1 m/s	8.5 m/s	0.1	0.59
Port Elizabeth (South Africa)	7.5 m/s	8.9 m/s	0.2	0.58
Murcia (Spain)	2.6 m/s	5.9 m/s	0.03	0.35
Nottingham (United Kingdom)	1.3 m/s	5.3 m/s	0.01	0.31
Point Barrow (Alaska, U.S.)	6.6 m/s	8.8 m/s	0.25	0.59

Figure 1.5: Comparison of AWE's and wind turbines' CF for different locations [7]

AWE systems' layout

As already mentioned, the AWE systems are comprised of three main parts. The flying structure, the tether and the generator, a simple representation of the system can be seen in Figure 1.6. It also has several required systems, such as the sensors and the control units. The structure can be divided into two main categories:

- glider: this type of structure is characterized by being a rigid one with some wings attached to it. As a result, they resemble a drone in shape, as it can be seen in figure 1.7a.
- wing: this flying structure is analogous to the one find while kite surfing, commonly resembling a rectangular parachute, as it is portrayed in Figure 1.7b.

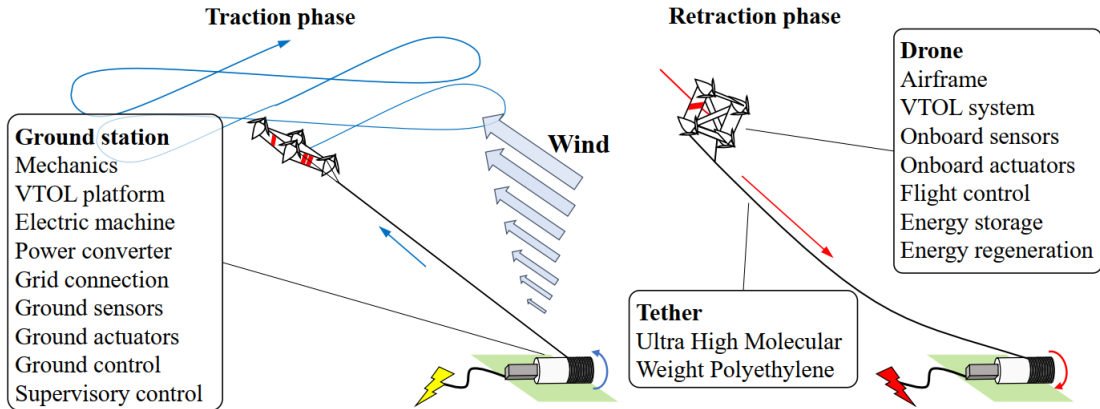


Figure 1.6: Schematic system representation



(a) Glider scheme [3] .

(b) Wing scheme [3].

Figure 1.7: AWE systems schemes

The tether, shown above as the lines attached to the structures, has the function of connecting the flying structures to the generator in the ground. To accomplish that, it is required to it that it is capable of sustaining high strains with the smallest diameter in order to minimize its weight and the aerodynamic drag that cause lost of energy.

The generator is responsible for converting the drone's movement in electricity. There are two main categories, the on-board generators(also called OBGs) and the ground generators (also knowns as GLGs). As the disposition differs, also the operating principle does. With an OBG system, the electricity is generated on-board and then transmitted to the ground usually by the tether. On the other hand, the GLG system relays on the reeling motion driven by the flying structure to produce electricity.

On the side of the sensor system, usually the flying structure is equipped with an inertial measurement unit (providing GPS, three accelerometers, three gyroscopes and one

magnetometer). The ground station is provided with load sensors for the tether's load assessment and also with the capacity to measure wind speed and direction through an anemometer. Some other sensors may be needed depending on the configuration, for instance a sensor for measuring the control action applied. In the case of a glider, measuring the control surfaces' deflection. This thesis focuses on a GLG system with a glider flying structure named Kitemill AS. As a result, to the previously mentioned sensors, it is necessary to provide the glider with sensors for measuring the rotors' speed.

The scope of the present work is to produce a control strategy, including set of references, controllers, assessment of the phase of the mission online, that enables a successful full-cycle mission. The main focus is set to the transition between the end of a generation phase cycle and the starting of the next one. During this moment, the drone must fly back towards the generator, usually with a loose tether, and reengage it again to start a new generation phase. This transition is very delicate, hence a methodology to tackle it is proposed and assessed using a non-linear simulator.

In this thesis it is presented a new methodological approach to design the control subsystem for the retraction phase. The idea behind this contribution is to create a scheme that divides the retraction phase in different parts. Each of them is specifically tackled to solve their unique problems. Once the division is done, the key parameters on which the feasibility of the transition depends are chosen. The effect of each of them is studied and it is presented through the change in the trajectory and their physical explanation. Finally, a set of parameters is chosen for the case study chosen and the resulting trajectory is presented.

2 | System description and operating strategies

2.1. System description

The kite(referred as "drone" in the remained) under study is a quad-rotor fixed-wing hybrid that can be seen in Figure 2.1, inspired by that of the company KItMill AS. It shows the drone with a standard configuration, having a longer wing close to its centre of gravity, where the ailerons are located, and a T-shape tail to position the elevator and the rudder. The main benefit of the hybrid configuration is the capability to take off and land vertically (VTOL capabilities) thanks to the addition of the four motors, while it remains aerodynamically efficient to follow the pumping pattern for energy generation. The ground station features a winch connected to an electric machine that serves both as generator and motor during pumping operation, together with all the required subsystems. The analysis, modelling and design is made in continuous time for simplicity reasons. As such, the time variable is t and it is presented along with any variable depending on it. t is always positioned besides any variable to the immediate right and as follows " (t) ". This time variable is defined as $t \in \mathbb{R}$. The system is working in cross-wind for a key reason, the effect of the freestream is constant during the whole operation. The reason for this is the following, we first analyse the ideal situation in which the drone is drawing the ∞ -shape in a plane perpendicular to the ground while the freestream can be safely assumed to act parallel to the ground. The plane in which the drone is moving is also perpendicular to the direction of the freestream. In that situation, wherever the drone is, the influence of the freestream will always be accounted in the same way. That means that its direction with respect to the chord is not changing, thus its contribution to the attack angle is constant. On the other hand, the one contributing to the angle of attack that can be modified at will is the speed of the drone itself. The angle of attack is computed as the angle between the chord direction and the relative wind direction. The latter is calculated as $V_{freestream}(t) - V_{drone}(t)$, which are both vectorial quantities. Thus, by acting upon the latter, it is possible to modify the angle of attack.

Conversely, if the drone was flying parallel to the ground, there would be times in which the effect of the freestream would increment the lift, others in which it would reduce it and others in which it would have no effect. All of them happening for every 8-shape. This behaviour, similar to the one appearing in every helicopter's blades, is undesirable. As a result, the solution is to fly as perpendicular to the freestream as possible. Usually the lift force is much bigger than the weights of the different parts in this kind of systems and assuming it is perpendicular to the 8-shape plane, the angle of the 8-shape plane from the vertical can be very small. The remaining force can be used to produce energy.



Figure 2.1: 5 kW prototype of Kitemill AS

2.2. Operation scheme

In normal conditions, free from any fault, the working principle of the system can be organized as follows:

1. **Vertical take-off.** When the wind conditions at the targeted operating altitude are suitable to generate energy, the drone takes off using the 4 equipped propellers. These are capable of sustaining the combined weight of the drone plus the tether while keeping the attitude of the drone under control for this suitable atmosphere conditions.
2. **Transition from hovering to power generation.** The drone moves to the desired position in which the tether must be engaged. Once the tether force is acting upon the drone, it speeds up and reaches the correct attitude and speed that allow for the weight to be sustained only by the aerodynamic forces at the expected altitude where the power generation phase will start.
3. **Power generation.** The drone enters the power generation mode via the so-called 'pumping operation'. This procedure consists on two phases, the traction phase

and the retraction phase (as shown in figure 1.6). During the former, the drone flies fast in crosswind patterns (i.e. roughly perpendicular to the wind flow) and the tether is reeled-out under high force, generating energy. On the other hand, during the retraction phase the drone glides towards the ground station while the tether is reeled-in using a very low force. For connecting these two phases, two suitable transitions are devised, which enable a cyclic generation of power. During this phase, the propellers are not used except for the recharging of the batteries and as the power supply to the onboard electronics and actuators. As a result, the dynamic equations describing this phase are similar to the ones used for modelling an aeroplane's behaviour, where the aerodynamic forces keep the drone flying. This model is extended to consider the presence of the tether.

4. **Transition from flight to hovering.** This phase is usually enabled when either the wind is too low to generate energy or it is too strong to keep the operation safe. Hence, the drone slows down and starts to depend on the propellers to keep the approximation to the landing position and the hovering stage safe.
5. **Vertical landing.** The drone performs a controlled vertical landing in hovering mode.

2.3. Reentry strategies

In the literature there is a common consensus regarding the type of trajectory most beneficial to power generation. On the other hand, there are several reentry strategy options, which describes how the aircraft is flown from the ending of the last traction phase to a suitable position for starting the next one. Some of the options available are Free-flight (term referring to the absence of help from the ground station, hence implying that the tether is slack) reentry, Complete rotation around the ground station and Climb and Descend reentry [13]. The approach chosen in the present work is Free-flight. The idea behind it is to transition from taut-tether to loose-tether flight when the maximum admissible unwound tether length is reached. Then, the drone glides toward an Target point upstream, while the generator winds up the tether. The winding must be done in a way that minimize the tether forces. Once the Target point is reached, a point where the unwound tether length reaches the minimum acceptable value, the drone moves to achieve the correct attitude to restart the generation phase, at the same time aiming to engage the tether smoothly.

2.4. Coordinate systems

There is a range of coordinate systems used for having an accurate and easy description of the drone-tether-winch system.

1. **Ground station frame** (from now onwards *Earth frame* or *ef*): it is characterized by being an inertial coordinate system fixed to the ground station where the x-axis points to the North, the y-axis is oriented East and z-axis points down (commonly referred as NED coordinate system).
2. **Drone frame - sphere coordinates** (from now onwards *sphere coord.* or *sphere*) : it is based on describing the drone position in spherical coordinates, which are distance, $\theta_{sphere}(t)$ and $\phi_{sphere}(t)$. A set of new axis is then placed on the gravity centre of the drone ($L_N(t)$, $L_E(t)$ and $L_D(t)$) The graphic representation of them can be seen in figure 2.2. The calculus of this angles can be accomplished by using the relations presented in equation (2.2). Then, to express a vector from the sphere coordinate system into the Earth frame the rotation matrix shown in equation (2.1) is needed, where "c" represents "cosine" and "s" means "sine".

$$R_{sphere2ef} \begin{bmatrix} -c(\phi_{sphere}(t))s(\theta_{sphere}(t)) & -s(\phi_{sphere}(t)) & -c(\phi_{sphere}(t))c(\theta_{sphere}(t)) \\ -s(\phi_{sphere}(t))s(\theta_{sphere}(t)) & c(\phi_{sphere}(t)) & -s(\phi_{sphere}(t))c(\theta_{sphere}(t)) \\ c(\theta_{sphere}(t)) & 0 & -s(\theta_{sphere}(t)) \end{bmatrix} \quad (2.1)$$

$$\theta_{sphere}(t) = \arctan\left(\frac{z_{ef}(t)}{\sqrt{x_{ef}(t)^2 + y_{ef}(t)^2}}\right) \quad (2.2a)$$

$$\phi_{sphere}(t) = \arctan\left(\frac{y_{ef}(t)}{x_{ef}(t)}\right) \quad (2.2b)$$

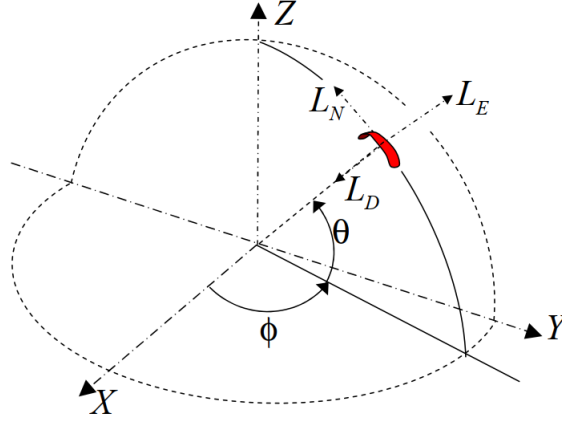


Figure 2.2: Sphere coordinates

3. **Drone frame - tether** (from now onwards *drone tether frame* or *tether*) : both the origin and the axis directions coincide with the ones explained for the *sphere* system. However, this system is introduced to point out the angles required for the attitude control during the traction phase. In that part, the objective is to have the drone pointing North in the *sphere* while the line of the tether coincides with Down in *sphere*. In order to achieve that, three angles are introduced in table 2.1.

angle	symbol	derivative's symbol
rotation around N_{sphere}	$\phi_{tether}(t)$	$\dot{\phi}_{tether}$
rotation around E_{sphere}	$\theta_{tether}(t)$	$\dot{\theta}_{tether}$
rotation around D_{sphere}	$\psi_{tether}(t)$	$\dot{\psi}_{tether}$

Table 2.1: drone's earth frame: symbolic description

The first and second angles are particularly important because they show whether the axis perpendicular to the plane formed by the wings coincides with the Down axis from the *sphere* coordinates. When these 2 are collinear, the drone is using the wind effect to keep himself flying while pulling the tether.

the calculus of all these angles is based on the data collected from the attitude.

4. **Drone frame - NED** (from now onwards *drone earth frame* or *def*): its origin is position at the centre of gravity of the drone and the convention from x,y and z is the same presented in the previous point. The notation regarding these representation is summarize in table 2.2.
5. **Drone frame - body** (from now onwards *body frame* or *bf*): it is attached to the drone, the x-axis coincides with the longitudinal axis of the drone, the y-axis

state	state symbol	state's derivative symbol
$P_{x_{def}}$	$x_{def}(t)$	$\dot{x}_{def}(t)$
$P_{y_{dfe}}$	$y_{def}(t)$	$\dot{y}_{def}(t)$
$P_{z_{def}}$	$z_{def}(t)$	$\dot{z}_{def}(t)$
rotation around North	$\phi_{def}(t)$	$\dot{\phi}_{def}(t)$
rotation around East	$\theta_{def}(t)$	$\dot{\theta}_{def}(t)$
rotation around Down	$\psi_{def}(t)$	$\dot{\psi}_{def}(t)$

Table 2.2: drone's earth frame: symbolic description

points to the right when seeing the drone from above and the z-axis completes the right-hand system pointing downwards. Considering this layout, the rotation around the x-axis is called rolling, while the rotation around the y-axis is named pitching(positive when the drone's nose point to the sky) and around the z-axis is called yawing. While the angles are represented by Greek letters, their derivatives are commonly associated with P,Q and R. This relations are clearly stated in table 2.3.

state	state symbol	state's derivative symbol
$P_{x_{bf}}$	$x(t)$	$u(t)$
$P_{y_{bf}}$	$y(t)$	$v(t)$
$P_{z_{bf}}$	$z(t)$	$w(t)$
roll	$\phi(t)$	$P(t)$
pitch	$\theta(t)$	$Q(t)$
yaw	$\psi(t)$	$R(t)$

Table 2.3: drone's states: symbolic description

6. **Drone frame - wind** (from now onwards *wind frame* or *wf*): As the two previous ones, the origin is at the centre of gravity of the drone. However, the x-axis in this case has the same direction of the incoming wind, the y-axis points to the right when seeing the plane from above during steady flight condition and then the z-axis points upwards to follow the right-hand convention. In this situation, the drag force, force along the x-axis, is positive during a steady flight and the lift force is also positive along the z-axis.

The angles describing the attitude of the aeroplane are used to create a new representation based on quaternions. The initialization of the quaternion (q) is stated in (2.3). This representation is updated in the simulation as presented in section Quaternion update and it used to overcome the singularity problem of the attitude's Euler-based representation.

$$q = \begin{bmatrix} \pm(\cos(\frac{\phi(t)}{2})\cos(\frac{\theta(t)}{2})\cos(\frac{\psi(t)}{2}) + \sin(\frac{\phi(t)}{2})\sin(\frac{\theta(t)}{2})\sin(\frac{\psi(t)}{2})) \\ \pm(\sin(\frac{\phi(t)}{2})\cos(\frac{\theta(t)}{2})\cos(\frac{\psi(t)}{2}) - \cos(\frac{\phi(t)}{2})\sin(\frac{\theta(t)}{2})\sin(\frac{\psi(t)}{2})) \\ \pm(\cos(\frac{\phi(t)}{2})\sin(\frac{\theta(t)}{2})\cos(\frac{\psi(t)}{2}) + \sin(\frac{\phi(t)}{2})\cos(\frac{\theta(t)}{2})\sin(\frac{\psi(t)}{2})) \\ \pm(\cos(\frac{\phi(t)}{2})\cos(\frac{\theta(t)}{2})\sin(\frac{\psi(t)}{2}) - \sin(\frac{\phi(t)}{2})\sin(\frac{\theta(t)}{2})\cos(\frac{\psi(t)}{2})) \end{bmatrix} \quad (2.3)$$

When a transformation between the body frame and the drone earth frame is needed, the equation (2.4) is used.

$$T_{b,f2def} = \begin{bmatrix} c(\theta)c(\psi) & c(\theta)s(\psi) & -s(\theta) \\ s(\theta)c(\psi)s(\phi) - s(\psi)c(\phi) & s(\theta)s(\psi)s(\phi) + c(\psi)c(\phi) & c(\theta)s(\phi) \\ s(\theta)c(\psi)c(\phi) + s(\psi)s(\phi) & s(\theta)s(\psi)c(\phi) - c(\psi)s(\phi) & c(\theta)c(\phi) \end{bmatrix} \quad (2.4)$$

2.5. Tether properties

It is assumed that a tether made of dyneema sk78, a polymeric material, is used in our system. The properties of this material are from [16]. It is assumed that the tether will have a diameter of 10 mm, which leads to a breaking load of 102 kN.

3 | Mathematical models

In this section, the mathematical models of the different components of the systems are presented. First, the tether model and its hypothesis are explained. Finally, the equations describing the behaviour of the drone are presented.

3.1. Tether model

The tether is a crucial element in AWE systems. Although its importance, it is possible to simplify its model in any degree possible, without losing the generality of the complete mission simulated and studied. In this work, it is decided to take a simple approach to its modelling, a simple spring, joining the generator and the drone. As the tether is unwound by the generator, the natural length of the spring is changed accordingly. The table 3.1 summarizes the parameters of the tether.

Title of Table (optional)

Paramet	value
K_{tether}	$2.366E+6 \frac{N}{m}$
ρ_{tether}	$975 \frac{kg}{m^3}$

Table 3.1: Representative values for the State machine

3.1.1. Tether Forces

The following two sections contain the two main tether forces. First, the force related to the longitudinal deformation of the tether is presented, elastic force. Then, the force due to its drag is approximated.

Tether elastic force

The force produced by the tether follows the simple equation describing a spring effect and it's presented below. Where, $l_{tether}(t)$ is the length of the tether unwound and $l_{tether_0}(t)$ is the actual length of the tether. This linear simple equation is changed in the model, because $l_{tether_0}(t)$ has a minimum value, which is $l_{tether}(t)$. As a result, it is not possible to compress the tether.

$$F_{tether}(t) = \max(0, K_{tether}(l_{tether}(t) - l_{tether_0}(t))) \quad (3.1)$$

Tether drag force

As the tether is considered as a simple spring, the effect of its drag is considered using an approximation [13]. It is based on an increment in the drag coefficient on the drone and it is computed based on the following formula. Where, $C_{D_{cross-section}}$ is the drag coefficient of the cross-section, d_{tether} is the tether's diameter and S is the wing's area.

$$C_{D_{tether}} = \frac{C_{D_{cross-section}} d_{tether} l_{tether}(t)}{8S} \quad (3.2)$$

3.1.2. Length of the tether

For the sake of simplicity, it is considered that the controller of the winch system is fast enough to be regarded as instantaneous. As a result, the tether length is directly defined according to the strategy proposed in the next chapters.

3.1.3. Matlab solver

This model represents a stiff behaviour, as the mass of the tether is small while the elastic constant is big in comparison and the friction coefficient is also small. As a result, every tiny deformation will lead to a force big enough to cause huge accelerations. This is a problem when considering numerical stability. Thus, it is decided to use the solver `ode15s` in *simulink*, purposely devised for this stiff situations.

3.2. Hybrid drone model

As it has been explained before, the drone modelled is a combination of a fixed wing system with 4 rotors whose axis of rotation are always parallel to the z axis of the drone.

First, the model of the system acting as a fixed wing plane is studied and then the model for the quadcopter behaviour is presented.

3.2.1. Aerodynamic data

The aerodynamic data for the *Kitemill* aircraft was taken from [12]. This information is used to approximate the aerodynamic coefficient of the drone in every instant using the following formulas, being the coefficients from (3.3a) to (3.3c) used to calculate the aerodynamic forces and coefficients obtained from (3.3d) to (3.3f) are used to calculate the aerodynamic moments.

$$C_D(t) = C_D(\alpha(t)) \quad (3.3a)$$

$$C_Y(t) = C_Y(\beta(t), \delta_r(t)) + C_{Y_P} \frac{P(t) b}{2V_a(t)} + C_{Y_R} \frac{R(t) b}{2V_a(t)} \quad (3.3b)$$

$$C_L(t) = C_L(\alpha(t), \delta_e(t)) + C_{L_Q} \frac{Q(t) \bar{c}}{2V_a(t)} \quad (3.3c)$$

$$C_m(t) = C_m(\alpha(t), \delta_e(t)) + C_{m_Q} \frac{Q(t) \bar{c}}{2V_a(t)} \quad (3.3d)$$

$$C_n(t) = C_n(\alpha(t), \delta_a(t)) + C_n(\beta(t), \delta_r(t)) + C_{n_P} \frac{P(t) b}{2V_a(t)} + C_{n_R} \frac{R(t) b}{2V_a(t)} \quad (3.3e)$$

$$C_l(t) = C_l(\alpha(t), \delta_a(t)) + C_l(\beta(t), \delta_r(t)) + C_{l_P} \frac{P(t) b}{2V_a(t)} + C_{l_R} \frac{R(t) b}{2V_a(t)} \quad (3.3f)$$

3.2.2. Aerodynamic forces and moments

Once the coefficients are obtained, the next step is to calculate the forces and moments derived from them. They will be then added to the ones produced by the rotors. The following equations represent the forces.

$$\text{drag} \quad D(t) = 0.5 \rho V_a(t)^2 S (C_D(t) + C_{D_{\text{tether}}}(t)) \quad (3.4a)$$

$$\text{lift} \quad L(t) = 0.5 \rho V_a(t)^2 S C_L(t) \quad (3.4b)$$

$$\text{sideforce} \quad Y(t) = 0.5 \rho V_a(t)^2 S C_Y(t) \quad (3.4c)$$

These forces are expressed in the wind system of coordinates, so they are transformed to the body axis as it is shown below (F_A stands for aerodynamic forces along a given axis shown in the lowest subscript).

$$\begin{bmatrix} F_{A_x}(t) \\ F_{A_y}(t) \\ F_{A_z}(t) \end{bmatrix} = \begin{bmatrix} \cos(\alpha(t))\cos(\beta(t)) & \sin(\beta(t)) & \sin(\alpha(t))\cos(\beta(t)) \\ -\cos(\alpha(t))\sin(\beta(t)) & \cos(\beta(t)) & -\sin(\alpha(t))\cos(\beta(t)) \\ -\sin(\alpha(t)) & 0 & \cos(\alpha(t)) \end{bmatrix} \begin{bmatrix} -D(t) \\ Y(t) \\ -L(t) \end{bmatrix} \quad (3.5)$$

On the side of the aerodynamic moments represented in the body axis, they can be calculated as follows. Where (3.6a) is the rolling moment or moment around the x body axis, (3.6b) is the pitching moment or moment around y body axis and (3.6c) is the yawing moment or moment around the z body axis.

$$l(t) = 0.5 \rho (V_a)^2(t) S b C_l(t) \quad (3.6a)$$

$$m(t) = 0.5 \rho (V_a)^2(t) S \bar{c} C_m(t) \quad (3.6b)$$

$$n(t) = 0.5 \rho (V_a)^2(t) S b C_n(t) \quad (3.6c)$$

3.2.3. Motors' effect

When considering the traction force and the forces produced by the rotors, the following terms should be considered in the different body axis. Where the subindex in T_i refers to the rotor position, as it is shown in figure 3.1, where the convention for positive rotation is added.

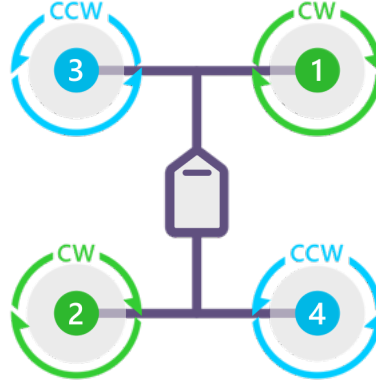


Figure 3.1: Drone's motor numeratio

$$F_{T_x} = 0 \quad (3.7a)$$

$$F_{T_y} = 0 \quad (3.7b)$$

$$F_{T_z}(t) = -(T_1(t) + T_2(t) + T_3(t) + T_4(t)) \quad (3.7c)$$

The same logic applies for the moments produced by the rotors which are separated by their influence on the different axis as follows, where Q_i represent the torque of the i^{th} positioned rotor.

$$l_R(t) = -T_1(t) + T_2(t) + T_3(t) - T_4(t) \quad (3.8a)$$

$$m_R(t) = T_1(t) - T_2(t) + T_3(t) - T_4(t) \quad (3.8b)$$

$$n_R(t) = Q_1(t) + Q_2(t) + Q_3(t) + Q_4(t) \quad (3.8c)$$

3.2.4. Dynamic equations

All the different components are included in order to write the differential equations for the fixed-wing drone. The idea is to follow the approach of the Newton's Laws and express everything in terms of the drone's speeds. Equations from (3.9a) to (3.9c) are the expres-

sions needed to calculate the states related to linear movement, while equations ranging from (3.9d) to (3.9f) defines the dynamic of the states related to angular movements.

$$\dot{U}(t) = \frac{F_{Ax}(t) + F_{Tx}(t)}{mass} + g_x(t) + W(t)Q(t) + V(t)R(t) \quad (3.9a)$$

$$\dot{V}(t) = \frac{F_{Ay}(t) + F_{Ty}(t)}{mass} + g_y(t) + U(t)R(t) + W(t)P(t) \quad (3.9b)$$

$$\dot{W}(t) = \frac{F_{Az}(t) + F_{Tz}(t)}{mass} + g_z(t) + V(t)P(t) + U(t)Q(t) \quad (3.9c)$$

$$\dot{P}(t) = (c_1R + c_2P)Q(t) + c_3(l(t) + l_R(t)) + c_4(n(t) + n_R(t)) \quad (3.9d)$$

$$\dot{Q}(t) = c_5 R(t) P(t) - c_6(P(t)^2 - R(t)^2) + c_7(m(t) + m_R(t)) \quad (3.9e)$$

$$\dot{R}(t) = (c_8P + c_2R)Q(t) + c_4(l(t) + l_R(t)) + c_9(n(t) + n_R(t)) \quad (3.9f)$$

The terms c_i in the above equations are related to the inertia of the drone and they are defined as follows.

$$\begin{aligned} c_1 &= \frac{(J_{yy} - J_{zz})J_{zz} - J_{xz}^2}{\Gamma} & c_4 &= \frac{J_{xz}}{\Gamma} & c_7 &= \frac{1}{J_{yy}} \\ c_2 &= \frac{(J_{xx} - J_{yy} + J_{zz})J_{xz}}{\Gamma} & c_5 &= \frac{J_{zz} - J_{xx}}{J_{yy}} & c_8 &= \frac{(J_{xx} - J_{yy})J_{xx} + J_{xz}^2}{\Gamma} \\ c_3 &= \frac{J_{zz}}{\Gamma} & c_6 &= \frac{J_{xz}}{J_{yy}} & c_9 &= \frac{J_{xx}}{\Gamma} \end{aligned} \quad (3.10)$$

where $\Gamma = J_{xx}J_{zz} - J_{xz}^2$

while the decomposition of the gravity in the body axis is done as shown below.

$$\begin{aligned} g_x(t) &= 2g(q_1(t)q_3(t) - q_0(t)q_2(t)) \\ g_y(t) &= 2g(q_2(t)q_3(t) - q_0(t)q_1(t)) \\ g_z(t) &= g(q_0(t)^2 - q_1(t)^2 - q_2(t)^2 + q_3(t)^2) \end{aligned} \quad (3.11)$$

Finally, the side slip angle derivative and the angle of attack derivative expressions are presented below, along with the equation for the free stream velocity with angle of attack and side slip angle to the x-axis body frame.

$$\begin{aligned} \dot{V}_T(t) &= \frac{\dot{U}(t)U(t) + \dot{V}(t)V(t) + \dot{W}(t)W(t)}{V_a(t)} \\ \dot{\alpha}(t) &= \frac{\dot{W}(t)U(t) - \dot{U}(t)W(t)}{U(t)^2 + W(t)^2} \\ \dot{\beta}(t) &= \frac{\dot{V}(t)V_a(t) - \dot{V}_a(t)V(t)}{V_a(t)^2 \cos(\beta(t))} \end{aligned} \quad (3.12)$$

3.2.5. Quaternion update

In order to update the quaternion representation the its derivative can be written as follows. Then, the next pose of the drone is obtained by integrating this derivative along with the rest of the state's derivatives.

$$\dot{q}(t) = 0.5 \begin{bmatrix} -q_1(t) & -q_2(t) & -q_3(t) \\ q_0(t) & -q_3(t) & q_2(t) \\ q_3(t) & q_0(t) & -q_1(t) \\ -q_2(t) & q_1(t) & q_0(t) \end{bmatrix} \begin{bmatrix} P(t) \\ Q(t) \\ R(t) \end{bmatrix} \quad (3.13)$$

4 | Control System

The first step towards the design of the control strategy is identifying the control actions, which are the speed of each motor and deflection of the control surfaces. The control surfaces available in the drone under study are the ailerons, the elevator and the rudder. Their effects can be seen in the aerodynamic coefficients and the value of their deflection is written as δ_i with $i = a, e, r$ for the ailerons, elevator and rudder, respectively.

In addition, it is important to know which are the measuring capabilities of the system. It is assumed that the drone have an IMU powerful enough to provide a good sampling frequency and small errors. At the same time, it is necessary to have a GPS, to locate the drone in the Earth Frame.

This chapter is divided by how is the behaviour of the drone, called hovering control and airplane mode control. However, the first part is the explanation on how is the control system layout, where a rough overview of the functioning of the system as a whole is given. Later, the subsystem in charge of orchestrating the whole mission, the state machine, is described. Subsequently, the controllers for the hovering control are explained in detailed. Finally, the controllers for the airplane mode control are introduced and described in details.

4.1. Control layout

The proposed system is based on a cascade approach, where the closed-loop dynamics at the the lowest level are used as the basis the design of the higher levels. At the same time, there will be parallel controllers in different levels. The switching among them is done according to the phase in which the drone is and to some other variables, chosen to represent crucial points, that will be explained in more detailed later.

4.2. State machine

The whole mission consists on 7 Phases, each of them representing a distinct phase with its own problems and, thus, controllers and references as solutions. Hence, it is crucial to have a subsystem capable of recognizing the Phase in which the mission is at any time and also able to discern when that phase must change. Moreover, each Phase is coupled with a set of references that are the ones fed to the control system. This role is played by the state machine, and its 7 Phases will be described in the next paragraphs to finally present its pseudo-code.

4.2.1. Representative values

There are several values that will be used to represent key points where the Phase may change, if all the other conditions are met. Also there are some that are vital for the correct definition of the path.

Symbol	Explanation
l_{min}	minimum tether length during the generation phase
l_{max}	maximum tether length during generation phase
θ_{obj}	position in the sphere coordinate $\theta(t)$ of the Target points
ϕ_{obj}	position in the sphere coordinate $\phi(t)$ of the Target points this value is the positive one
y_{obj}	position in y_{ef} of the Target points when the tether length is equal to l_{min} , this value is the positive one
x_{obj}	position in x_{ef} of the Target points when the tether length is equal to l_{min}

Table 4.1: Parameters used in the State machine

4.2.2. Possible Phases

Phase 0 - Take off

The first possible Phase occurs during the take off, as shown in figure 4.1. It is assumed that the drone is going to start always pointing northwards. Thanks to the VTOL capabilities of the drone, it engages the motors to keep itself parallel to the ground while gaining altitude. On the other hand, the control surfaces remain unused. As a result,

the main reference in this phase is the desired altitude, while the references for the body angles are all 0. While rising in altitude, the tether is reeled out at a pace that keeps it loose. Thus, the tether's length is always 10% bigger than the distance from the drone to the generator.

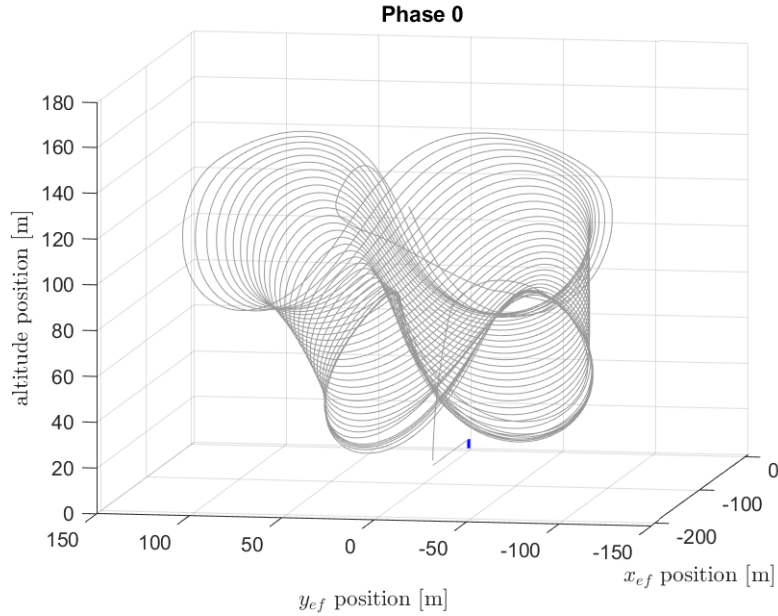


Figure 4.1: Phase 0

Phase 1 - Approach sphere's surface

Once the desired altitude is reached, the Phase changes to the number 1, shown in blue in figure 4.2. The objective in this phase is to reach almost l_{min} , the drone must move along the x_{ef} axis during this phase. As it is done in Phase 0, the motors are the only ones engaged again. The references for their controller are an altitude one, keeping the same value that it had in the previous Phase, and 3 for the attitude. These ones are based on the desired ending point of Phase 1, which is a point that leaves the tether length at a value that is 99% of l_{min} . During the whole procedure, the tether is reeled out at a pace that keeps it loose. In this work, the tether's length is always 10% bigger than the distance from the drone to the generator. As the drone must engage the tether, its unwound length is restricted to l_{min} .

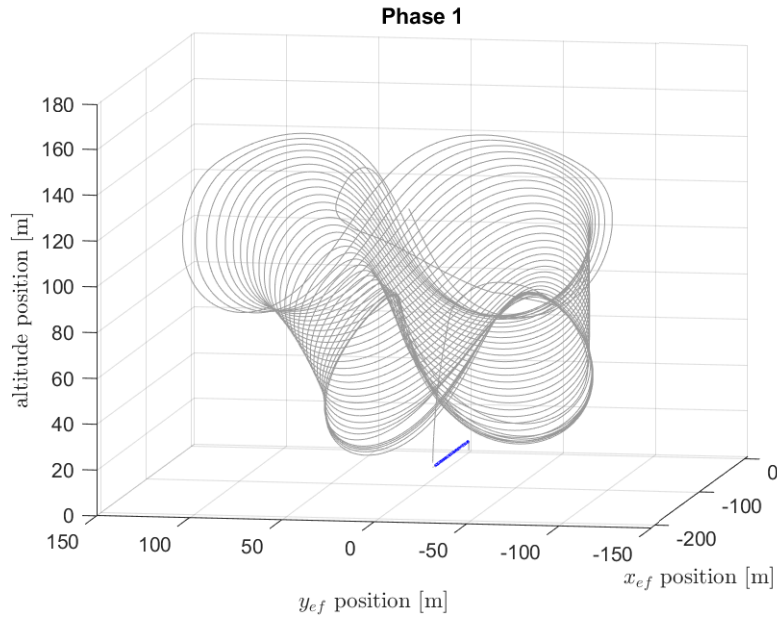


Figure 4.2: Phase 1

Phase 2 - Tether engaging

This is a short Phase, the idea is to produce the engagement of the tether in a smooth way. Thus, after changing to this Phase the reference is moved to a value a little bit bigger than l_{min} , as it can be seen in figure 4.3. As the proportional characteristic of the controller dominates and the error is small, the movements are slow. Hence, the tether is engaged without producing sudden huge forces on the vehicle. This Phase is kept for 3 seconds, to allow the drone to stabilize. This is necessary because as the drone engages the tether, being the latter an undamped body (analogous to a spring without damper), there will be oscillations, that are to be eliminated before starting to climb. To conclude, the set of references will follow the same logic as the ones in the previous Phase, the only different will be in the values for the objective position.

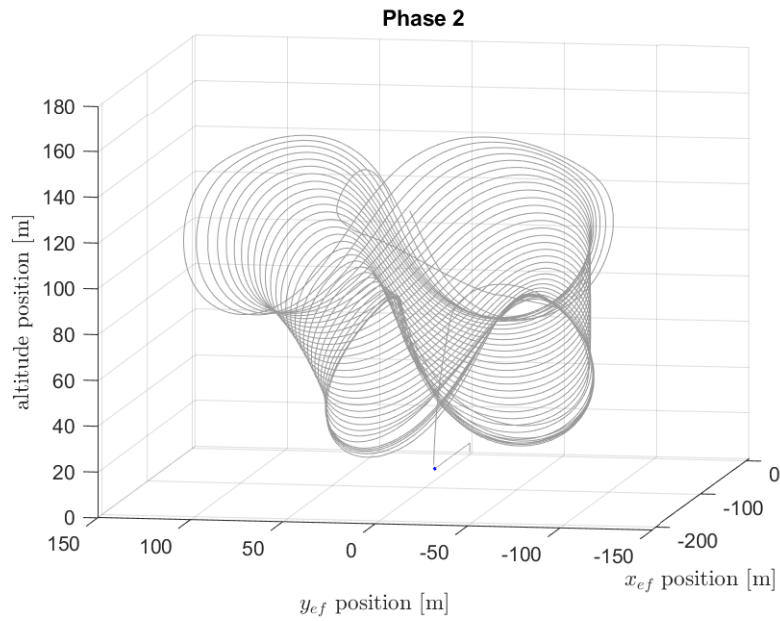


Figure 4.3: Phase 2

Phase 3 - Climbing

Once the drone reaches Phase 3, the tether is taut and it is time to start climbing, movement portrayed in figure 4.4. As the tether is already engaged, the drone climbs on the sphere. Hence, the idea is to make the drone quickly gain altitude while keeping it on the x_{ef} axis. In addition, the nose should start to point upwards, reaching the attitude that will characterize the dynamic in Phase 4. In order to produce this movement, the set of references and variables to control changes. In the mean time, the tether is kept with a length equal to l_{min} .

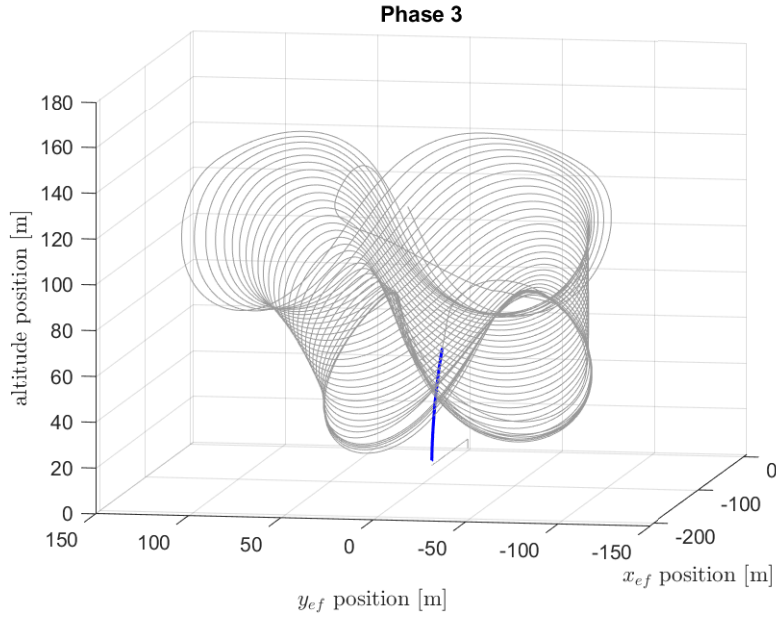


Figure 4.4: Phase 3

First, the control cascade layout is simplified. Before, the attitude was controlled based on the position in the space of some key points, that were transformed into references for the angles defining the attitude (roll, pitch and yaw), to finally become signals to define the motors' speed. Now, the first part of this cascade control is removed. As a result, the references for this control layer are given as angles directly.

Second, up to now, the inner controller has as input the angular errors of the Euler angles. However, this is changed for the Phase 3. Now, the pitch and roll angles are exchanged for the tether angles, while the third angle is still the yaw one. It is possible to replace $\theta(t)$ by θ_{tether} and $\phi(t)$ by ϕ_{tether} for control purposes. The reason behind this is that the pitching movement of the drone, affects directly the value of θ_{tether} . The analogous connection exists between the other pair of angles.

Third, the set of references changes. The altitude reference now is a simple relationship between the previous value of the altitude and the current reference. In here, the logic used is that the current reference value should be always 30 meters higher than the previous altitude of the drone. The motivation behind this choice is to produce an always increasing reference, that enables the drone to reach any required altitude for the switching to Phase 4. Similar is the approach taken for the attitude references. The reference used for ϕ_{tether} is 0, because in this phase is important for the drone to have its wings forming a plane parallel to the sphere. The case of θ_{tether} is comparable to the one described above, however, the starting conditions are very different. For ϕ_{tether} , the starting condition is

very close to 0 already. On the other hand, θ_{tether} starts with a high value that must be close but not equal to 0, i.e. nose up and with the longitudinal axis of the drone almost tangential to the sphere. This great error may lead to too aggressive movements that are undesirable. Thus, the approach taken for the reference is based on a simple relation in between the current reference for the angle and its previous value. The idea is to make it decrease to a value close to zero, so the new reference must always be a fraction of the previous angle value. As a result, the drone is bound to increase its altitude while pointing its nose up, all contained in the x_{ef} axis.

To finish this Phase, a certain altitude is chosen. As the reduction of the error in θ_{tether} is much faster, it is not used as a condition. The altitude value in which Phase 4 is reached depends on the capacity of the drone to enter the generation phase properly. One of these conditions is a value of u_r that is big enough to allow the control surfaces to impact on the dynamic properly.

Phase 4 - Stabilization

Once the required altitude is reached and the drone is fast enough, the Phase 4 is reached. In here, the drone starts to aim alternatively to two different points, both defined in the spherical coordinates, as it can be seen in figure 4.5. Once the drone is close enough to one of them, the objective is switched to the other one. The measure of closeness is related to the ϕ_{sphere} coordinate of the drone. When its absolute value is bigger than the absolute value of ϕ_{sphere} for the current objective, the objective changes. In another words, the Target points define a region inside the sphere, contained between them; when the drone exits this region from any side, the reference becomes the Target point defining the opposite limit. In this Phase, the control and reference system change again.

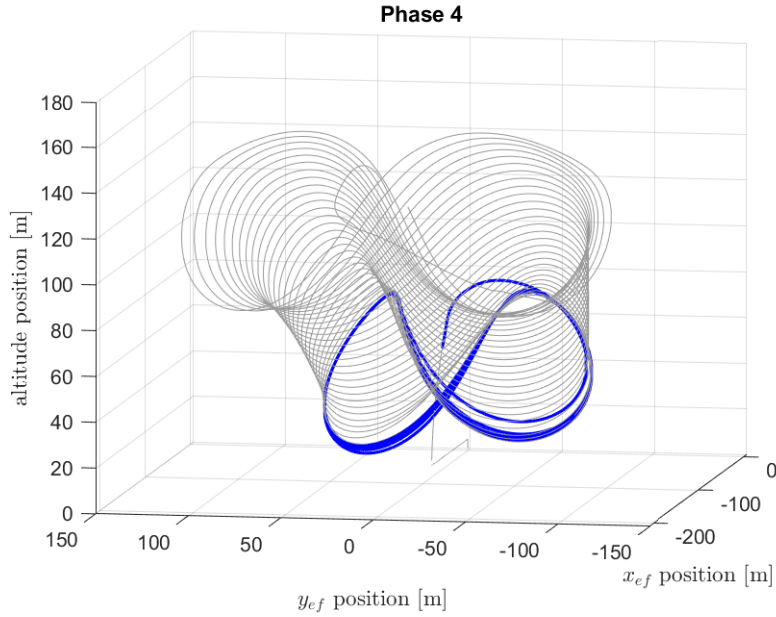


Figure 4.5: Phase 4

The control actions are now the elevator, rudder and ailerons, thus the controller changes. The errors being fed to it are still related to the tether angles and there is a change in the third one. Before, $\phi(t)$ was used, but now the error is computed in relation to the velocity angle. This angle shows where the velocity vector is pointing, contained in the plane tangential to the sphere in the drone position, and the reference of it is calculated to make the drone move towards the objective. When talking about the other two angles, θ_{tether} is used for controlling the velocity and ϕ_{tether} changes to try to take the side slip angle to zero. The logic behind this choices are in the control action that they provide. There are not many forces acting on the drone that are big enough to be used as a possible control action, one is the lift and the other one is the tether force. The former one is discarded because it can only be projected into the axis of the drone by α and β , to use it as a control force. However, α should be kept in a certain range of values and ideally in one that maximizes the aerodynamic efficiency. Moreover, and most importantly, β should be zero at any given time. As the result, they are not a good choice for angles to control. The option of the tether force remains, this value can be easily decomposed into the drone body axis by changing the two tether angles, which are directly related to $\theta(t)$ and $\phi(t)$ as explained before. This is the approach used because it gives a simple control structure to control the drone dynamic. Controlling its velocity is done by changing θ_{tether} , which produces a variation in the projection of the tether force into the longitudinal axis of the drone. On the other hand, ϕ_{tether} is leveraged to project the force into the y axis and compensate the side slip angles. The reduction to zero of β enables also the drone's

capability to produce turns.

This Phase is a transition one. The tether length is kept constant during the full span of Phase 4. The reason motivating this choice is to make the system more robust. In fact, when Phase 3 is finished, the drone may be in plenty of different conditions. Hence, it is proposed to wait for it to carry out a few cycles at constant tether length so it gets ready for the generation phase. The drone is bound to produce several cycles of switching between the Target points, while it mitigates the problems that may arise from the starting condition.

Phase 5 - Generation

Once the drone is flying in a regular manner while switching Target points, Phase 5 starts. It is characterized by the reeling out of the tether, which is the source of the electricity production, as it can be seen in figure 4.6. This new element leads to a more complex dynamic, because the reeling out leaves the drone with a variable length of the tether. As such, there is one precaution to be taken. It is how to start the reeling out, this should not be too harsh because it may produce some instability but not too slow as there is a loss in time. This issue is tackled by creating a signal that slowly increases the reeling out speed to finish in a constant value, which amount to the desire value for energy generation.

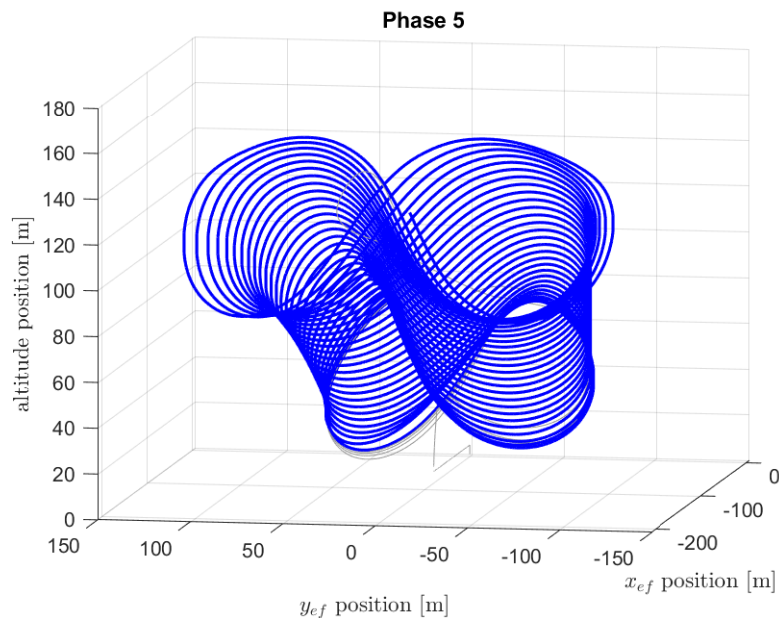


Figure 4.6: Phase 5

On the side of the controllers and references used, they are exactly the same as in Phase 4.

Phase 6 - Retraction

This stage in particular is composed by several parts, the sum of them is presented in figure 4.7:

- part 1: the drone, with a loose tether, starts the manoeuvre to transition to the generation phase by turning. For that, it is crucial to consider the distance to the Target point from the place where part 1 begins. Both the altitude difference and the distances in x and y should be considered. As a result, the references are to be compared with the body angles. The pitch angle is independent from the other 2 and it is used for controlling the altitude with which the drone arrives Target point, the arrival is assessed in the horizontal plane only. On the other hand, the yaw angle depends on the roll angle. The latter is chosen with respect to the distance from the beginning of part 1 to the Target point and the former is used to control the side-slip, thus allowing for a coordinated turn.
- part 2: The drone is already heading towards the Target point in the x-y plane. This parts starts when the earth speed vector is align with a vector starting at the current position and aiming at the objective.
- part 3: Once the drone is close enough to the point, it is given as references a high roll and pitch angles. The idea is to make the drone turn towards the outside and, at the same time, make it point downwards. At the same time, a reference to the yaw angle is proposed, with the scope of make the drone point to the next Target point.
- part 4: Once the drone is pointing downwards and it starts to turn outwards, the references are shifted to the tether angles. In this situation, the drone is already engaged with the tether, hence the reference for the theta tether angle is the same used in Phase 4 and 5. On the other hand, ϕ_{tether} is used to control the side slip angle. In this part, the reference is not given for the velocity angle, it is for the yaw angle and its scope is the same as in part 3, to make the drone point towards the next Target point.

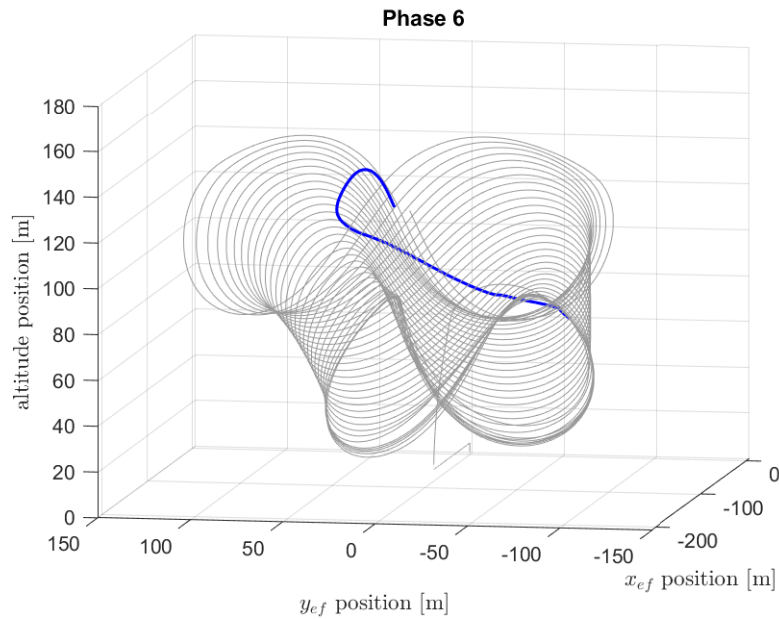


Figure 4.7: Phase 6

4.3. Hovering control

During hovering, the motors are responsible for the attitude and altitude control. In figure 4.8 it is possible to see how is the control logic. This phase comprises Phase 0 - Take off, Phase 1 - Approach sphere's surface, Phase 2 - Tether engaging and Phase 3 - Climbing, however the first three of them have a substantial difference with respect to the last one. The latter is characterized by a taut tether and the set of controllers are different, as explained before, and the control block is presented in figure 4.8 as "Taut tether control". The first three Phases have a cascade controller with one layer more than the one present in Phase 3, the control block is presented in figure 4.8 as "Loose tether control". While the drone is moving with a loose tether, the generator is in charge of reeling out to prevent strong tether forces. The dynamic of the attitude and altitude can be decoupled to analyse and synthesize controllers separately. The main idea for the attitude controller is to arrange a cascade control with a number of layers.

Section Taut tether control contains the inner and middle layer controllers, as they are the only ones needed in this Phase for attaining the desire attitude. Both of them are used also during the loose tether phase, that is why their description is not added in section Loose tether control. However, this section contains the explanation of the outer layer, which is only used during the first three Phases. In addition, the altitude controller is presented in section Altitude controller, and it is used for both taut and loose tether

phases. At the end of this section, the Control allocation - Hovering logic is presented.

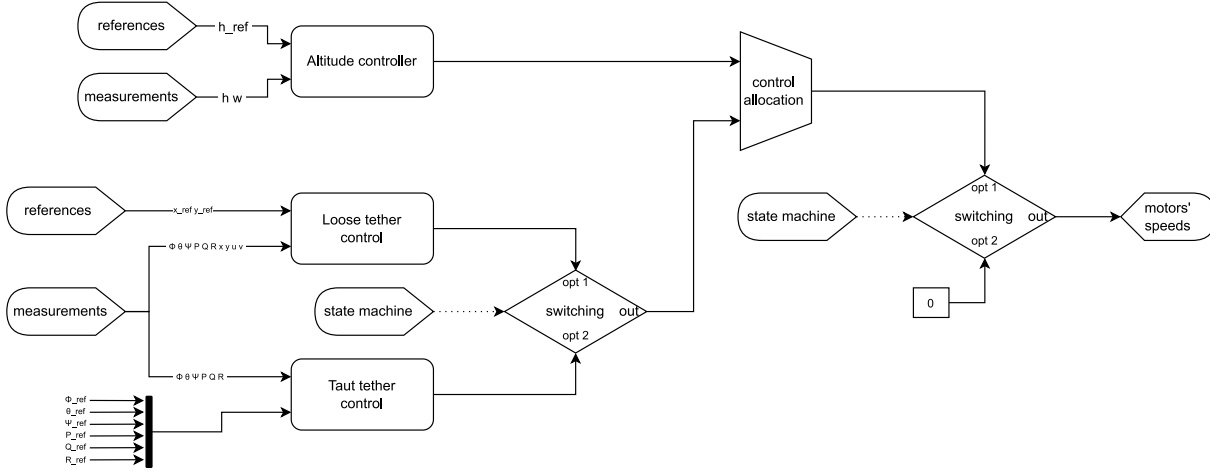


Figure 4.8: Complete hovering control block diagram

4.3.1. Altitude controller

To tackle the control of the altitude of the drone in hovering mode, the strategy is also leveraging on the decoupling of the attitude and altitude dynamics. So, the dynamical model is only composed into two variables, the altitude and its derivative. This state space model is enlarged so as to provide an integral action, reflected in the third row of the equation (4.1). The final model can be seen below, where the parameters relating \mathbf{W} and \mathbf{h} are taken from [10].

$$\begin{bmatrix} \dot{W}(t) \\ \dot{h}(t) \\ \dot{e}_h(t) \end{bmatrix} = A \begin{bmatrix} W(t) \\ h(t) \\ e_h(t) \end{bmatrix} \quad (4.1)$$

4.3.2. Taut tether control

As explained before, this controller is in charge of the attitude when the tether becomes taut and it is devised with a cascade scheme. It has two layers, called Inner layer and Middle layer, with their own inputs and outputs. A control scheme is presented below.

Inner layer - PQR controller

This layer returns a set of references for the motors' angular speeds based on a set of references for the angular speeds in the body axes. In order to achieve it, the controller computes the required moments around x,y and z to be applied to the drone based on the

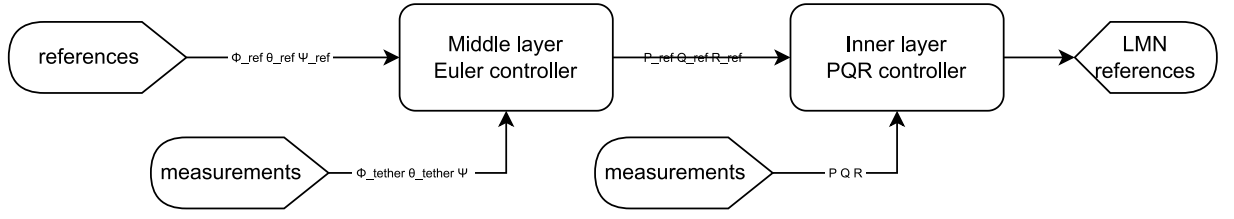


Figure 4.9: Schematic block diagram of the Taut Tether Control subsystem

inputs. Afterwards, these are merged with the force returned by the altitude controller into references for the motors' angular speeds as explained in section Control allocation - Hovering, when in hovering mode. On the other hand, while in airplane mode the moments are achieved by suitable aerodynamic moments.

Middle layer - Euler controller

The middle layer is in charge of tracking the angular position of the drone described by the three Euler angles in the *drone earth frame*. Hence, a reference for each of those is received as input and, after transforming from Euler to body angular speeds, the control actions are obtained in the form of body angular speeds. Below, it is possible to see the mathematical relationships describing the dynamic under control. These equations relate the Euler angles and their derivatives by a simple kinematic relationship and are reported below in the LaPlace domain.

$$\begin{aligned}\phi_{def} &= \frac{\dot{\phi}_{def}}{s} \\ \theta_{def} &= \frac{\dot{\theta}_{def}}{s} \\ \psi_{def} &= \frac{\dot{\psi}_{def}}{s}\end{aligned}\tag{4.2}$$

4.3.3. Loose tether control

This subsystem is responsible of the controlling of the attitude while the drone is flying with a loose tether. The inner and middle layers of this cascade control are shared with the 4.3.2, so their descriptions are not going to be repeated in this section. However, there is one difference with respect to the previous control subsystem, the loose tether control subsystem requires another layer in the cascade scheme. The new block scheme is shown in figure 4.10 and the explanation of the new layer can be found below. The existence of this new layer is driven by the necessity of the drone to move based on spacial references in the x_{ef} - y_{ef} plane during Phase 0 to 2.

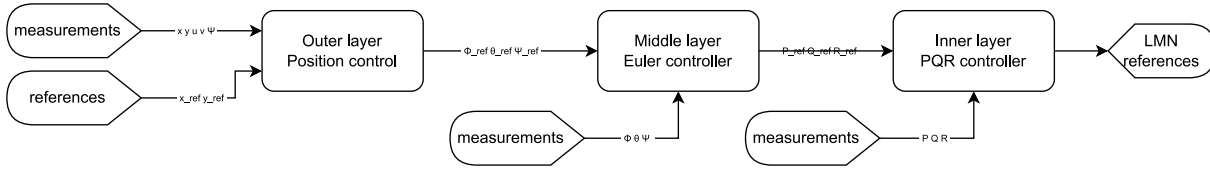


Figure 4.10: Schematic block diagram of the Loose Tether Control subsystem

Outer layer - Position control

The third layer of the attitude controller is used in the case of having the earth positions as references, inputs of this system, and $\phi_{ref}(t)$ and $\theta_{ref}(t)$ as outputs. There are several steps involved to reach to the desired output. First, as explained in section Position controller, based on the inputs the speeds in the earth coordinate system are calculated. Second, they are used as references for a control loop in which the references for $\theta(t)$ and $\phi(t)$ are computed following the procedure detailed in section Velocity controller.

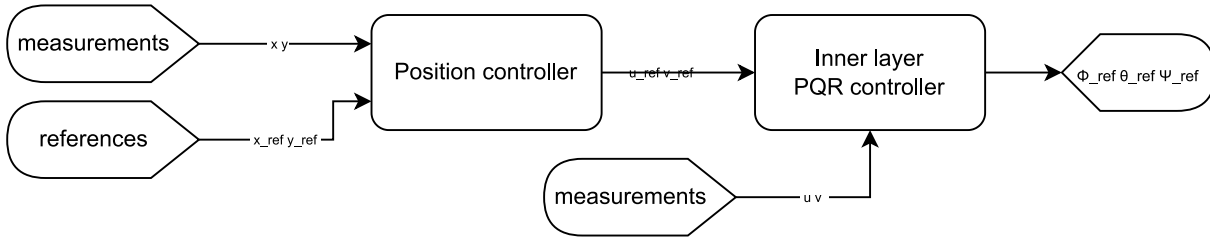


Figure 4.11: Schematic block diagram of the Position controller

Position controller The desired positions $x_{def}(t)$ and $y_{def}(t)$ are the inputs for this part while the outputs are necessary speed components in the Earth Frame, so as to reach the desired inputs. The relation in between them is the simple kinematic relationship between a variable and its derivative. Defining the position references by $P_{earth}(t) = [x_{def_{ref}}(t) \ y_{def_{ref}}(t)]$, the following equation describes the dependencies studied in the LaPlace domain.

$$P_{earth} = \frac{\dot{P}_{earth}}{s} \quad (4.3)$$

Velocity controller The inputs for this part are the speeds in the *Earth Frame* and the outputs are $\theta(t)$ and $\phi(t)$. Once, a small $\theta(t)$ is applied and the nose goes down, the total motors force will increase its projection on the forward direction a little. Then, the speed in this direction will also increase over time. A similar chain of thought can be used if only a small $\phi(t)$ angle appears, the only difference is that in the case in which the aeroplane's right wing goes down, the motors' force will have an increased projection

toward that side and a higher speed over time too. Based on them, a simplification on the relationship between forces and accelerations is used. As the nominal case represents the drone in a hovering situation, where the drone keeps its attitude and position constant, it can be assumed that the approximation of small angles holds. As a result, the following models are derived starting from the sum of forces in the x-y plane of the *Drone Earth Frame*.

$$\ddot{x}(t) = -\frac{F_{motors}(t)\sin(\theta(t))}{m} = -\frac{F_{motors}(t)\theta(t)}{m} = -\frac{W_{drone}(t)}{m}\theta(t) = g\theta(t) \quad (4.4a)$$

$$\dot{x}(t) = -g\frac{\theta}{s}$$

$$\ddot{y}(t) = \frac{F_{motors}(t)\sin(\phi(t))}{m} = \frac{F_{motors}(t)\phi(t)}{m} = \frac{W_{drone}(t)}{m}\phi(t) = g\phi(t) \quad (4.4b)$$

$$\dot{y}(t) = g\frac{\phi}{s}$$

The negative sign in the equation relating the speed in x and the $\theta(t)$ angle comes into play because of the sign convention for the latter. When it is positive, the drone raises its "nose" and the motors' force move the drone in the negative direction.

4.3.4. Control allocation - Hovering

Once the required moments and the force are computed, it is necessary to convert them into references for the motors' speed. This is achieved by calculating the sum of forces and moments, so as to achieve a satisfactory transformation. The final transformation matrix is shown in equation (4.5).

$$\begin{bmatrix} \omega_{motor_1}(t) \\ \omega_{motor_2}(t) \\ \omega_{motor_3}(t) \\ \omega_{motor_4}(t) \end{bmatrix} = \begin{bmatrix} b_1 & b_2 & b_3 & b_4 \\ -b_1x_p & b_2x_p & b_3x_p & -b_4x_p \\ b_1y_p & -b_2y_p & b_3y_p & -b_4y_p \\ c_1 & c_2 & c_3 & c_4 \end{bmatrix}^{-1} \begin{bmatrix} F_{motors_z}(t) \\ M_{motors_x}(t) \\ M_{motors_y}(t) \\ M_{motors_z}(t) \end{bmatrix} \quad (4.5)$$

Afterwards, it is necessary to implement a saturation to the angular speed references. In order to accomplish this, the main logic is to apply to the 4 motor reference speeds the same modifications, so they keep they relative distances (key for the attitude control). The main changes are done to prevent the existence of a reference smaller than 0. Then, the four of them are scaled to prevent the overcome of the maximum limit.

Algorithm 4.1 Angular speed references' saturation logic

```

1:  $\omega_{motors_{min}} = \min(\omega_{motors})$ 
2:  $\omega_{motors_{max}} = \max(\omega_{motors})$ 
3: if  $\omega_{motors_{min}} < 0$  then
4:    $\omega_{motors} = \omega_{motors} + \text{abs}(\omega_{motors_{min}})$   $\omega_{motors_{max}} = \max(\omega_{motors})$ 
5:   if  $\omega_{motors_{max}} > \omega_{motors_{lim-max}}$  then
6:      $k = \frac{\omega_{motors_{lim-max}}}{\omega_{motors_{max}}}$   $\omega_{motors} = k \omega_{motors}$ 
7:   end if
8: else if  $\omega_{motors_{max}} > \omega_{motors_{lim-max}}$  then
9:    $\omega_{motors} = \omega_{motors} - (\omega_{motors_{max}} - \omega_{motors_{lim-max}})$ 
10:  if  $\omega_{motors_{min}} < 0$  then
11:     $\omega_{motors} = \omega_{motors} + \text{abs}(\omega_{motors_{min}})$   $\omega_{motors_{max}} = \max(\omega_{motors})$ 
12:    if  $\omega_{motors_{max}} > \omega_{motors_{lim-max}}$  then
13:       $k = \frac{\omega_{motors_{lim-max}}}{\omega_{motors_{max}}}$   $\omega_{motors} = k \omega_{motors}$ 
14:    end if
15:  end if
16: end if

```

4.4. Airplane mode control

This control system is enabled during Phase 4 - Stabilization, Phase 5 - Generation and Phase 6 - Retraction, because in them the equipment used for controlling the drone's attitude and altitude are the control surfaces. A cascade controller strategy is used to allow the drone to complete the generation and retraction phase, with the transition in between them. There are two layers in the the cascade controller, the first one, Inner layer - attitude controller, is in charge of controlling the attitude by computing the references for the aerodynamic moments (l, m and n). However, as the generation and retraction phases are different based on their requirements, there are unique strategies for each of them. The transition is studied along with the retraction. Consequently, the Outer layer encompasses two different controllers, one for the Generation phase and another for the Retraction and transition phase.

4.4.1. Inner layer - attitude controller

This layer is in charge of acting on the attitude to follow the references that will allow the drone to leverage the generation phase to produce the energy needed and, when it is finished, come back to the starting position to restart the generation phase. Although the

generation and retraction phases have distinct strategies, all share the same inputs and outputs. The latter are the aerodynamic moments needed to follow the references, while the former are the related to the Euler angles and their derivatives.

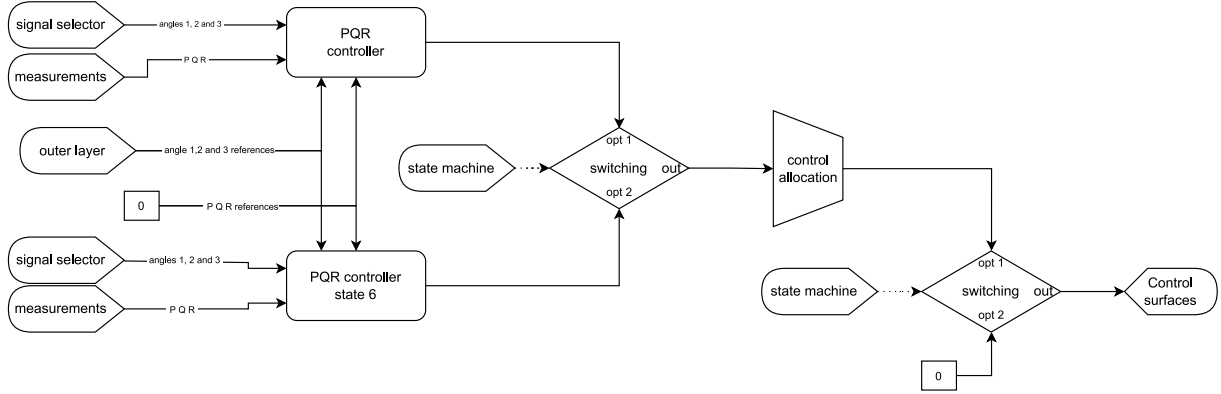


Figure 4.12: Schematic block diagram of the Inner layer for airplane mode

Generation phase

Starting from the non linear equations of the drone's dynamic, a linearized version is obtained. The variables considered for this controller are the three Euler angles, their derivatives and the integration of the error for $\psi(t)$, from now on $\psi_{error}(t)$. Although the controller is devised as stated before, the actual signals to control are the tether angles and the velocity angle. This leads to no problem, the reason behind it is the relation between the Euler angles and the three to be controlled. The first comment to be made is about the real inputs taken by the LQR controller, they are the errors between the references and the angles. The second consideration is related to the relation of the angles. By the way $\theta_{tether}(t)$ is defined, any variation in $\theta(t)$ is shown in $\theta_{tether}(t)$ in a one to one relation. Analogously, the relation between $\phi_{tether}(t)$ and $\phi(t)$ presents the same ratio of conversion. In the case of $\psi(t)$, the definition of $\gamma(t)$ is made in such a way that a variation in $\psi(t)$ can be seen in $\gamma(t)$. The relationships in this case becomes a little bit more complex, as it is one to one when both tether angles are zero. Not only cannot that situation be taken as normal, but also the actual scope of the tether angle controllers will lead to them not being null as the basis to keep the drone in the correct path. Nonetheless, the angles will be small enough to consider the variation they produce as negligible.

Retraction and transition phase

The approach chosen for this controller is similar to the previous one, a controller synthesized by the LQR methodology. However, the variables used as states are less. The

integral action in this case is not used. At the same time, the errors fed to the controller are diverse, depending on which part of the sixth phase the drone is in. The options are the errors of the tether angles and the velocity angle, the errors of $\theta(t)$, $\psi(t)$ and $\phi(t)$ or a mixture of them. When and why they are chosen is explained in details in Retraction and transition phase.

4.4.2. Outer layer

The outer layer is responsible of feeding the references to the inner layer controllers. While its own set of references are related to the Phase that the State machine chooses at any point. The options for the references are encompassed in the attitude of the drone, the wind angles and the Target points.

Generation phase

The generation phase is the first one in which the drone starts to behave as an airplane, where the ailerons, rudder and elevator are the main control actions. In addition, the references are computed based on the Target point at which the drone must aim and the speed relative to wind. There are three references to provide, one for $\theta(t)$, one for $\phi(t)$ and another for $\psi(t)$.

The reference for $\theta(t)$ is linked to $u_r(t)$. As explained before, the tether force is leverage to produce a modification in the speeds on the body frame. As such, the projection of this force on the longitudinal axis of the drone is subject to the value of $\theta_{tether}(t)$, which is modified by a changing in $\theta(t)$. As a result, a controller based on the error in $u_r(t)$ is developed, this error is computed with respect to a value of $u(t)$ that permits the control surfaces to have a big enough impact on the drone's dynamic. It is important to mention that the purpose of this controller is not to keep a perfect track of the speed, as those efforts will probably lead to a lost of the cross-wind state. The main objective of the control system is to keep the drone with the tether angles as close to 0 as possible. The consequence is the introduction of a saturation in the output, hence the reference of $\theta_{tether}(t)$ will be limited to a small range around 0.

Regarding $\phi(t)$, another SISO controller is devised. Its purpose is to contain, ideally nullify, the side-slip angle. In order to do this, the tether force projection is exploit once more. In this case, the projection on the $y(t)$ axis is crucial, as $\beta(t)$ value is subordinate to $v(t)$. A simple mathematical model is developed and used as a basis for this controller.

Finally, the $\psi(t)$ reference is computed. This is the one that allows the drone to track

the Target points. As explained before, the error fed to the inner layer comes from the velocity angle and its reference. The latter one is crucial to have a good shape in the figure drawn by the drone's path. For its calculus, it is required to have $\theta_{sphere}(t)$, $\phi_{sphere}(t)$ and the Target points. With that information, it is possible to calculate whether the drone should be pointing at one Target point or the other. The logic behind is rather simple and it takes into consideration where the drone is and which was the previous reference. Once the Target point is chosen, the computation of the reference angle takes place. As explained in [13], the reference is computed as shown in (4.6). However, this is not enough, as a switching between different references exists and the inner layer controller is sensitive to discontinuities in the input signal, a filter is added. This filter is also necessary to smooth the signal when switching in between reference points. The reason is that once the drone is close enough to an Target point, the signal jump abruptly towards the other one and a big discontinuity can be seen. However, the filter must allow the reference to be fast enough to keep a correct track of the objective. Under those conditions, the filter is designed.

$$\gamma_{ref}(t) = \arctan_2((\phi_{obj}(t) - \phi_{sphere}(t)) \cos \theta_{sphere}(t), -(\theta_{obj}(t) - \theta_{sphere}(t))) \quad (4.6)$$

Retraction and transition phase

Once the tether length reaches l_{max} , a new Phase starts. At that point the drone must fly back towards positive values of x_{ef} and the state machine changes to Phase 6 - Retraction. In order to accomplish this, the control action used are still the ailerons, the rudder and the elevator. As explained before, there are several parts forming this Phase and the set of references may change from one part to the other. Similarly, the signals to be controlled may change from a part to a different one. In the following paragraphs there are presented the different parts with their control strategies.

The control layout is a cascade control, having as the inner loop a MIMO controller synthesized based on the linearized equations of the drone and shaped by the LQR method. The variables coming into play are the three Euler angles and their derivatives and it is used across all the parts of this phase. This controller is fed by a signal selector, explained in details in 4.4.3 and the outer layer. The former changes the signals to control according to the part and the latter computes the references for the chosen set of signals.

Part 1 - turning As soon as the Phases becomes the sixth one, the drone must start turning towards an Target point. The choosing of it is related to which one the drone was heading to when in Phase five. The rule is to make the drone change the Target point when

Phase is changed. There is a reason behind this choice. It is the manoeuvre the drone performs when engaging the generation phase again. This manoeuvre is characterized by a sharp rolling and high pitching, the first one making the drone move far away from the generator and the second one making the nose point down. This movement is useful to prepare the control system to successfully and smoothly shift to the tether coordinates again. However, this logic will only work as expected when the attitude of the drone upon arrival to the moment of switching is marked by its longitudinal axis pointing towards the positive values of x_{ef} but also on the opposite direction of the generator on the y_{ef} . As a result, the drone must perform a coordinate turn to point towards the new objective.

The main responsible for the turning manoeuvre is the controller on $\phi(t)$. There are several points to remark in its design.

1. Roll reference computation : its reference is an angle deviation. This error comes from the angular difference ($\Delta ang(t)$) between the drone's speed vector (the angle is presented as $\epsilon_1(t)$ in the figure 4.14) and the vector that joins the current drone position and its Target point (the angle is presented as $\epsilon_2(t)$ in the figure 4.14), both in x_{ef} - y_{ef} plane.
2. Saturation : depending on when the Phase six starts, what leads to how is the attitude and speed of the drone at that precise point, the reference can be too big to be a sensible value. As a result, there is a saturation that limits the reference provided to the controller. However, at the same time the drone is turning it is also loosing altitude. The simultaneous occurrence of the two has as a consequence the mutual interference in their respective dynamics. Thus, when the drone has to loose a lot of altitude, a given saturation produces a different result in comparison to when the drone has to decrease its altitude only a little. The solution to this situation is the implementation of a variable saturation that changes according to the altitude that needs to be lost when computed at the very beginning of the sixth Phase.

With this considerations in mind, the development of the controller is done following the affine parameterization methodology and its output corresponds to a reference to $\phi(t)$.

There is another requirement for a coordinated turn, the controlling of $\psi(t)$. The idea in this kind of turns is to keep the acceleration vector projection in the y axis null, however this must be translated to some reasonable and attainable condition for the development of a controller. The requirement found is related to the $\beta(t)$ angle. The value of this angle changes due to the existence of an acceleration in the y axis, situation that must be prevented. Thus, $\psi(t)$ is acted upon so as to keep $\beta(t)$ angle constant, but this is not

enough. The existence of a non-zero $\beta(t)$ is usually accompanied by a later displacement of the drone, situation to be avoided as well. As a result, this controller's objective is to keep $\beta(t)$ as close to zero as possible.

Finally, the controller in charge of the reference for $\theta(t)$ aims at arriving at the switching point with a correct altitude. Some considerations should be made as the basis of its development.

1. Pitch reference computation : big discontinuities in the reference must be avoided thus, the idea is to give as altitude reference a linearly decreasing value, which depends on the distance between the drone and the Target point in the x_{ef} - y_{ef} plane.
2. Saturation : as the difference may be big at the beginning, there is a limit to how much the value of $\theta(t)$ can oscillate around zero.

The controller's synthesis is preceded by a mathematical description of the relation between $\theta(t)$ and the altitude, shown in equation . With this, an affine parameterization approach is used for the synthesis of the controller.

Part 2 - transition start Once the drone is close enough to the Target point, the references change but the signals to control are still the Euler angles. The new set of references aims to put the drone in a favorable condition to switch again to the tether angles. In order to do that, the nose must point down and the intrados must face the generator. The point in which this part starts must be tuned properly and carefully. If the drone flies past the Target point too much, during the turning, or after it, when the drone is engaging the tether again, there are high chances that the sudden force of it will make the drone unstable and lead to its fall. On the other hand, if it does not fly past the objective, or it does but it is too little, there are high possibilities that the tether will be engaged too soon, preventing the drone to reach the desire attitude due to the interference of the tether force.

This turn has to be done while keeping $\beta(t)$ as close to zero as possible. As done before, $\psi(t)$ is used for controlling $\beta(t)$, while $\theta(t)$ is used for making the drone point downwards and $\phi(t)$ has to change to take the intrados to the desire condition. It would be possible to simply produce a change in the references and let the controllers handle the situation, however that results in abrupt changes and saturation of the controllers. Moreover, it is common for the closed loop system to have an exponential behaviour under those conditions which means more aggressive control action application at the beginning. This situation is not desirable, hence, the main development for this part is to propose a set

of references which derives in a less demanding manoeuvre for the controllers.

The solution is to provide linear references for the three angles with a final saturation for $\phi(t)$ and $\theta(t)$ (named $\theta_{stg6-line}(t)$, $\phi_{stg6-line}(t)$ and $\psi_{stg6-line}(t)$). In this situation the control's layout changes and the only controller remaining is the one present in the inner layer. Once the drone has followed the signals up to the constant part of the references, it will have the desired attitude. If, apart from achieving the aimed attitude, the drone has lost some meters of altitude, the new part starts.

Part 3 - tether angles The drone is pointing downward, its intrados (lower side of the wing, characterized by a high pressure in the airflow) is facing the generator and the tether is taut. During the previous manoeuvre, due to the fact that the rolling and yawing moments will make the drone fly away from the generator, the tether becomes taut. Another important result from the previous part is the gain in speed of the drone. Consequently, the control surfaces' capacities are enough to fully control the drone. As the idea is to keep gaining speed and put the drone in a condition to restart the generation phase, there is the necessity to use the tether angles as signals once again. However, the references are different from before.

First, the control scheme used during this phase is a cascade control, as mentioned before. Also, the inner layer is a controller based on the LQR method and the linearized drone's dynamic equation. However, the outer layer is a mix of different approaches. The errors fed to the controller are those described in (4.7). The objective is to put the drone in a position where $\theta_{tether}(t)$ is zero, which is advantageous for coming back to the generation phase. At the same time, $\phi_{tether}(t)$ is in charge of keeping $\beta(t)$ contained and it will allow a seamless transition, as it is the same duty it has while in the generation phase. On the side of $\psi(t)$, the reference is still the linearly increasing, or decreasing depending on the Target point. This results in the drone's longitudinal axis moving towards the opposite Target point, another decision taken to make the transition to the generation phase as smooth as possible.

$$\theta_{error}(t) = -\theta_{tether}(t) \quad (4.7a)$$

$$\phi_{error}(t) = \phi_{\beta ref}(t) - \phi_{tether}(t) \quad (4.7b)$$

$$\psi_{error}(t) = \psi_{stg6-line}(t) - \psi(t) \quad (4.7c)$$

This part is the last one of the sixth Phase, as such, when it ends, the state machine is switched to the generation phase again, represented as Phase four. This transition occurs when the absolute value of $\theta_{tether}(t)$ is smaller than a certain value.

4.4.3. Signal selector

A crucial part of the management of the airplane mode control is the signal selector. As explained above, there are several changes in terms of the variables to control during the different parts. A pseudo-code is presented in Algorithm 4.2 to portray clearly how this selection works and which are the variables that comes into play.

Algorithm 4.2 Signal selector logic

```

OUT = SignalSelector(Phase,PhasePart, EulerAngle, TetherAngles,  $\gamma$ )
1: if Phase  $\neq$  6 then
2:   OUT = [TetherAngles;  $\gamma$ ]
3: else
4:   if PhasePart == 3 or PhasePart == 4 then
5:     OUT = [TetherAngles;  $\psi(t)$ ]
6:   else
7:     OUT = EulerAngle
8:   end if
9: end if

```

The idea behind this controller is to provide the values of $[P_{ref}(t), Q_{ref}(t), R_{ref}(t), W_{ref}(t)]$, from which the required moments are computed by the inner-most controller. As in the hovering version, there are also two dynamic to control. The first one is related to the altitude, while the second one is related to the attitude of the drone.

For the altitude part, the reference are the three euler angles defining the attitude of the drone. These are converted into references for their derivatives. As the inner-most controller requires $[P_{ref}(t), Q_{ref}(t), R_{ref}(t)]$, a non-linear transformation is used and it is based on matrix.

On the other hand, the altitude controller exploits two different signals to accomplish a satisfactory tracking of the altitude. These inputs are the pitch angle and the longitudinal speed. In order to successfully achieve this objective, first it is necessary to compute steady flight condition.

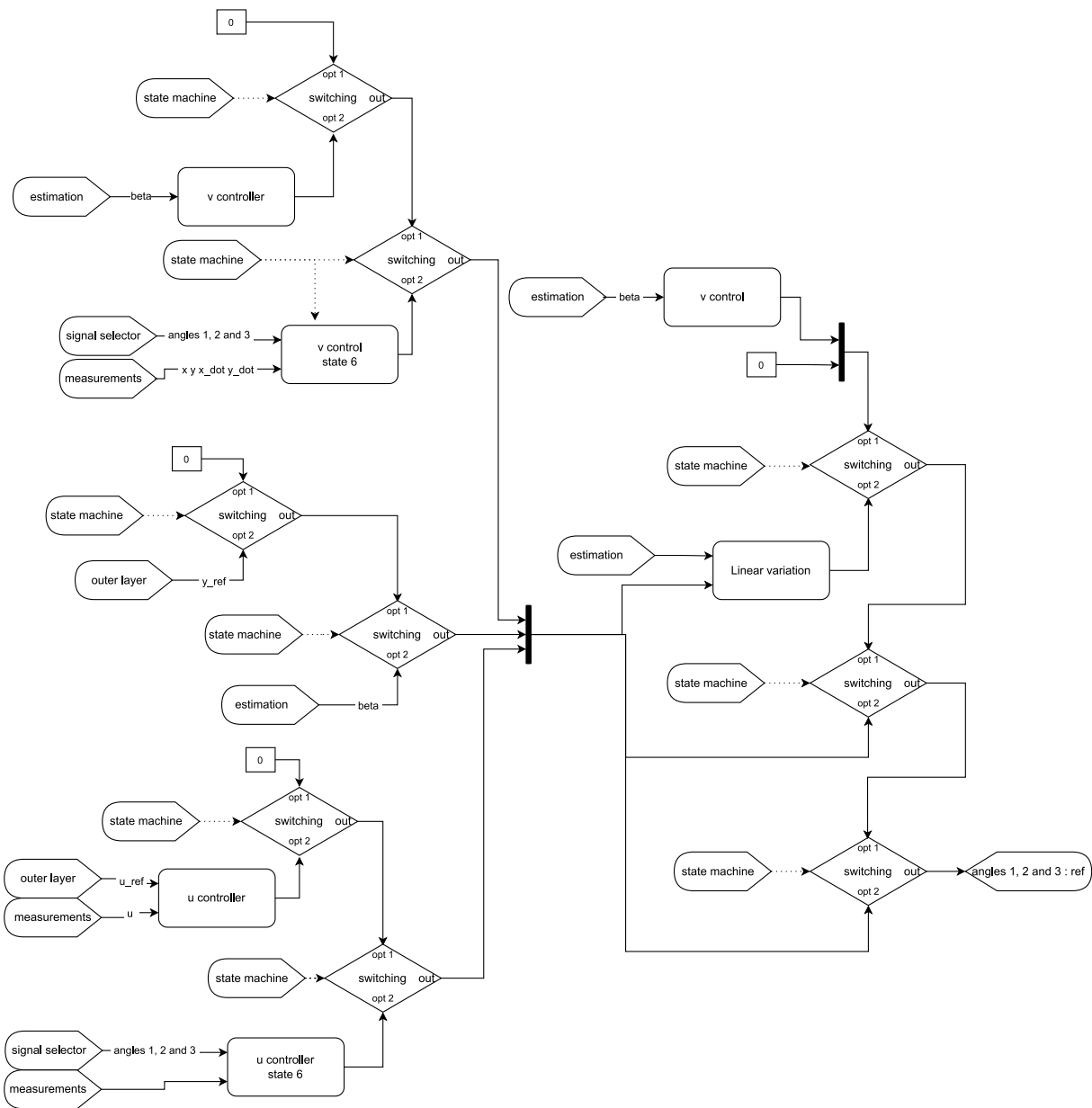


Figure 4.13: Schematic block diagram of the Outer layer for airplane mode

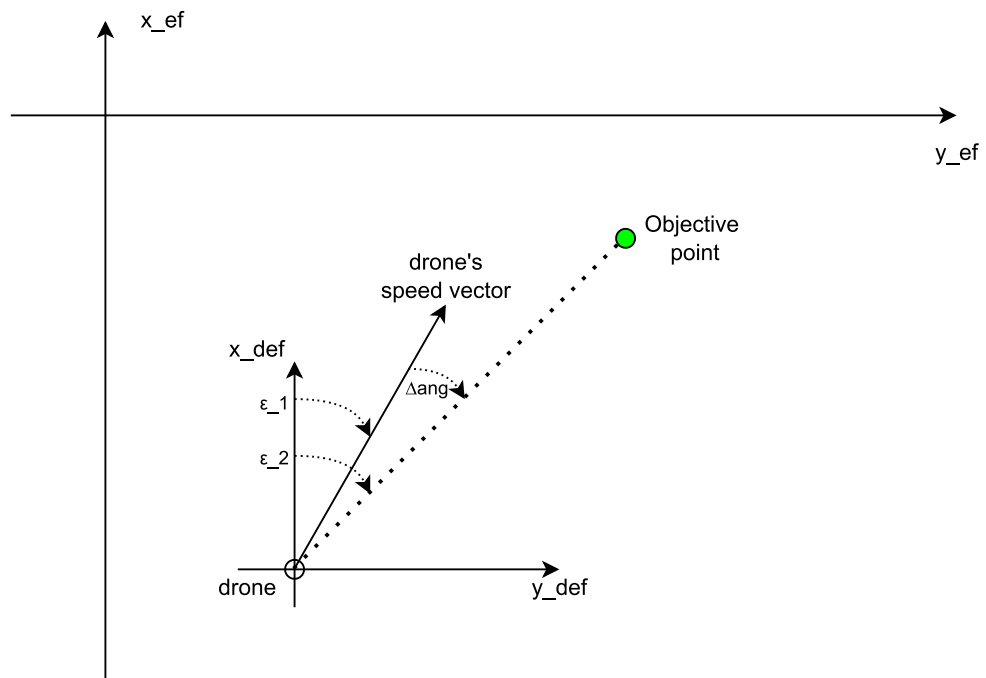


Figure 4.14: Angular error during Gliding

5 | Results

In the present chapter the actual synthesis of the controllers is explained. Following the same logic as in the previous chapter, this one is divided in hovering control and airplane mode control. After describing the controllers' design, the set of references that allows a successful mission are presented in all details. Then, an outline of the whole strategy for the transition is described. Finally, the simulation results for all phases are shown.

5.1. Hovering controllers synthesis

As explained in the previous chapter, there are several controllers needed for achieving a successful mission. Their numerical development is presented in the following subsections.

5.1.1. Hovering's cascade control decoupling

The proposed control scheme during hovering is a cascade layout. It amount to three layers, at most, and all of them must be ideally decoupled. To achieve this, the closed loop poles of each layer must be separated by a large-enough margin. It is normal to use as a metric the settling time of each of the systems and compare them, and this is the approach taken in this thesis. First of all, it is vital to have some rough limits for the value of the poles. The first one is a speed limit, all control system are dependent on a measurement system, which cannot accurately sample at any desire rate. The hovering cascade control requires a gyroscope to acquire the samples of the Euler angles and their derivatives. In the market, it is possible to find products with a sampling frequency of 2000 Hz [1]. In practice, considering the Nyquist frequency, there are sensible data available at 1000 Hz. On the other side, the outer layer, as explained before, is in charge of the tracking of some points in the x_{ef} - y_{ef} plane. There is not necessity for the drone to fly to those points at high speed, nor to saturate the motors, thus a settling time of a several seconds is reasonable. With those rough limits in mind, the first proposed poles are the ones of the outer limit with a settling time of 20 seconds, which translates to a pole in -0.2. Considering a separation with a multiplication of 5 in between controllers' poles, the following table sum up the controllers and their proposed poles.

Title of Table (optional)

Controller	poles
Inner layer controller	-50
Middle layer controller	-5
Velocity controller	$-1 \pm i$
Position controller	-0.2

Table 5.1: Hovering controllers' proposed poles for their synthesis

5.1.2. Altitude controller - Hovering

Based on the generic matrix representation presented in section 4.3.1, the parameters completing the matrix are presented below, which are taken from [10]. This system is used for the synthesis of the controller.

$$\begin{bmatrix} \dot{W}(t) \\ \dot{h}(t) \\ \dot{e}_h(t) \end{bmatrix} = \begin{bmatrix} -0.3289 & 2.322 \times 10^6 & 0 \\ -1 & 0 & 0 \\ 0 & -1 & 0 \end{bmatrix} \begin{bmatrix} W(t) \\ h(t) \\ e_h(t) \end{bmatrix} \quad (5.1)$$

To synthesize the controller, the LQR [8] approach is used to obtain the matrix of gains K_{aHe} . As the method requires, the matrix Q_{aHe} and R_{aHe} .

$$Q_{aHe} = \begin{bmatrix} 0.1 & 0 & 0 \\ 0 & 25 & 0 \\ 0 & 0 & 5 \end{bmatrix} \quad (5.2a)$$

$$R_{aHe} = 1 \quad (5.2b)$$

$$K_{aHe} = \begin{bmatrix} 12.0191 & -14.8848 & 4.4721 \end{bmatrix} \quad (5.2c)$$

The last one is used to compute the force that the motors as a whole should provide, represented by the next equation.

$$F_{motor}(t) = K_{aHe} \begin{bmatrix} W(t) \\ h(t) \\ e_h(t) \end{bmatrix} \quad (5.3)$$

5.1.3. Inner layer controller - Hovering

As can be seen in the equations (3.9d) to (3.9f), the system is non-linearly coupled. However, when the model is linearize around a stationary condition with P, Q and R null, the non-linear coupling terms disappear. Thus, the only coupling terms that remain are the linear terms related to the control actions as can be seen in the representation of the linear system in its matrix form below.

$$\begin{bmatrix} \dot{P}(t) \\ \dot{Q}(t) \\ \dot{R}(t) \end{bmatrix} = \begin{bmatrix} 0 & 0 & 0 \\ 0 & 0 & 0 \\ 0 & 0 & 0 \end{bmatrix} \begin{bmatrix} P(t) \\ Q(t) \\ R(t) \end{bmatrix} + \begin{bmatrix} c_3 & 0 & c_4 \\ 0 & c_7 & 0 \\ c_4 & 0 & c_9 \end{bmatrix} \begin{bmatrix} l_R(t) \\ m_R(t) \\ n_R(t) \end{bmatrix} \quad (5.4)$$

Based on this relationships, and adding to them the linear dynamic of the Euler angles, the full matrix representation of the drone's behaviour is written and presented in (5.5). The constants defining the dynamic have also been replaced by their numerical values.

$$\begin{bmatrix} \dot{P}(t) \\ \dot{Q}(t) \\ \dot{R}(t) \end{bmatrix} = \begin{bmatrix} 0 & 0 & 0 \\ 0 & 0 & 0 \\ 0 & 0 & 0 \end{bmatrix} \begin{bmatrix} P(t) \\ Q(t) \\ R(t) \end{bmatrix} + \begin{bmatrix} 0.5748 & 0 & -0.0063 \\ 0 & 3.5714 & 0 \\ -0.0063 & 0 & 0.5465 \end{bmatrix} \begin{bmatrix} l_R(t) \\ m_R(t) \\ n_R(t) \end{bmatrix} \quad (5.5)$$

The aerodynamic moments are not considered as control action, rather they are considered disturbances produced by the relative speed due to both the movement of the drone and the wind.

As the tracking of references is not necessary at this level, the addition of an integral action is discarded. Hence, the control is synthesized using an LQR approach and, particularly, the *lqr matlab's* function. The choice of Q_{PQR} and R_{PQR} are driven by the resulting system's close loop poles that have to be close to the one shown in table 5.1. The equations below depict the choices made for Q_{PQR} and R_{PQR} , as well as the resulting controller K_{PQR} .

$$Q_{PQR} = 1 \times 10^3 \begin{bmatrix} 6.56 & 0 & 0 \\ 0 & 0.26 & 0 \\ 0 & 0 & 6.56 \end{bmatrix} \quad (5.6a)$$

$$R_{PQR} = \begin{bmatrix} 1.11 & 0 & 0 \\ 0 & 1.11 & 0 \\ 0 & 0 & 1.11 \end{bmatrix} \quad (5.6b)$$

$$K_{PQR} = \begin{bmatrix} 76.87 & 0 & 0 \\ 0 & 15.37 & 0 \\ 0 & 0 & 76.87 \end{bmatrix} \quad (5.6c)$$

As a result of the application of K_{PQR} to the linear system, the set of close loop poles presented below are obtained. They are close enough to the values proposed in section 5.1.1.

$$pole_1 = -44.29 \quad (5.7a)$$

$$pole_2 = -41.91 \quad (5.7b)$$

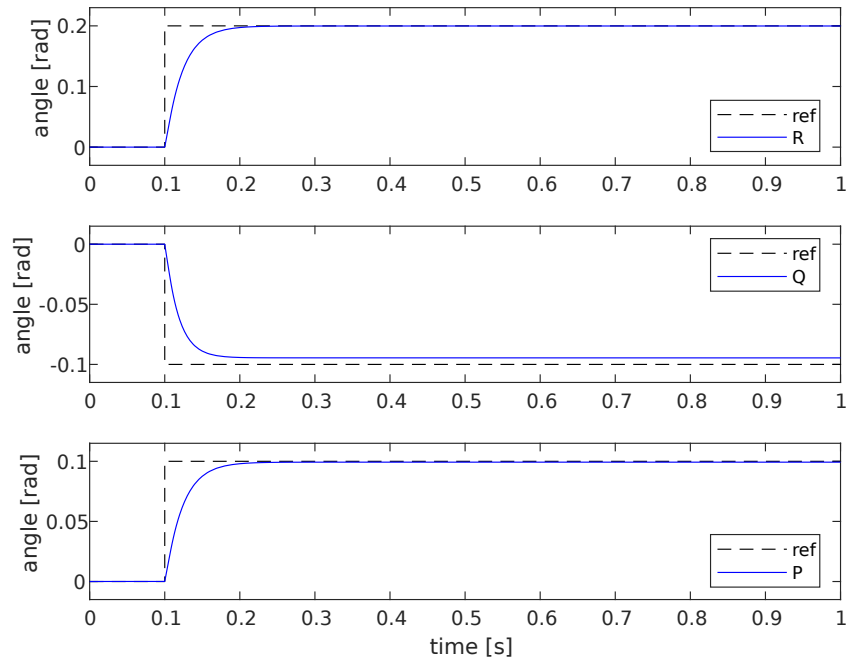
$$pole_3 = -54.91 \quad (5.7c)$$

This controller is tested on the non-linear model. To conduct it, the drone is fixed to a point, only allowing rotations. In such a condition, a step is fed as reference for the three angular velocities at the same time. As it is possible to see in figure 5.1, the controller is capable of tracking the error very fast. The three tracking presents a settling time close to 0.1 seconds. The poles computed based on the closed loop of the linear ideal system, equation (5.7), show a settling time between 0.1 and 0.072 seconds. This values are acceptable because the settling times are in the same order of magnitude and the errors can be related to some non-modelled dynamics, which in the big picture does not have an important effect. On the side of the control actions required to accomplish this movements, there is a very notorious peak at the beginning, portrayed in figure 5.1b, typical result to a step in the reference, which does not saturate the control action, maximum value of $1250 \frac{rad}{s}$.

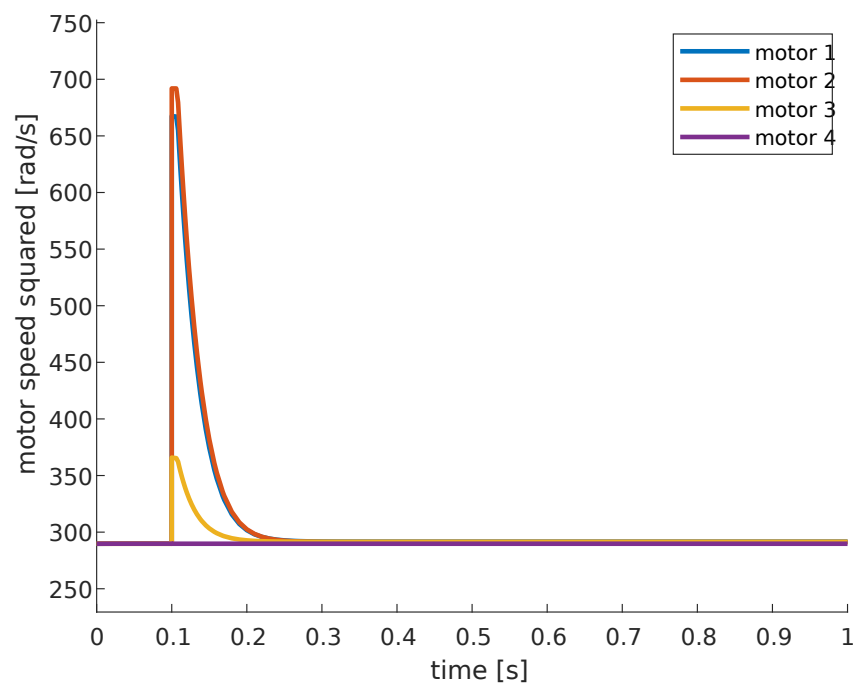
Another test is run on the controller. This time a ramp is fed to the controller, in the figure 5.2 presents the result obtained. It is possible to see the correct tracking of the signal, with some delay as expected. In addition, it is possible to see how the control actions are less important in this situation.

5.1.4. Middle layer controller - Hovering

As a result from the equations presented in section 4.3.2, it is simple to understand that the dynamic of the three variables is independent to the others. Thus, the idea is to propose a closed transfer function with a desired behaviour for each of them separately.

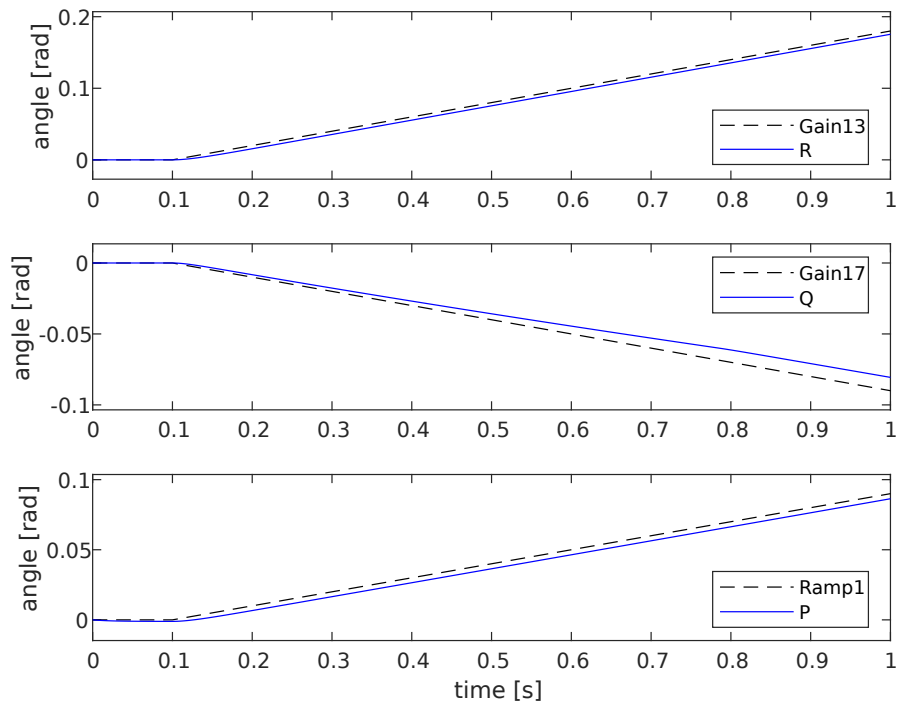


(a) Reference tracking

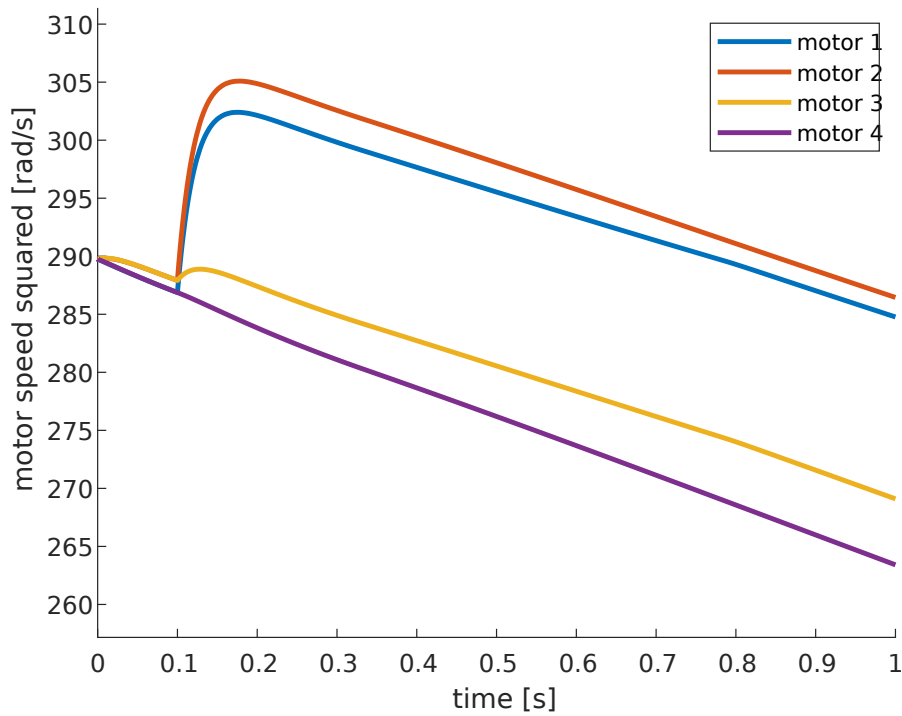


(b) Control action

Figure 5.1: Reference tracking with a step reference in P, Q and R



(a) Reference tracking



(b) Control action

Figure 5.2: Reference tracking with a step reference in P,Q and R

The chosen method to obtain the controllers' function is affine parameterization[8]. First, it is necessary to decide how should the close loop dynamic should be. To propose a complementary sensitivity function(T), there is the need to know the relative degree of the plant, which is one in this case as they are simple derivatives. The chosen T is $\frac{a+c*s}{(s+b)^2}$.

To find the values of the constants it is crucial to consider that this layer has another one inside, the requirements are devised based on the objective of decoupling them as explained in section 5.1.1. Hence, the time constant of the system has to be close to the one presented in Hovering controllers' proposed poles for their synthesis. As a result, b must be 5. On the other hand, a is chosen to be equal to the independent coefficient of the denominator. In the case of c , as an integral action is not desired, any value expect from the coefficient accompanying s in the denominator is acceptable, and for simplicity a value of 1 is chosen. By following the rest of the Affine Parameterization's method it is possible to find the following transfer functions, being $K_{euler-hovering}$ the controller.

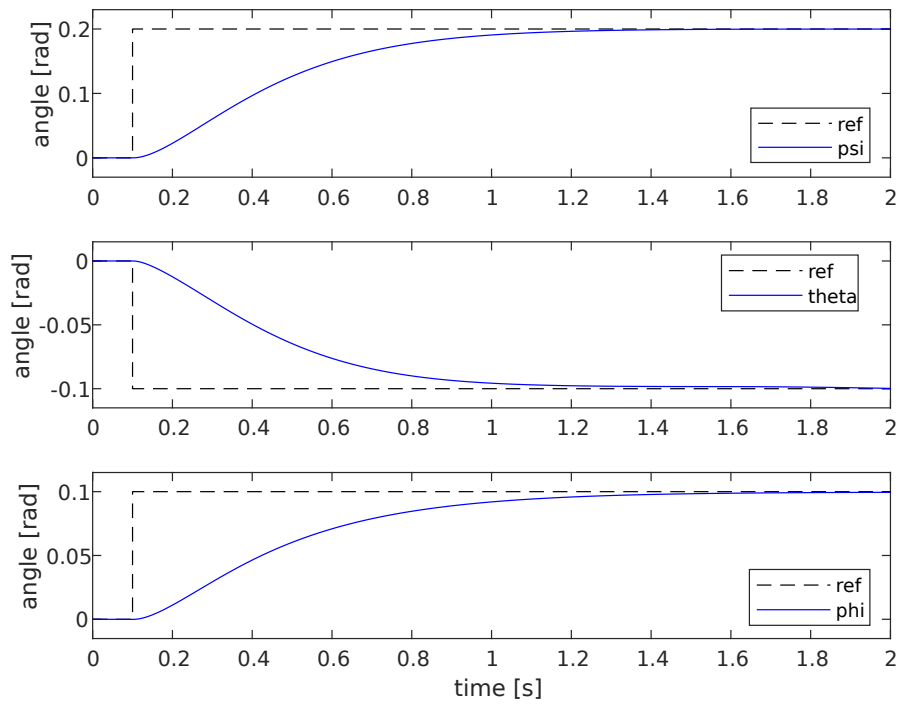
$$T_{euler-hovering} = \frac{s + 25}{s^2 + 10s + 25} \quad (5.8a)$$

$$Q_{euler-hovering} = \frac{s^2 + 25s}{s^2 + 10s + 25} \quad (5.8b)$$

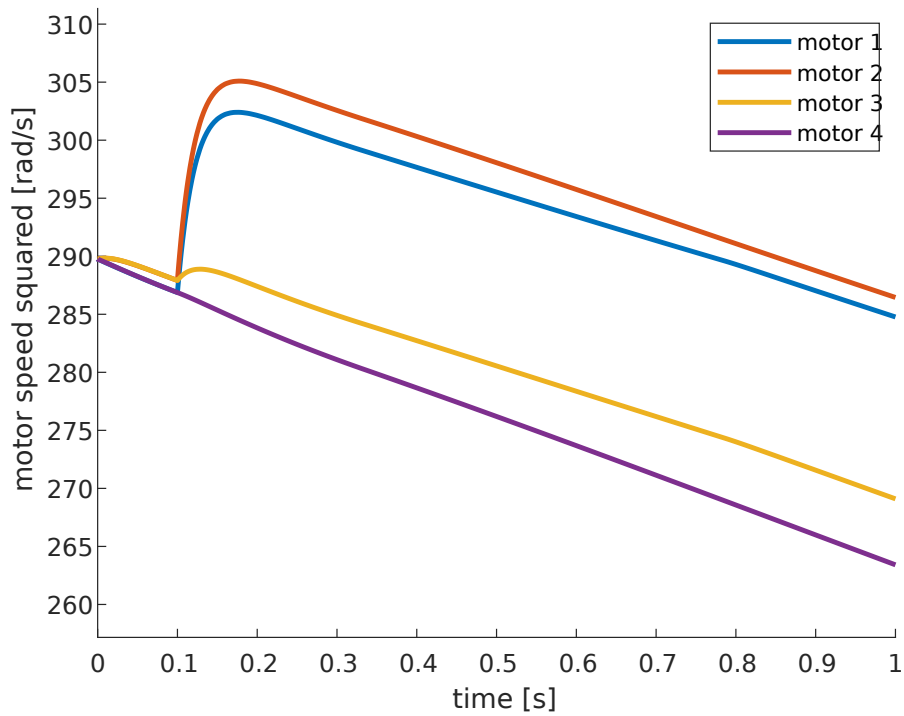
$$K_{euler-hovering} = \frac{s + 25}{s + 9} \quad (5.8c)$$

With the controller developed, some test are done on the closed loop system using the non linear model. As before, the drone is fixed to a point in the space while it only possible for it to rotate. The close loop includes the controller of P,Q and R. As a result, it is also a test for a part of the cascade control. The results to a step input are presented in Figure 5.3, the first thing to notice is the correct reference tracking. The second remarkable result comes from the settling time, it is expected for the settling to happen in one second according to the synthesis, which is accomplished in the test. This result is important as it shows that the dynamic of the two systems is decoupled. It is also important to highlight that the control actions are far from the saturation level.

As previously done, the controller is tested with another signal. This time a ramp is used and the results are presented in 5.4. It is possible to see an acceptable tracking of the references with a smaller peak in the control action.

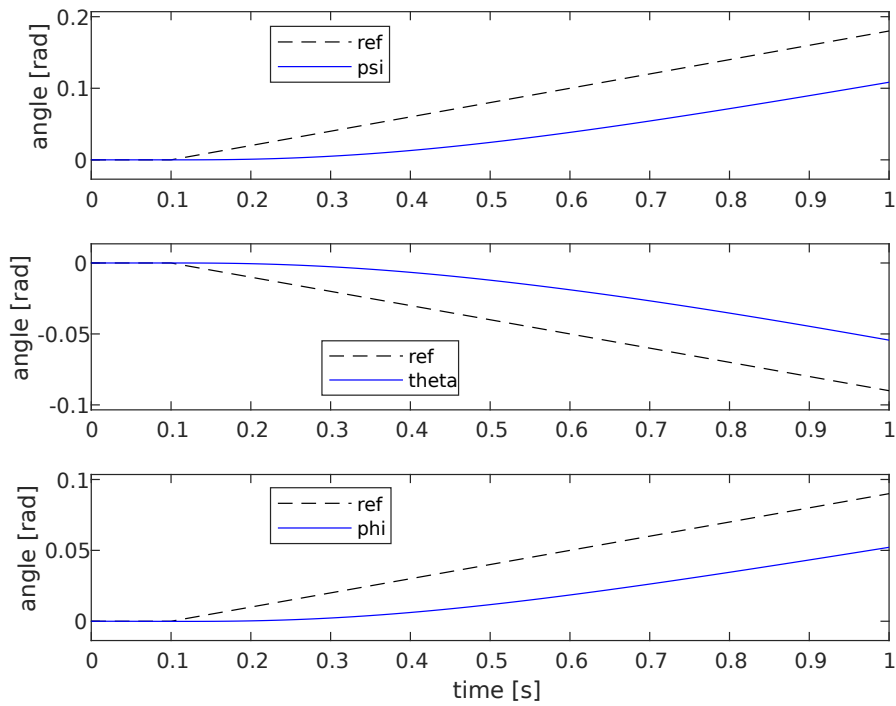


(a) Reference tracking

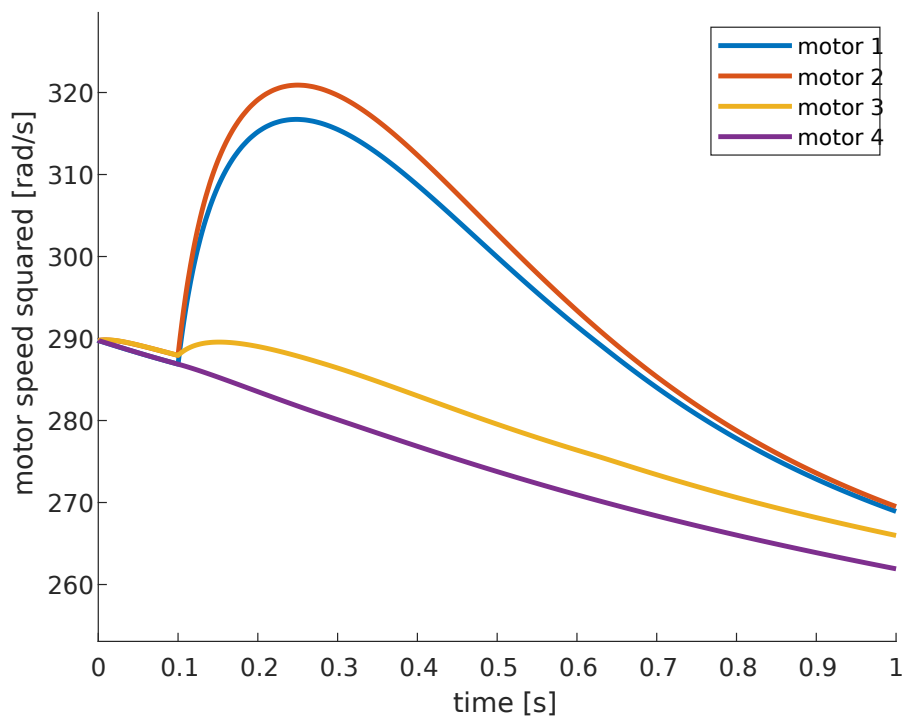


(b) Control action

Figure 5.3: Reference tracking with a step reference in the Euler angles



(a) Reference tracking



(b) Control action

Figure 5.4: Reference tracking with a ramp reference in the Euler angles

5.1.5. Velocity controller - Hovering

Having the transfer functions presented in section 5.1, which are independent from each other, two controls are synthesized by the affine parameterization methodology. It is important to follow the guidelines presented in Hovering controllers' proposed poles for their synthesis, which means that the decoupling of the different layers is accomplished. Below it is possible to see the desired closed loop function, equation (5.9a) whose poles are 10 times slower than those of equation (5.10a). Thus, it is possible to assume that the closed loop dynamics are decoupled.

$$T_{velocity-hovering} = \frac{s + 2}{s^2 + 2s + 2} \quad (5.9a)$$

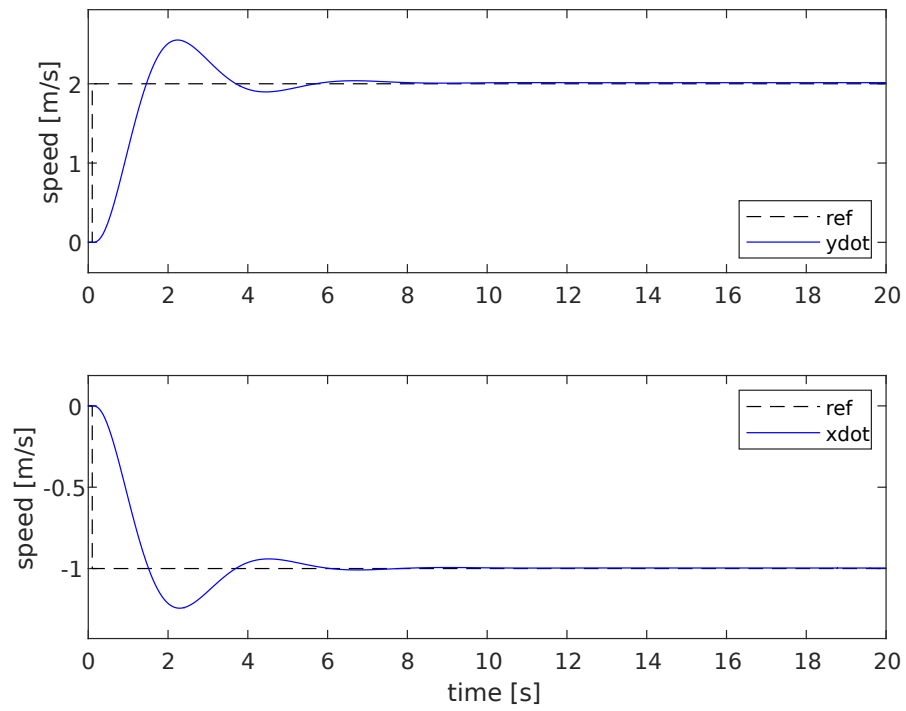
$$Q_{velocity-hovering} = \frac{0.10s^2 + 0.20s}{T + 0.1} \quad (5.9b)$$

$$K_{velocity-hovering} = \frac{0.10(s + 2)}{(s + 1)} \quad (5.9c)$$

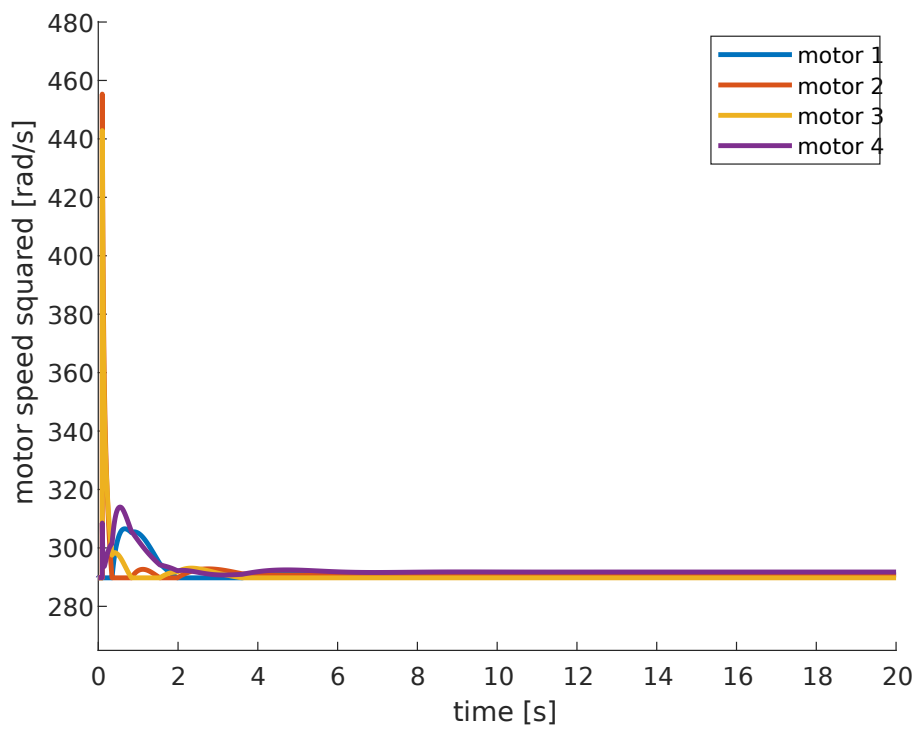
The controller presented in equation (5.9c) is used for both angular controllers. As a result, the references for the $\theta(t)$ and $\psi(t)$ angles are calculated and fed to the Middle layer controller - Hovering.

To test these controllers, the same pattern of tests is used. However, this time the drone is able to translate and rotate, thus it is a test on the six degree of freedom model. First a step input is fed, which results are presented in 5.5. The previous two controllers are present in this test, hence it is also an assessment on how much coupled are the dynamic of the different layers of the cascade control. The synthesis is done with a settling time of 5 seconds as objective. From the figures, it is simple to see that the achieved settling time is a little bigger than the one desired. There are several explanations for it, first of all is the possibility that the dynamics are slightly coupled. Moreover, the simulation is run in the fully non linear model, which is another source of errors. Nevertheless, the achieved settling time is close enough to the desired one. On the side of the control actions, there is a clear peak in motors' speed. However, it remains far from the saturation level, so it brings no problem.

The second test includes a ramp reference. The resulting dynamic of the close loop drone is satisfactory. It is possible to see from figure 5.6 that the tracking of the reference is acceptable, with the expected delay. On the side of the control actions, the motors' speeds depicted are far away from the saturation level, which is a good sign.

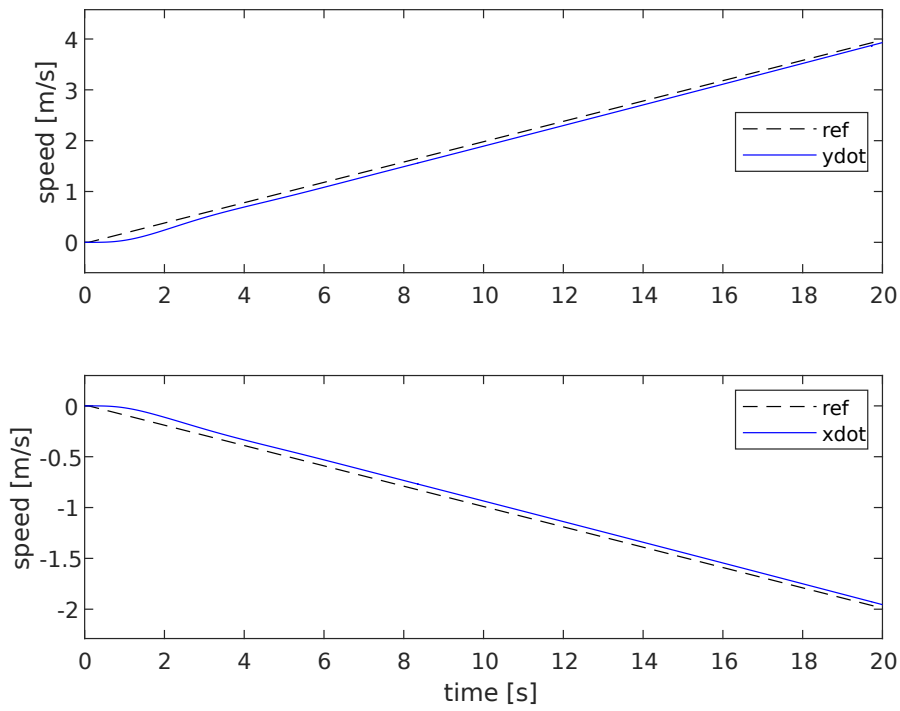


(a) Reference tracking

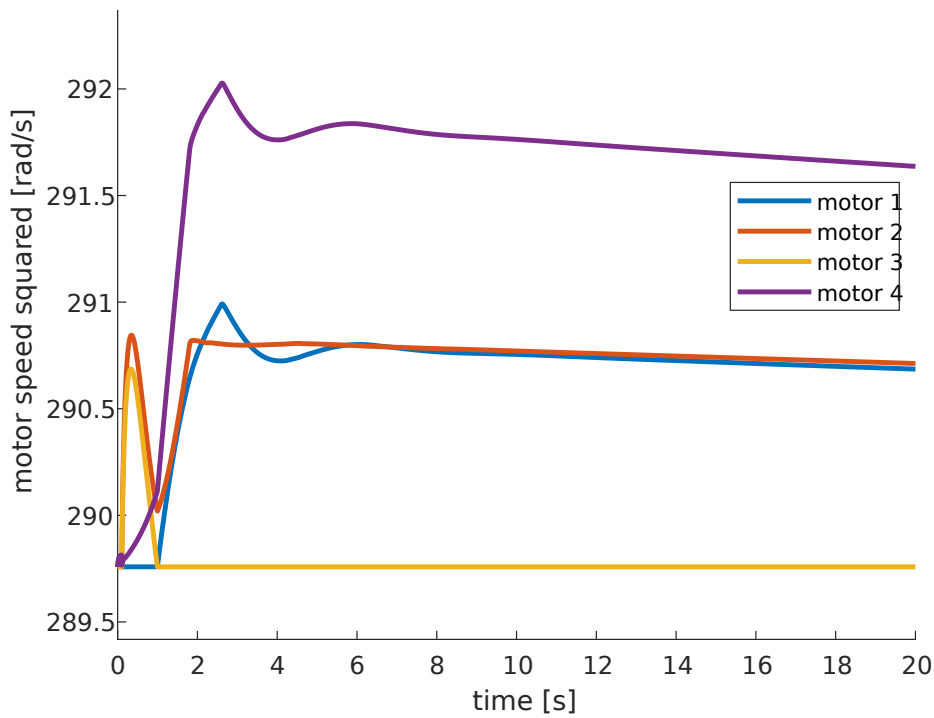


(b) Control action

Figure 5.5: Reference tracking with a step reference in \dot{x}_{ef} and \dot{y}_{ef}



(a) Reference tracking



(b) Control action

Figure 5.6: Reference tracking with a ramp reference in \dot{x}_{ef} and \dot{y}_{ef}

5.1.6. Position controller - Hovering

The method followed to synthesize the controller is Affine Parameterization. This is the outermost layer of the cascade control for Loose tether control. As such, the poles used for shaping the complementary sensitivity function are chosen based on chain of thought presented in section 5.1.1. There is another consideration to be made regarding this controller, this is the outermost layer and its objective is to track some points in x_{ef} - y_{ef} plane. Consequently, it is regarded as important to add an integral action to the control. To force the presence of an integrator in the controller, the coefficient in the numerator have to be selected so as to match the constant of the denominator for the same power of s . The logic is as follows, if the plant has no poles in the origin, only matching the independent coefficient is enough. If the plant has one pole in the origin, this exact case, the coefficient of s^1 and s^0 must be the same. All the transfer functions can be seen below, and it is important to point out the desired presence of the integral action in the controller.

$$T_{position-hovering} = \frac{0.4s + 0.04}{s^2 + 0.4s + 0.04} \quad (5.10a)$$

$$Q_{position-hovering} = \frac{0.4s^2 + 0.04s}{s^2 + 0.4s + 0.04} \quad (5.10b)$$

$$K_{position-hovering} = \frac{0.4(s + 0.1)}{s} \quad (5.10c)$$

It is important to mention that a modification to $K_{position-hovering}$ is made. As a nested control, the saturation restricting the motors' speeds has a direct effect on the capabilities of this controller. As such, there is always the possibility for the saturation to occur and, thus, a winding-up of the integrator. The solution is an anti-windup scheme, as explained in [8], where controller transfer function is divided into two, with the following values.

$$K_{position-hovering_\infty} = 0.40 \quad (5.11a)$$

$$K_{position-hovering} = \frac{-0.25}{(s + 0.1)} \quad (5.11b)$$

This is the last layer of the hovering cascade control. As it is a translation controller, the six degree of freedom model is used. First, a step is fed and the results are shown in figure 5.7. The expected settling time is 20 seconds, however the results portray a different reality. This characteristic time amount to 25 seconds. This difference is probably related to difference between the linear model used for the synthesis and the non-linear simulator. More specifically, the sources of discrepancies may be the controllers not being

fully decoupled or the linear equations used as the basis of the Affine Parameterization methodology lacking the representation of some important dynamics. Nevertheless, the error is not big enough to be regarded as a problem. On the side of the control actions, it is noticeable how close to the saturation level the motors' speeds are. However, as the saturation level is not reached, there is no problem.

The second test done has as input a ramp signal. The results presented in figure 5.8 show a correct tracking of the reference, with the clear effect of the integrator being displayed. When comparing the control effort, it is possible to see how the motors' speeds required in this test are about a half of the ones used to keep track of the step.

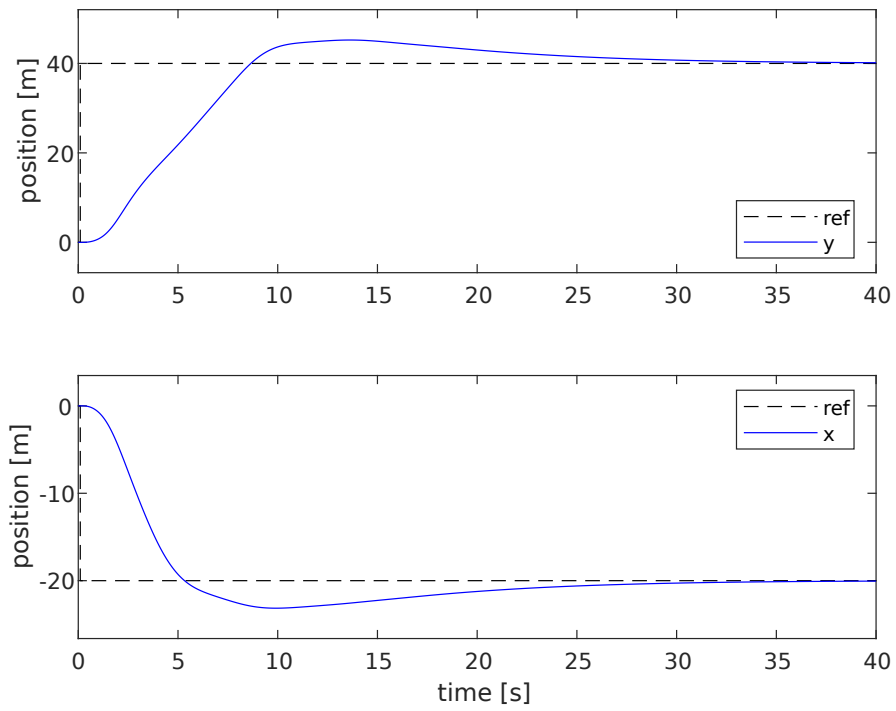
5.2. Airplane controllers synthesis

5.2.1. Generation Inner layer - Airplane

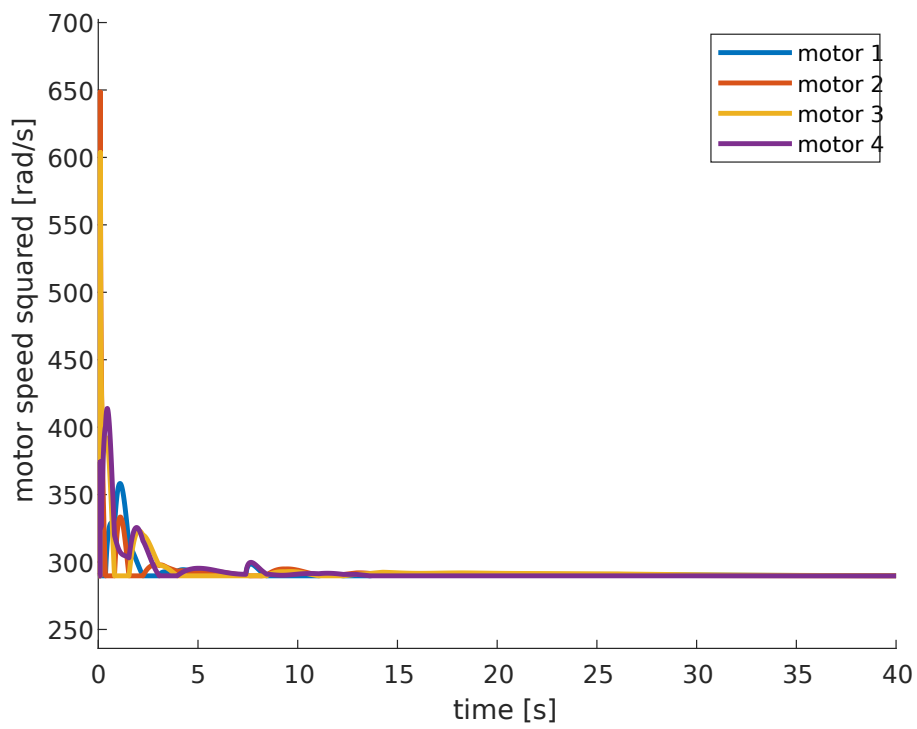
The controller used in this phase is based on an LQR methodology. First, it important to present the linearized representation of the drone's dynamic.

$$\begin{bmatrix} \dot{\phi}(t) \\ \dot{\theta}(t) \\ \dot{\psi}(t) \\ \dot{P}(t) \\ \dot{Q}(t) \\ \dot{R}(t) \\ \psi_{error}(t) \end{bmatrix} = \begin{bmatrix} 0 & 0 & 0 & 1 & 0 & 0 & 0 \\ 0 & 0 & 0 & 0 & 1 & 0 & 0 \\ 0 & 0 & 0 & 0 & 0 & 1 & 0 \\ 0 & 0 & 0 & 0 & 0 & 0 & 0 \\ 0 & 0 & 0 & 0 & 0 & 0 & 0 \\ 0 & 0 & 0 & 0 & 0 & 0 & 0 \\ 0 & 0 & -1 & 0 & 0 & 0 & 0 \end{bmatrix} \begin{bmatrix} \phi(t) \\ \theta(t) \\ \psi(t) \\ P(t) \\ Q(t) \\ R(t) \\ \int \psi_{error}(t) \end{bmatrix} + \begin{bmatrix} 0 & 0 & 0 \\ 0 & 0 & 0 \\ 0 & 0 & 0 \\ 0.57 & 0 & -0.01 \\ 0 & 3.57 & 0 \\ -0.01 & 0 & 0.55 \\ 0 & 0 & 0 \end{bmatrix} \begin{bmatrix} \delta_a(t) \\ \delta_e(t) \\ \delta_r(t) \end{bmatrix} + \begin{bmatrix} 0 \\ 0 \\ 0 \\ 0 \\ 0 \\ 0 \\ 1 \end{bmatrix} \psi_{ref}(t) \quad (5.12)$$

Matrices Q and R are the ones defining how the closed loop of the system is going to behave. Following the same chain of thought explained in 5.1.1, a maximum speed for the controller depends on the measurement system. As a basis for the control development, the next equations present the matrix Q_{PQR} and R_{PQR} used, along with the resulting K_{PQR} .

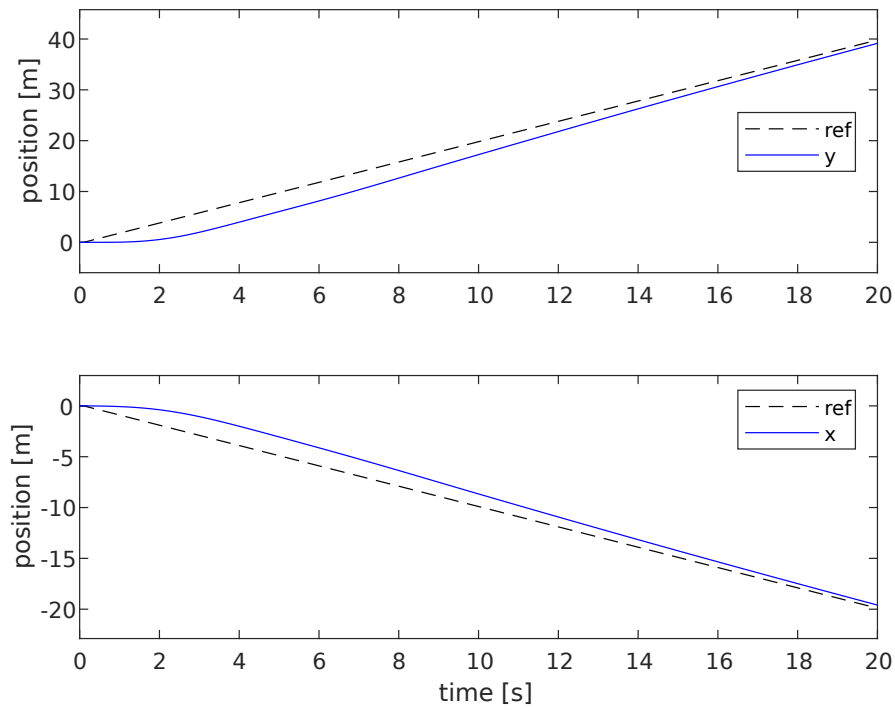


(a) Reference tracking

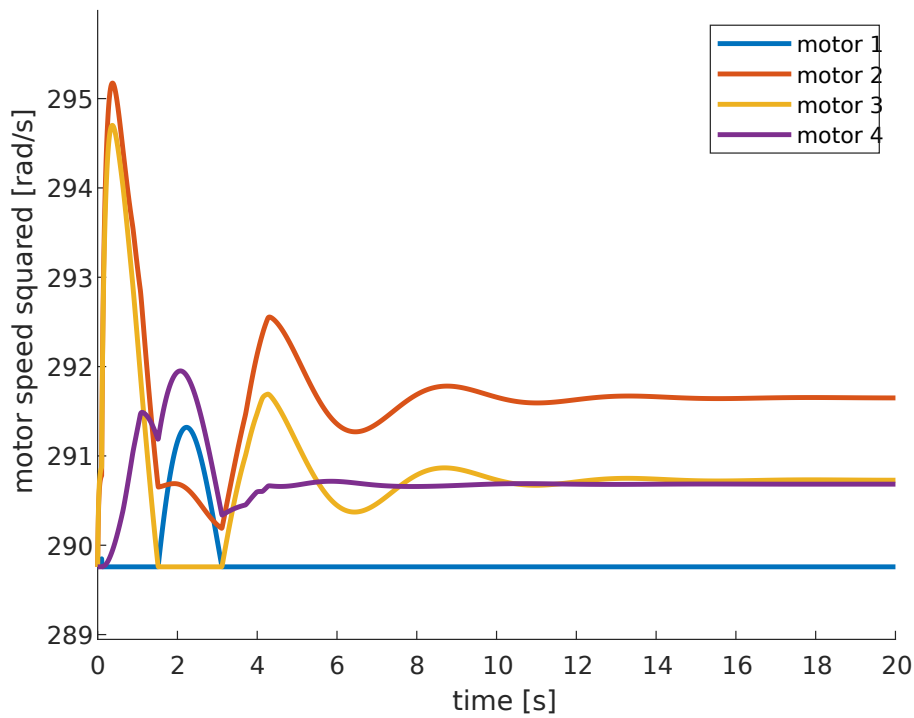


(b) Control action

Figure 5.7: Reference tracking with a step reference in x_{ef} and y_{ef}



(a) Reference tracking



(b) Control action

Figure 5.8: Reference tracking with a ramp reference in x_{ef} and y_{ef}

$$Q_{PQR} = 1.0e + 05 \begin{bmatrix} 18.24 & 0 & 0 & 0 & 0 & 0 & 0 \\ 0 & 164.14 & 0 & 0 & 0 & 0 & 0 \\ 0 & 0 & 0.07 & 0 & 0 & 0 & 0 \\ 0 & 0 & 0 & 0.05 & 0 & 0 & 0 \\ 0 & 0 & 0 & 0 & 0.01 & 0 & 0 \\ 0 & 0 & 0 & 0 & 0 & 0.20 & 0 \\ 0 & 0 & 0 & 0 & 0 & 0 & 0.05 \end{bmatrix} \quad (5.13a)$$

$$R_{PQR} = \begin{bmatrix} 1.11 & 0 & 0 \\ 0 & 1.11 & 0 \\ 0 & 0 & 1.11 \end{bmatrix} \quad (5.13b)$$

$$K_{PQR} = \begin{bmatrix} 128.12 & 0 & -0.02 & 9.46 & 0 & -0.01 & 0.01 \\ 0 & 384.35 & 0 & 0 & 5.10 & 0 & 0 \\ 0.15 & 0 & 15.55 & 0.03 & 0 & 13.63 & -6.71 \end{bmatrix} \quad (5.13c)$$

$$(5.13d)$$

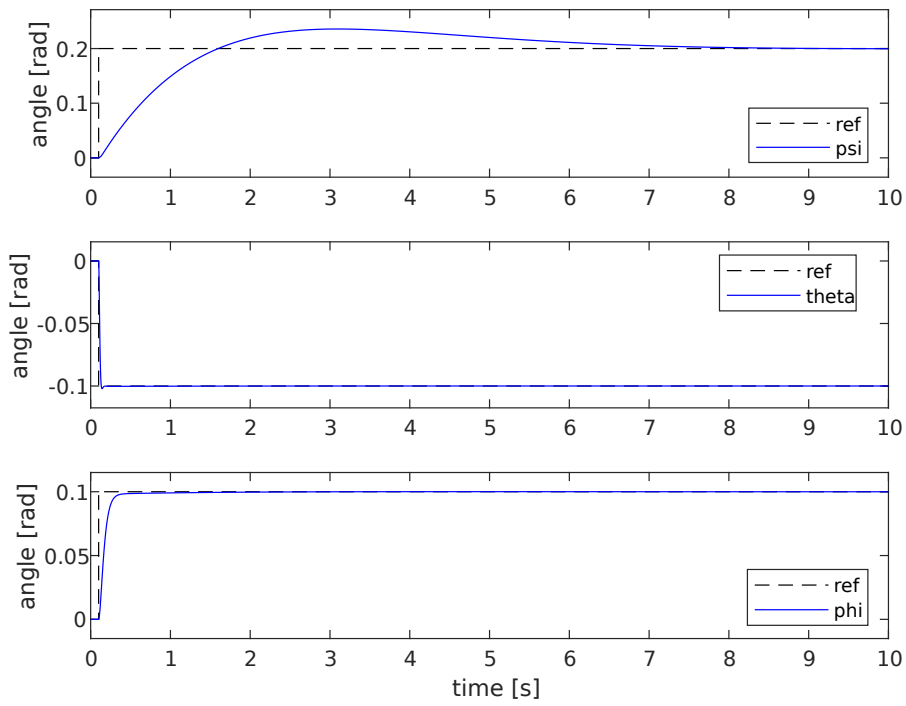
Once the controller matrix is computed, it is time to test the controller. For that, the drone is flying with a constant relative speed of 30m/s. As its incidence is perfect, there is no side-slip angle and the angle of attack is null. In order to test the controller, a step is fed to the system. However, it only affects the Euler angles, their derivatives have as reference a 0 value throughout the test.

5.2.2. Retraction and Transition Inner layer - Airplane

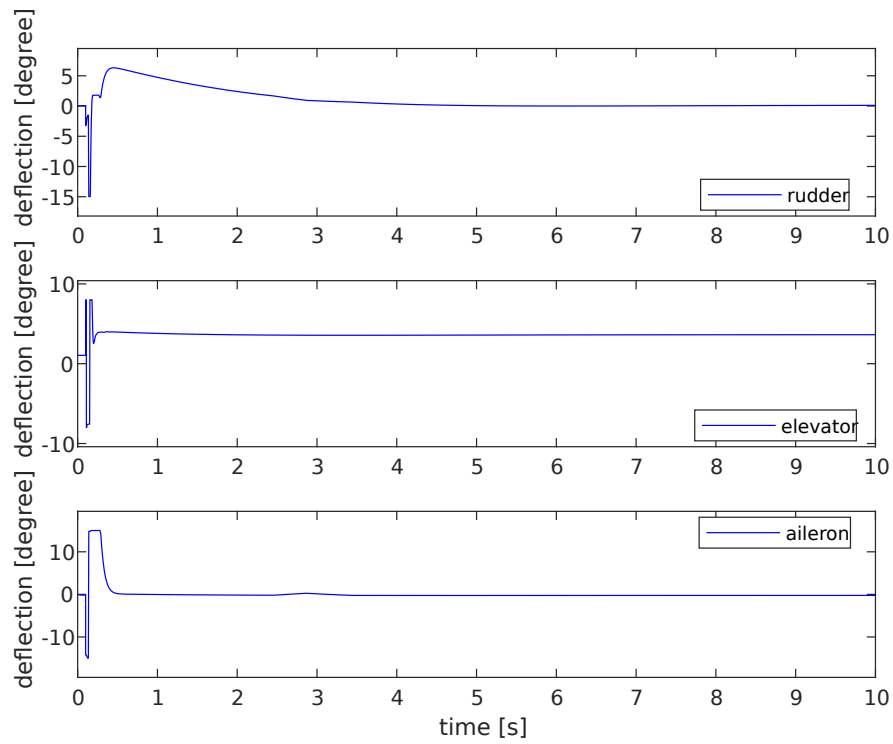
During Phase 6, the inner controller is synthesized based on the same linearization as in 5.2.1. However, there is a major difference, the integral action is no longer required and the matrix linear system is presented below.

$$\begin{bmatrix} \dot{\phi}(t) \\ \dot{\theta}(t) \\ \dot{\psi}(t) \\ \dot{P}(t) \\ \dot{Q}(t) \\ \dot{R}(t) \end{bmatrix} = \begin{bmatrix} 0 & 0 & 0 & 1 & 0 & 0 & 0 \\ 0 & 0 & 0 & 0 & 1 & 0 & 0 \\ 0 & 0 & 0 & 0 & 0 & 1 & 0 \\ 0 & 0 & 0 & 0 & 0 & 0 & 0 \\ 0 & 0 & 0 & 0 & 0 & 0 & 0 \\ 0 & 0 & 0 & 0 & 0 & 0 & 0 \end{bmatrix} \begin{bmatrix} \phi(t) \\ \theta(t) \\ \psi(t) \\ P(t) \\ Q(t) \\ R(t) \end{bmatrix} + \begin{bmatrix} 0 & 0 & 0 \\ 0 & 0 & 0 \\ 0 & 0 & 0 \\ 0.57 & 0 & -0.01 \\ 0 & 3.57 & 0 \\ -0.01 & 0 & 0.55 \end{bmatrix} \begin{bmatrix} \delta_a(t) \\ \delta_e(t) \\ \delta_r(t) \end{bmatrix} \quad (5.14)$$

Following the LQR method and keeping in mind the restrictions due to the measurement



(a) Reference tracking



(b) Control action

Figure 5.9: Airplane mode - reference tracking with a step reference to the Euler angles

system capabilities, a choice regarding the $Q_{PQR-Phase6}$ and $R_{PQR-Phase6}$ is made such that the resulting close loop dynamic is fast enough to decouple the inner and outer layers. The control matrix obtained to achieve this goal, $K_{PQR-Phase6}$ is shown in the next lines, along with $Q_{PQR-Phase6}$ and $R_{PQR-Phase6}$.

$$Q_{PQR-Phase6} = 1.0e + 05 \begin{bmatrix} 18.24 & 0 & 0 & 0 & 0 & 0 \\ 0 & 164.14 & 0 & 0 & 0 & 0 \\ 0 & 0 & 1.64 & 0 & 0 & 0 \\ 0 & 0 & 0 & 0.05 & 0 & 0 \\ 0 & 0 & 0 & 0 & 0.01 & 0 \\ 0 & 0 & 0 & 0 & 0 & 1.50 \end{bmatrix} \quad (5.15a)$$

$$R_{PQR-Phase6} = \begin{bmatrix} 1.11 & 0 & 0 \\ 0 & 1.11 & 0 \\ 0 & 0 & 1.11 \end{bmatrix} \quad (5.15b)$$

$$K_{PQR-Phase6} = 1.0e + 02 \begin{bmatrix} 12.80 & 0 & -0.02 & 0.95 & 0 & -0.02 \\ 0 & 3.8427 & 0 & 0 & 0.51 & 0 \\ 0.08 & 0 & 0.38 & 0.01 & 0 & 3.69 \end{bmatrix} \quad (5.15c)$$

$$(5.15d)$$

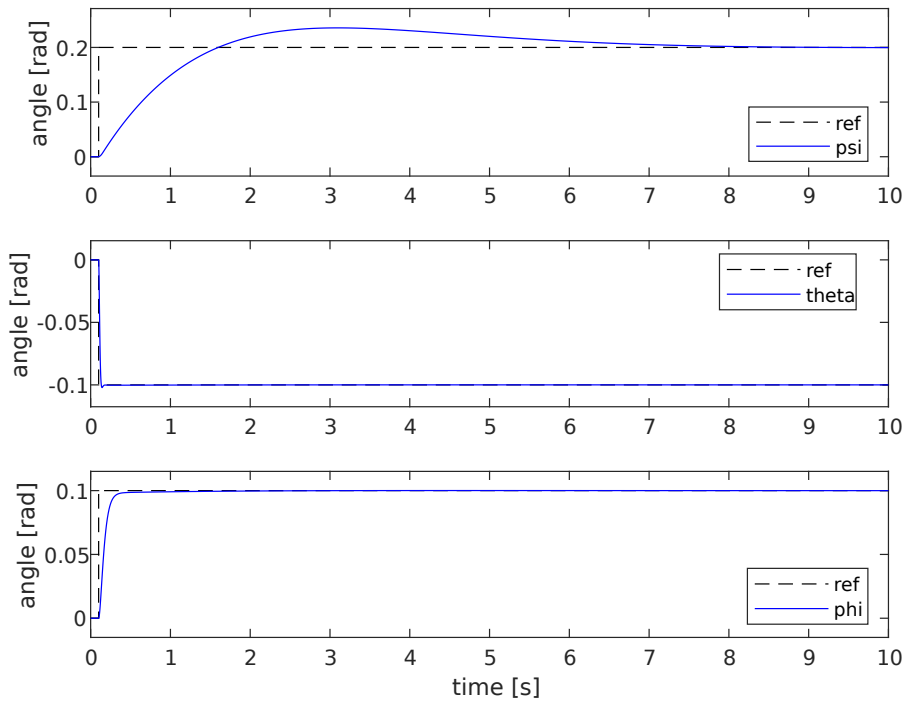
With the controller matrix already calculated, there is the need for testing the controller. For that, the drone is flying with a constant relative speed of 30m/s. As its incidence is perfect, there is no side-slip angle and the angle of attack is null. In order to test the controller, a step is fed to the system. However, it only affects the Euler angles, their derivatives have as reference a 0 value throughout the test.

5.2.3. Generation Outer layer - Airplane

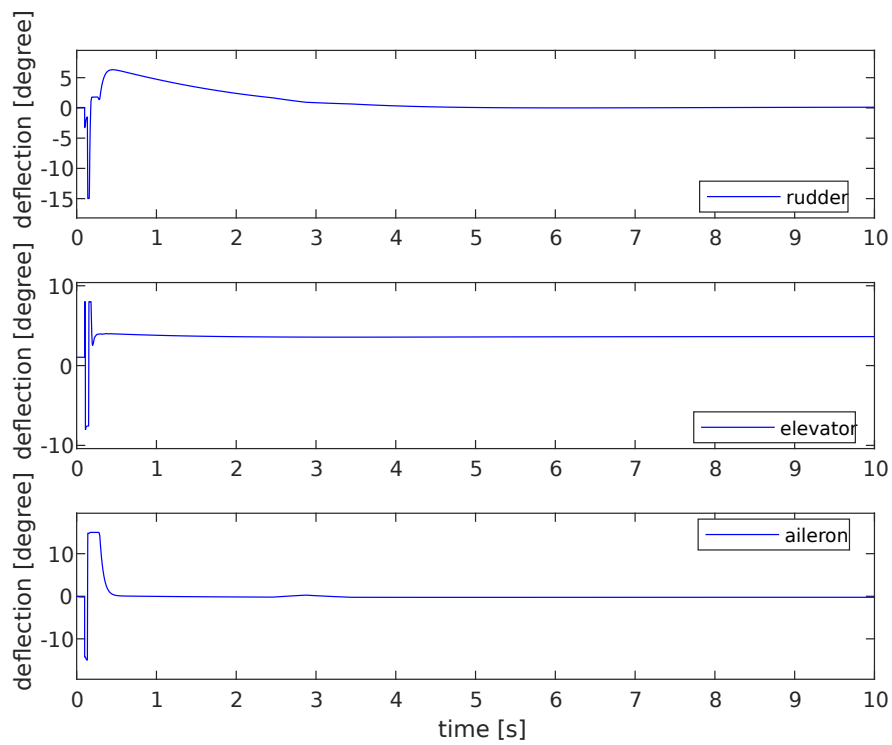
The outer layer during the generation phase is composed of three SISO linear controllers. Each of them provides one reference for only one Euler angle, that is fed to the inner layer.

Forward speed controller

The first step is to produce a mathematical model that accurately represents the dynamic of the system, perfection is not required, it is enough with the representation of the more important parts of the dynamic. In the situation studied, and as explained before, the force to be projected and used for the control of the forward speed is the tether force.



(a) Reference tracking



(b) Control action

Figure 5.10: Airplane mode - Phase 6 - reference tracking with a step reference to the Euler angles

Simply writing the sum of forces in the longitudinal axis and equalling it to the mass times the acceleration in the longitudinal axis, an equation to describe the dynamic is found. After simplifying it due to small angles, considering a constant relative speed and neglecting some terms, a final form of the equation, written in LaPlace form, adequate for control development is found and presented below.

$$\frac{u}{\theta_{tether}} = \frac{1262}{s + 1.718} \quad (5.16)$$

Once a mathematical model is obtained, some requirements must be set to develop the controller. First, an integrator is not needed, hence it is avoided. Second, the controller must be fast enough to have a good tracking of the forward speed, as it will be reflected in all the other controller. On the other hand, the amount of time the control surfaces are saturated should be kept at a minimum. With the requirements in mind, the Affine Parameterization method is used to synthesize the controller, below it is possible to find the transfer functions used.

$$T_{u-airplane} = \frac{0.9}{s + 1} \quad (5.17a)$$

$$Q_{u-airplane} = 43e - 4 \frac{s}{s + 1} \quad (5.17b)$$

$$K_{u-airplane} = 7.13e - 4 \frac{s + 1.72}{s + 0.1} \quad (5.17c)$$

There is another consideration to make, the necessity to keep the drone in cross-wind. Because of that, the output of this controller must be limited. An excess in speed is not as problematic as a lack of it. As a result, the reference for θ_{tether} has a maximum value of 6 degrees and a minimum of 2.

Side slip angle controller

During the part of the mission where the drone behaves as an airplane, it is crucial to keep the side slip angle contained near zero. For this task, a controller that provides a reference for ϕ_{tether} is synthesized. The mathematical model used starts as the dynamic equations along the y axis. The forces considered are the weight and the tether projection, the aerodynamic lateral force is disregarded. The assumption of ϕ_{tether} being small enough for the trigonometrical function to take their linear form is regarded as valid. As a result, the following equation is found.

$$\frac{\beta}{\phi_{tether}} = \frac{1000}{4.78s} \quad (5.18)$$

To synthesis the controller, the Affine Parameterization method is used. The next equations show the different transfer function used and obtained.

$$T_{\beta-airplane} = \frac{38s + 400}{s^2 + 40s + 400} \quad (5.19a)$$

$$Q_{\beta-airplane} = \frac{0.18s^2 + 1.91s}{s^2 + 40s + 400} \quad (5.19b)$$

$$K_{\beta-airplane} = 0.18 \frac{s + 10.53}{s + 2} \quad (5.19c)$$

As it is mentioned in the previous section, the system is based on the cross-wind dynamic. Thus, the feeding of a too big of a reference for ϕ_{tether} will lead to serious problems. The solution is to limit the reference values to the range contained between -30 and 30 degrees.

5.2.4. Retraction and transition Outer layer - Airplane

Phase 6, the one characterizing the part under study, is heterogeneous when analyzed under the perspective of the control.

Retraction and transition - Gliding

The first and second part inside the sixth Phase have as purpose taking the drone to the Target point by modifying the velocity vector until it points toward the desired point. In order to accomplish this, and as it was explained thoroughly in 4.4.2, the signals to be controlled are the Euler angles.

The generation phase may end in a variety of conditions, both in altitude and attitude. Hence, the control strategy in part one and two must be able to tackle this differences and provide a way for the drone to arrive at part three in an appropriate condition.

Altitude controller - airplane The first step to synthesize this controller is to develop a mathematical model. It is based on the sum of all forces in the z_{ef} axis. While gliding, the main forces to be considered are the weight of the drone and the lift. Using the assumption of small angles and hypothesizing that the lift is contained in the z axis, the vertical component of the lift can be computed by multiplying its value by $\theta(t)$. As a result, the following equation can be found.

$$\frac{h}{\theta} = \frac{111}{s^2} \quad (5.20)$$

Once this equation is obtained and by using the Affine Parameterization method, a controller is devised. The equations presented below are the ones taking part in this procedure.

$$T_{h-airplane} = \frac{27s + 27}{s^3 + 9s^2 + 27s + 27} \quad (5.21a)$$

$$Q_{h-airplane} = 0.24 \frac{s^3 + s^2}{s^3 + 9s^2 + 27s + 27} \quad (5.21b)$$

$$K_{h-airplane} = 0.24 \frac{s + 1}{s + 9} \quad (5.21c)$$

The choice of this complementary sensitivity function is made following the some guidelines. First, there is no necessity of the integrator. Second, the control action can be saturated, but the aim is to keep the time in which that situation occur at minimum. Also, it has to be fast because the distance from the starting point of the manoeuvre until the end is small. However, not too fast so as to couple the dynamic of this controller with the inner layer one. It can be seen that the poles defining the T functions are of the same order of magnitude, in the current case all of them are -3.

5.3. References

Another vital part of the control system is the choice of the set of references. As mentioned before, the controllers are arranged in a cascade fashion. Thus, all the controllers that are placed inside the loop defined for another one do not need a set of reference to be defined. Conversely, the controllers located in the outermost layers need a set of references, that are the ones defining how the mission is performed.

5.3.1. Hovering - Phase 1

Once the drone reaches the altitude of 5 meters, it moves towards the limits delimiting the sphere of radius l_{min} . To accomplish this, the next references are fed to the control system.

Altitude

The altitude must be kept at 5 meters, thus the altitude controller, defined in 5.1.2, is fed with this constant value.

Point in x_{ef} - y_{ef} plane

To lead the drone to the limits of the sphere, the controller presented in 5.1.6 is fed by the following values.

$$x_{ref1} = \sqrt{l_{min} * 0.99^2 - 25} \quad (5.22a)$$

$$y_{ref1} = 0 \quad (5.22b)$$

5.3.2. Tether engaging - Phase 2

Once the drone arrives to a position that is very close to the limit of the sphere, thanks to the references explained in the previous section, it is time to engage the tether. The new set of references are presented in the equations below.

$$h_{ref2} = 5 \quad (5.23a)$$

$$x_{ref2} = 1.5\sqrt{l_{min}^2 - h_{ref2}^2} \quad (5.23b)$$

$$y_{ref2} = 0 \quad (5.23c)$$

5.3.3. Climbing - Phase 3

The tether is already engaged and the drone is still, ready to start climbing. To achieve this, the references in the x_{ef} - y_{ef} plane are presented in the next equations.

$$x_{ref3} = 1.5\sqrt{l_{min}^2 - 25} \quad (5.24a)$$

$$y_{ref3} = 0 \quad (5.24b)$$

On the side of the altitude reference, an always increasing reference is given. It is represented by the equation (5.25). The combination of that equation and (5.24) is going to produce the following desired outcomes.

1. As the altitude increases, due to the related controller, the position in x_{ef} moves further away from the reference. It is important to remember that the drone moves

on the surfaces of a sphere of constant radius. The resulting increase in error derives in a bigger control action, which means that the nose is pointing upper.

2. As the nose points upper and the reference of altitude is always 30 meters above the current value, the tether's force increases. The result is an increase in speed, due to the tether's force projection.

$$h_{ref_3}[t] = h_{ref_3}[t - 1] + 30 \quad (5.25)$$

5.3.4. Generation - Phase 4 and 5

Once the altitude to arrive to Phase 4 is reached, a transition to the generation phase starts. The set of references are the same for Phase 4 and 5. As explained in 4.2.2, the signals to control are the tether angles and the velocity angle. Their references are presented in the next paragraphs.

The first one is related to u . In 5.2.3, the controller and its saturation is presented. The reference fed is a constant value that contributes to a contained value of $\alpha(t)$ and $\beta(t)$, at the same time it allows the control surfaces to have a big enough effect on the drone's dynamic. The value chosen is 50 m/s.

The second reference is fed to the controller presented in 5.2.3. As the ideal situation is to have a null side slip angles throughout the whole generation phase, the reference given is zero.

The third reference to be presented is given to modify the velocity angle, and thus is fed directly to the controller explained in 5.2.1. The logic behind this reference must capture the switching between Target points, at the same time it must change their position in the space to prevent the increase in size of the ∞ shape as much as possible. The logic behind the update of the Target points is presented in Algorithm 5.1. Considering that the $\theta_{sphere}(t)$ coordinate of the points is kept constant, the other coordinate is changed based on the position of the drone. The function *NewTargetPoint*, shown in Algorithm 5.1, returns the new angular position on sphere coordinates. That function uses the following equations to compute the desired value.

$$d[t] = norm(drone_position[t - 1], 2) \cos(40) \quad (5.26a)$$

$$\text{OUTPUT : } \phi_{sphereObjective-Points} = atan\left(\frac{y_{Objective-Position}}{d[t]}\right) \quad (5.26b)$$

Once it is decided whether a new reference is needed, and its value, there is another choice to make. The last step is to assess if it is due time to feed the new reference to the controller. The logic behind that decision is presented in Algorithm 5.2. To put it into words, while the drone is far away from the Target point, the reference is not updated. The meaning of this can be better seen under a simple example, at time k the drone recalculates the reference to $\phi_{sphere_{ref}}(t) = 30$. As long as the drone's $\phi_{sphere}(t)$ is not 1 degree apart from the reference, the reference will still be 30 degrees. It does not matter that the distance from the drone to the generator is still increasing. However, once the error is small enough, the reference is updated to $\phi_{sphere_{ref}}(t) = -28$, as an example. That will be the reference value until the drone's $\phi_{sphere}(t)$ is only 1 degree far from the reference. This update procedure is portrayed in figure 5.11. The left green Target point is old one and the green one on the right is the new one.

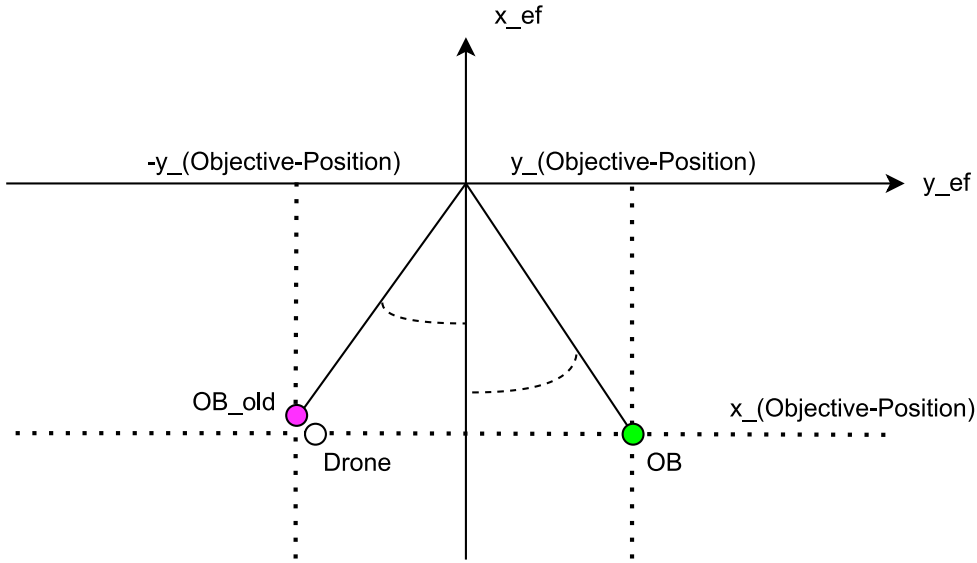


Figure 5.11: Target points' position update

Algorithm 5.1 Target points modification logic

$\phi_{sphere_{OB}} = \text{ObjectivePointsPostion}(\text{Phase}[t-1], \text{drone_position}[t-1], \text{switch_target}[t-1], \phi_{sphere_{OB}}[t-1])$

1: ϕ_{ref}

2: **if** $\text{Phase}[t-1] == 5$ **and** $\text{switch_target}[t-1] == \text{true}$ **then**

3: $\phi_{sphere_{OB}} = \text{NewTargetPoint}(\text{drone_position}[t-1])$

4: **else**

5: $\phi_{sphere_{OB}} = \phi_{sphere_{OB}}[t-1]$

6: **end if**

Algorithm 5.2 Objective selector logic

OUT = ObjectiveSelection(ϕ_{sphere} , OB_old, $\phi_{sphere_{OB}}$)**Require:** OB_old previous Target point**Require:** $\phi_{sphere_{OB}}$ previous Target point coordinate**Require:** ϕ_{sphere} : drone's sphere coordinate

```

1: if OB_old == 1 then
2:   if  $\phi_{sphere} < \phi_{sphere_{OB}} + \text{pi}/180$  then
3:     OB = 2
4:   else
5:     OB = OB_old
6:   end if
7: else
8:   if  $\phi_{sphere} < \phi_{sphere_{OB}} - \text{pi}/180$  then
9:     OB = 1
10:  else
11:    OB = OB_old
12:  end if
13: end if

```

5.3.5. Transition - Phase 6

The set of references in this Phase are crucial for the correct transition to start again the generation phase.

Gliding - part 1 and 2

The first part is the gliding, including the turning manoeuvre, of the drone to face the new Target point. There are three references to provide, one for each Euler angle.

The first one is related to how the drone will change directions, and it is the reference for $\phi(t)$. First, it is important to compute the angular distance between the drone's velocity vector and the line joining the drone and the Target point, calculated on the x_{ef} - y_{ef} plane. The figure 4.14 portrays how is the situation explained. The idea is to make the drone turn 10 degrees for each degree of angular error, with a variable saturation. The saturation level depends on the difference in altitude between the starting point of the manoeuvre and the Target point. The approach taken to tackle to construction of this variable saturation is the simulation of different possible starting conditions and finding the value that allows a correct turning of the drone for that specific case. As stated

before, it is found that the only parameter needed to determine the saturation is the difference in altitudes, table 5.2 presents the values found. With that information, an spline interpolation is made and used to calculate any saturation level required due to shifting to the sixth Phase in any point along the generation trajectory.

Altitude difference [m]	Saturation [degrees]
101.30	20
106.70	20
125.00	35
142.00	45
155.00	45
157.60	45

Table 5.2: Relation between altitude difference and $\phi(t)$ saturation value

The second reference has as objective keeping the side-slip angle controlled. For that, its value is fed to the $\psi(t)$ controller. The value taken is $\psi(t)$ plus $\beta(t)$. The idea is to have the same axis as the basis for measuring the angles and, thus, align the longitudinal axis of the drone to the relative wind speed.

The last reference's aim is to make the drone's altitude decrease from its value when shifting to the sixth Phase to the desired value to start sixth Phase's part three. The final value must be higher than the altitude of the Target points, because part three and four require the drone to lose altitude. The reference in altitude (h_{obj}) is 70 meters, approximately 10 meters higher than the reference points. However, it is important to avoid giving a jump in the reference. As a result, the calculus of its value is derived by the distance of the drone from the Target point chosen (named as d). When the drone has just started Phase 6, the maximum reference is fed, which amounts to the altitude at that point (h_{init}). As the drone gets closer, the altitude decreases linearly. The minimum reference altitude is the objective value of 70 meters.

$$h_{ref}(t) = \min(70, \frac{(h_{init} - h_{obj})d(t)}{d_{init}} + h_{init}) \quad (5.27)$$

Drop - part 3

The third part is crucial for the transition, it will lead the drone to have an appropriate attitude to engage the tether and shift to control the tether angles. To accomplish this,

the objective is to make the drone point down and turn to get far away from the generator. However, this cannot be done with an abrupt change in the references. As a result, from the previous reference values at the end of part 2, a linear variation of them is proposed.

The reference for $\theta(t)$ is an increasing value with a slope of 20 degrees per second. As this part is short, it is important for it to change quickly but not so fast that it could cause the existence of a too big of $\alpha(t)$. At the same time, it is not desirable to reach an angle bigger than 60 degrees. This reference is the same regardless of the Target point.

On the other hand, the references for $\phi(t)$ and $\psi(t)$ change signs depending on which point is being tracked. Even though they change sign, the absolute value is the same for both Target points. In the case of $\phi(t)$, the slope is 50 degrees per second and the saturation is in 50 degrees.

Different from the other two references, the $\psi(t)$ one does not present a saturation limit. The scope of it is to bring the drone to point to the opposite Target point, that will become the new one once the switching to Phase 4 is done. This strategy tries to minimize any jump in the reference when the change in reference is done. Once again, it exhibits a linear behaviour with a slope of 25 degrees per second. The increase in slope is motivated by the fact that it will reduce the effect of the side slip angle.

Engaging - part 4

The last part of the transition is characterized by an effort to bring the drone to an attitude enabling a smooth transition back to generation. In order to accomplish that, each reference is carefully chosen to have an impact in achieving the objective.

The first reference is the most important one and is related to the $\theta_{tether}(t)$. To start the generation phase in the best way possible, it is an advantage to have both tether angles in zero value. That condition is forced into this reference. On the other hand, the reference of $\phi_{tether}(t)$ is taken from the controller explained in section 5.2.3. Its objective being to reduce the side slip angle. The third reference is fed to $\psi(t)$. Its value is the continuation of the one used in section 5.3.5. As explained there, the reference for $\phi(t)$ is a continuously increasing value, which does not stop when shifting to part 4 nor it has a limit. The expected result from this choice is to keep moving the longitudinal axis towards the opposite reference point.

5.4. Strategy outline

It is important to condense all the strategy presented in a few sentences to have a guideline for new applications. The first part of the transition is arriving at the desired Target point in a way that is as parallel as possible to the y_{ef} axis. Once this is achieved, the more sensitive part starts. The main parameters to control how the transition is done are presented in the next paragraphs.

First, the objective in altitude to finish the gliding is crucial to prevent the drone for hitting the ground during the dive. This parameter is important when the shape obtained is good, but the drone is too close to the ground in the lowest point. This is clearly visible in figure 5.12

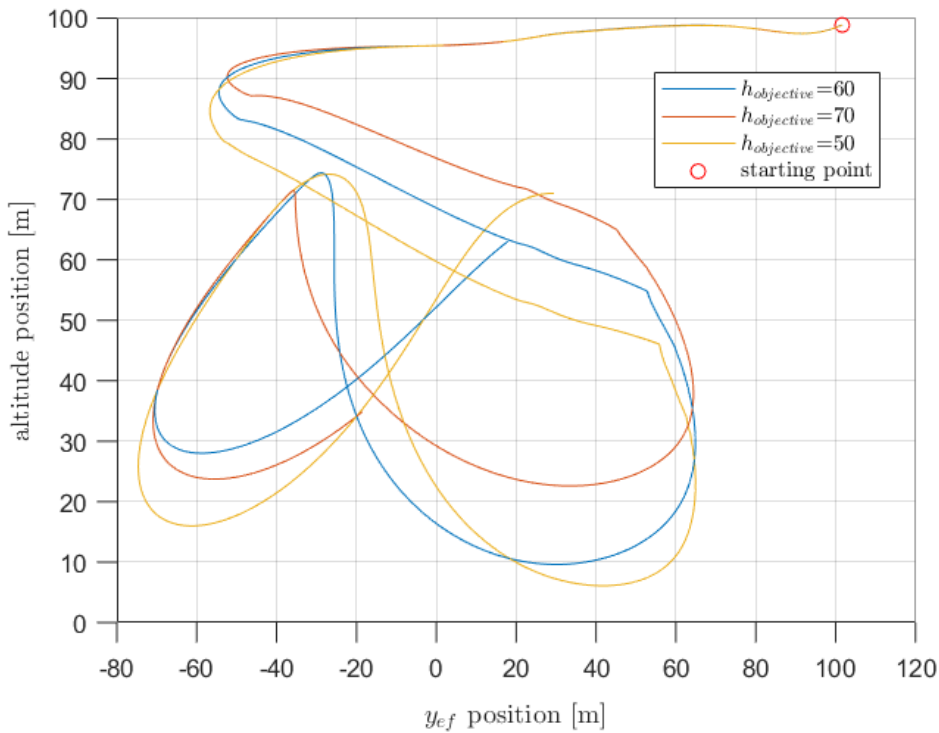


Figure 5.12: Phase 6 - Effect of change in the Target point's altitude

Second, the rate of change in $\psi_{ref}(t)$ plays an important role in how much the drone dives and how much it takes for the drone to point to the new Target point. As depicted in figure 5.13, the increase in the rate leads to the plane nearing the ground. At the same time, it makes the turning shape, while the drone is diving, to have an increase in radius.

Third, the parameter of *altitude drop* represents an important value in the switching from part 3 to part 4 of the sixth Phase. As such, it defines how big the linear variations in

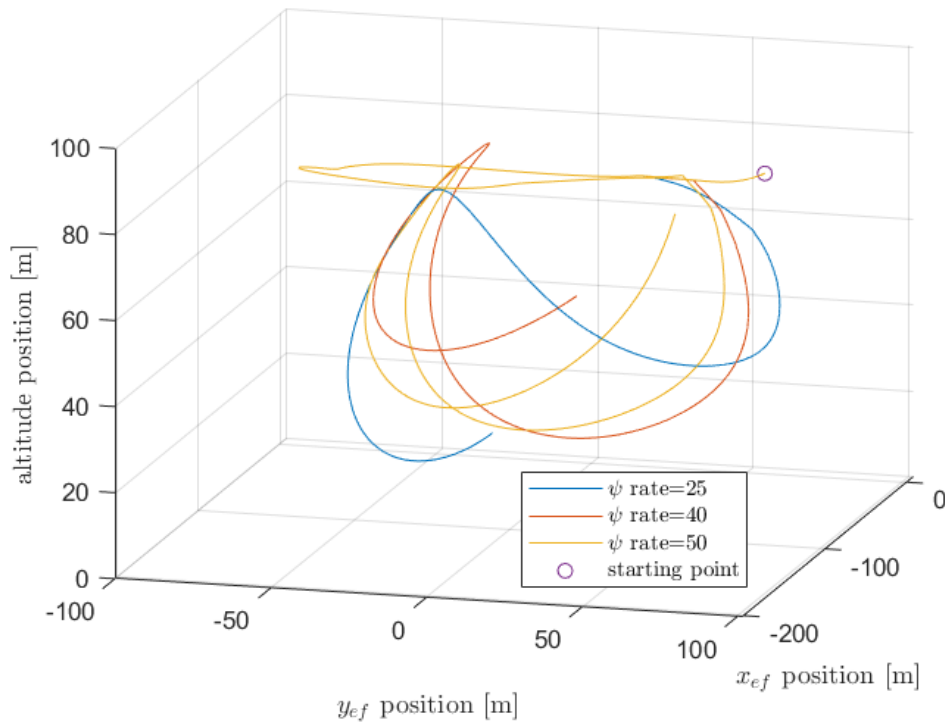


Figure 5.13: Phase 6 - Effect of change in $\psi(t)$ reference rate of change

the references on the Euler angles will reach, resulting in a different attitude at the end. The results can be seen in figure 5.14.

Fourth, the distance to switch in x_{ef} from the Target point, when switching to Phase 3 is crucial to engage the tether in the correct circumstances. If the tether is engaged too soon, its force will pull the plane with an angle producing undesired effects in the aerodynamic angles. At the same time, doing it too late has as a consequence higher tether forces in value, better align at the beginning but they will pull too much the airplane.

In the following table the sum-up of the effect of this four parameters are presented.

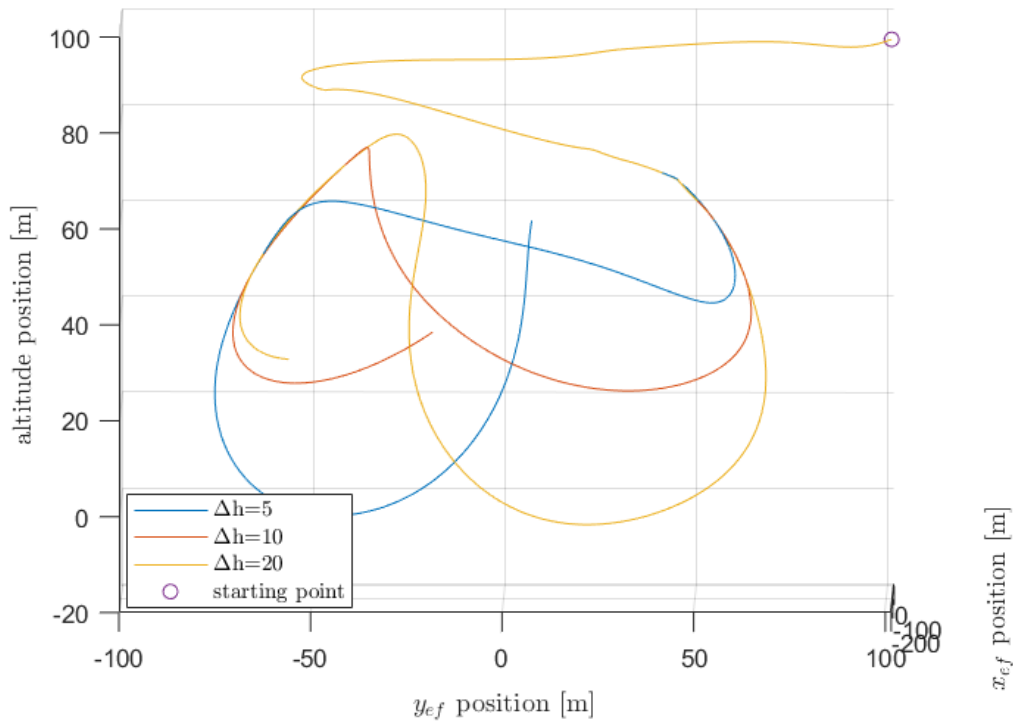


Figure 5.14: Phase 6 - Effect of change in the dive distance

Title of Table (optional)

Parameter	Sum-up of its effect
Objective altitude - gliding rate of change in $\psi(t)$	it is used to prevent the drone from hitting the ground when turning - how much to drop before changing
altitude drop distance to switch in x_{ef}	how much to dive before starting part 3 distance that affects mainly on how the tether is engaged

Table 5.3: Representative values for the State machine

5.5. Simulation

In this section the results of applying the controllers, layout and reference to the non-linear simulator are presented. The organization of the simulation sub-chapter dictates that at the beginning the results of Phase 1 and 2 are presented, related to the hovering part up to reaching the surface of the sphere draw with a radius of l_{min} . Then, it is presented the simulation of the climbing and stabilization, Phase 3 and 4. To proceed, the generation phase is shown. To finish, the results of the proposed strategy are portrayed, from Phase 6 to Phase 4. The simulations are performed with a wind speed of 5 m/s, along the x_{ef} direction towards its negative values. To run the simulations, a notebook Dell 7559 (with a processor i7 6700HQ) is used. The software is MATLAB R2021a.

5.5.1. Hover up to the sphere limits

The following figure, 5.15, portrays how the drone moves toward the limit of the smaller sphere, with radius of l_{min} . It is possible to see how the control manages to keep a good path, with no visible undesired movements. This is particularly important because the drone's wings produce disturbing aerodynamic forces, due to the relative wind speed.

The control actions are depicted in 5.16. It is interesting to remark some parts of it. First, the beginning oscillations are caused by the presence of the aerodynamic forces, which are compensated quickly. Second, the final motor's speed changes are a result of the engaging of the tether.

5.5.2. Climbing and stabilization phases

When the tether is engaged, the Phase 3 starts. The climbing is perfectly depicted in figure 5.17. The drone keeps increasing the altitude while the position on y_{ef} is null. Once the altitude is big enough, along with a high u_{rel} , the Phase 4 starts. The resulting ∞ -shape is clear and steady. It is possible to see that the periodicity of the movement is achieved, which is regarded as a sign of the drone being in a stable period movement.

The figures 5.18 contain important information about the feasibility of the trajectory. It possible to see how the aerodynamic angles are contained in sensible values. At the same time, on the right figure of the pair is drawn the relative speeds. There are two things that it is important to notice, the first one is the effect of the Forward speed controller. Although u_{rel} is oscillating, its values is contained in a range which results the small values of the aerodynamic angles. In addition, having a high valued relative speed derives in the control surfaces' effect being big enough so as to affect the dynamic of drone. The second

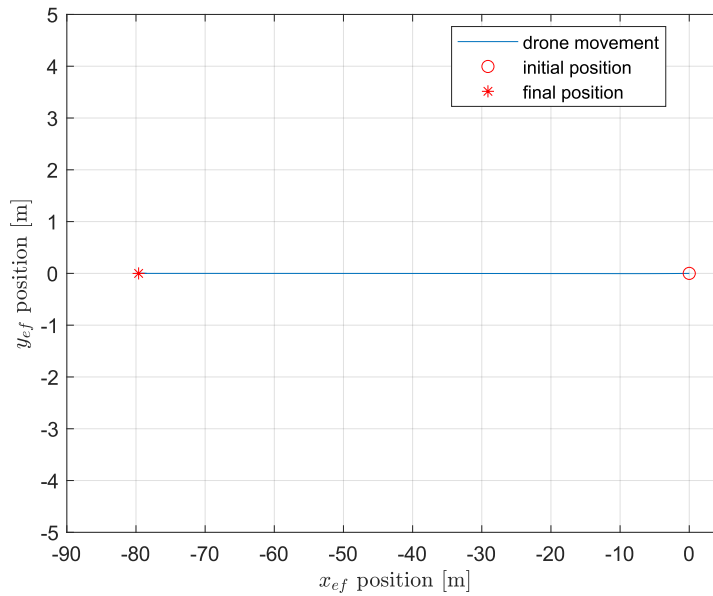
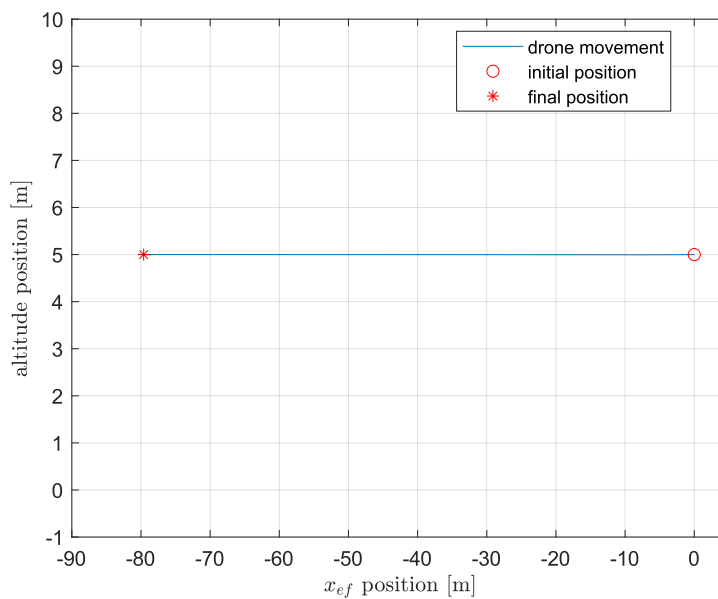
(a) drone movement in $x_{ef} - y_{ef}$ (b) drone movement in $x_{ef} - h$

Figure 5.15: Phase 1 and 2 - move to the edge of the sphere

remarkable consequence is related to the v_{rel} , which can be seen portrayed with small values. This is the outcome of the Side slip angle controller, that is crucial for mission to be accomplished.

The last figure, 5.19, presents the control surfaces deflection. At the start of the plot they are all null, as the control actions in Phase 3 are the motors' speeds. After shifting to

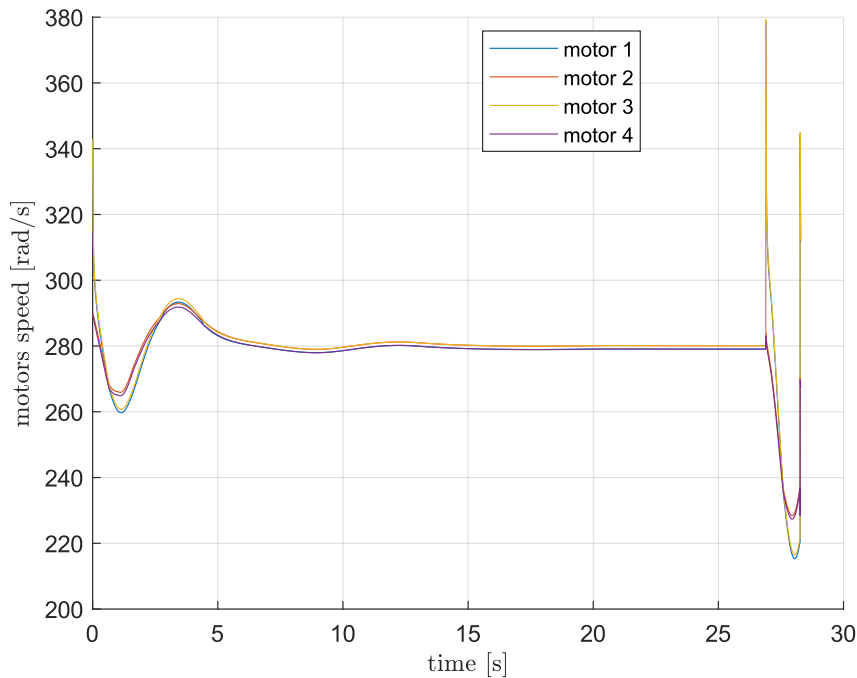


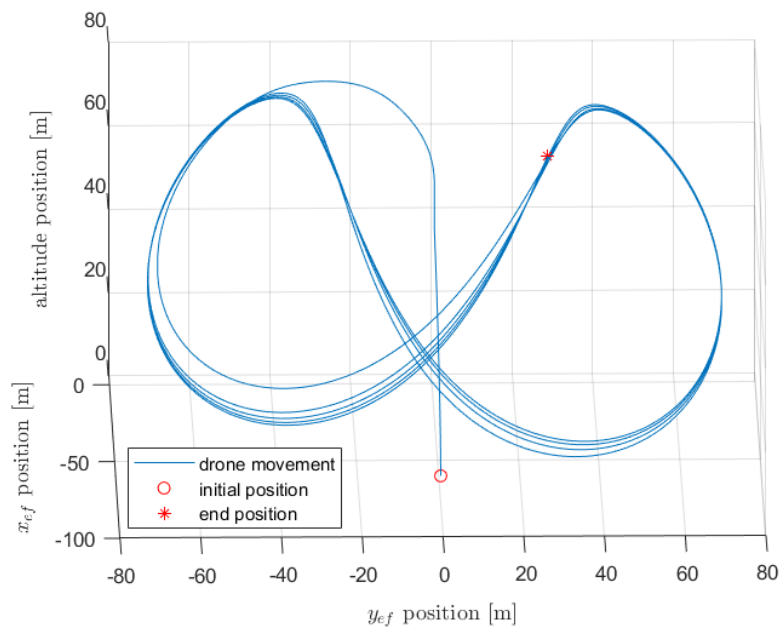
Figure 5.16: Phase 1 and 2 - motors' speed

Phase 4, the value of the deflection is not big as to be close to saturation, except from 2 isolated peaks. This is a good sign, because it leaves room for higher deflection values in case of gusts or any other wind fluctuation.

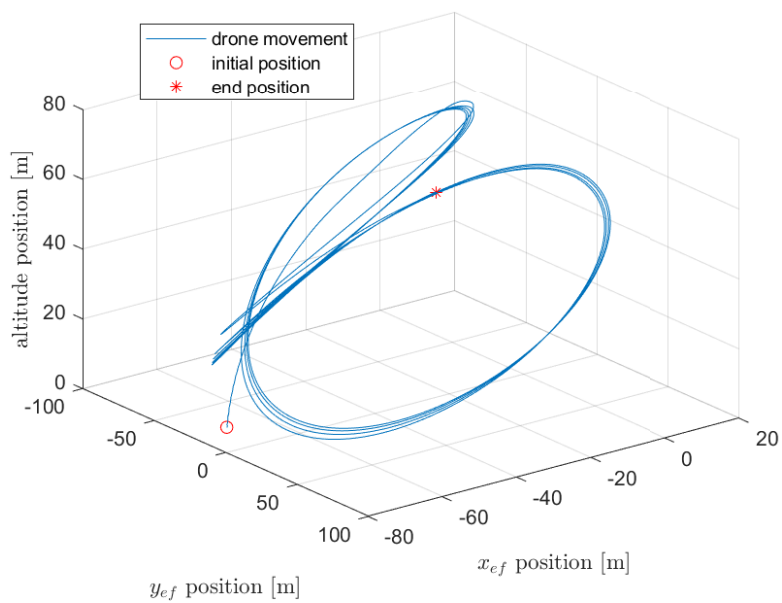
5.5.3. Generation phase

Once the system arrives to the generation phase, the tether starts to reel out. As a result, the ∞ -shape is not contained in the same sphere each loop. Conversely, the radius of the sphere increases along with the length of the reeled out tether. It is possible to see in figure 5.20 how is the new shape. The ∞ -shape is clearly depicted in the right hand plot.

This new dynamic of the system, introduced by the reeling out of the tether, influences the aerodynamic angles and the relative speeds, as it is shown in figure 5.21. Opposite to what is seen in Phase 4, the values of the variables plotted changed over time. It is noticeable, on the left figure, how the average of the angle of attack increases, but it is always in the linear region of the aerodynamic coefficients. At the same time, the side-slip angle's extreme values moves from the starting number to a bigger one, and then they are reduced. On the right hand figure, the most distinct variation is seen in the u_{rel} value, its average decreases but the most important change is on the increase of the difference between its higher and lower value. However, as shown in the left figure, it does not affect



(a)

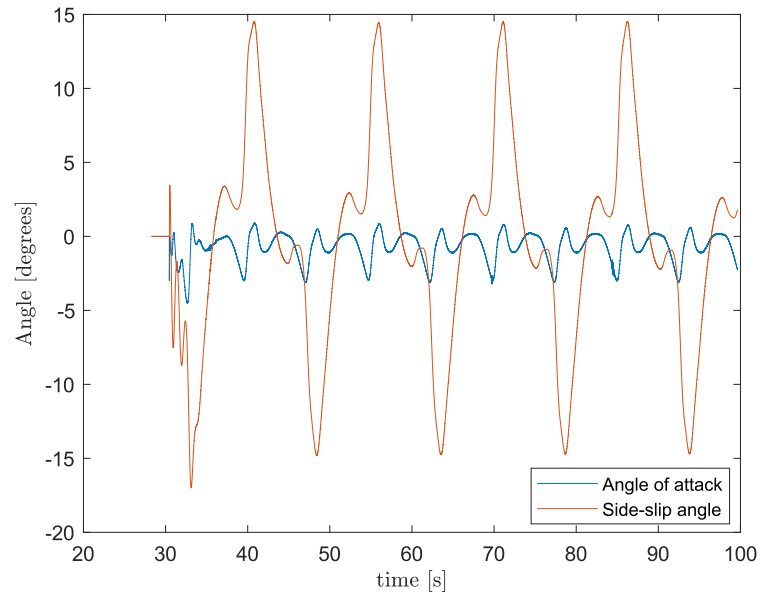
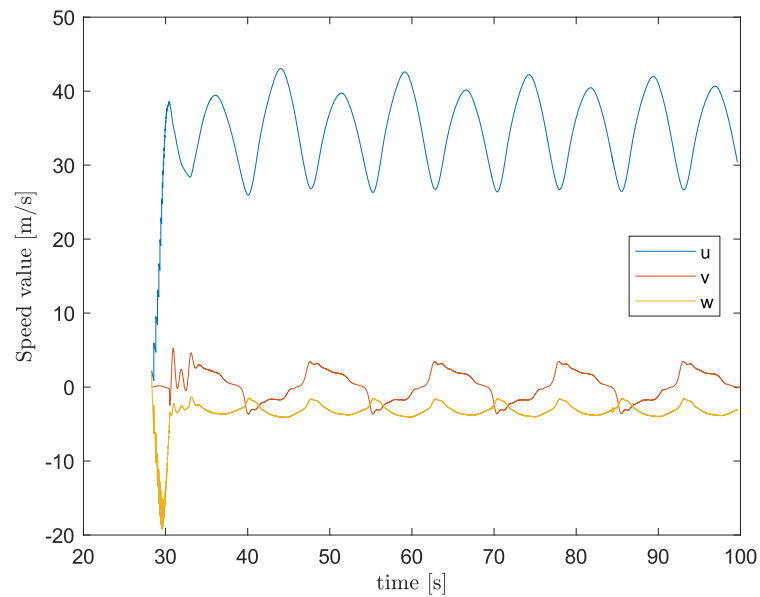


(b)

Figure 5.17: Phase 3 and 4 - climbing and stabilization

the aerodynamic angles negatively.

The control surfaces' deflections are presented in Phase 5 - control surfaces. The most remarkable point is the distance to the saturation level of all of them.

(a) α and β 

(b) body speeds

Figure 5.18: Phase 3 and 4 - speed and aerodynamic angles

5.5.4. Transition

Once the unwound tether has reached the maximum permissible length, the transition phase starts. As explained in section 4.2.2, the transition manoeuvre is simulated. Figure 5.23 presents the results. It is possible to see how the drone turns, aiming to the Target

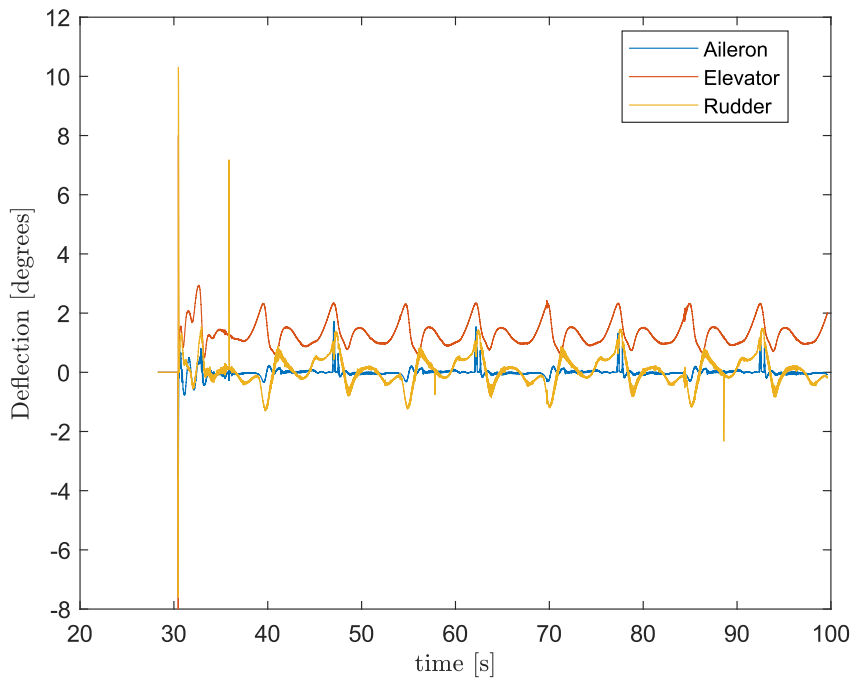


Figure 5.19: Phase 3 and 4 - control surfaces

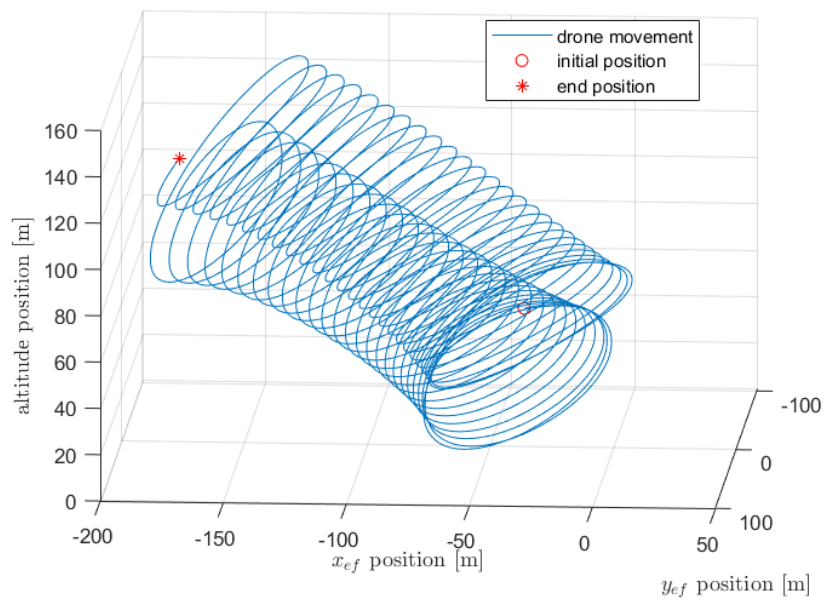
point 1, and approaches it. Once close enough, the drone dives and turns looking for the Target point 2. When it is in the correct position, it shifts back to Phase 4 and produces the ∞ -shape figures that are shown.

The next figure depicts the first part of the transition. It is possible to see the turning manoeuvre and the linear approximation toward the Target point. When looking at the decrease in altitude, it is clear that the result is not a perfect line. This is explained due to the difficulty to follow the reference under the gliding condition without arriving to a stall. However, It is important to notice that the end point is very close to the objective one.

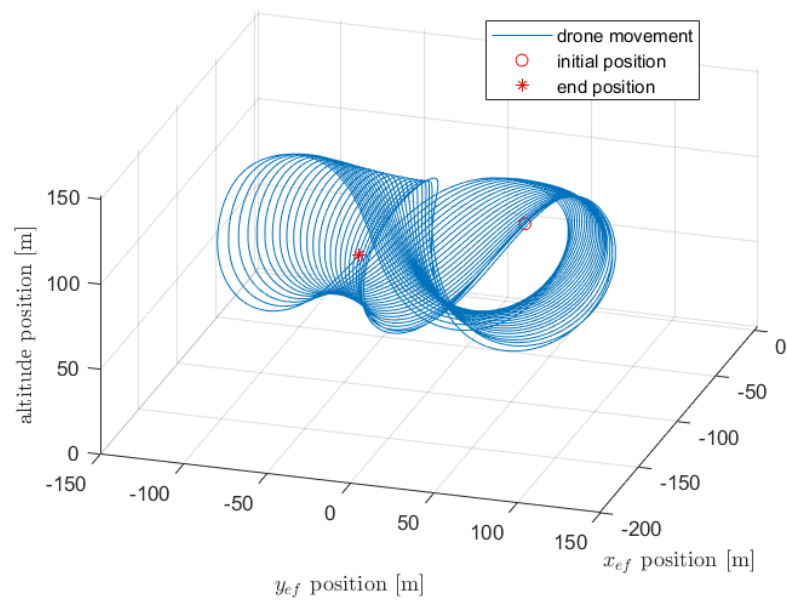
Figure 5.25 portrays how the next part of the sixth Phase takes place. The linear increase in the references is shown along with the signal of the variables to control. It is easily seen how the tracking occurs and the references are being followed.

Finally, the sixth Phase's last part takes place. In the following plot is possible to see how the controller enforces θ_{tether} to track the reference, same situation occurs for ϕ_{tether} . At the same time, the reference keeps increasing in the case of $\psi(t)$.

In addition to the case presented so far, in the figures below there are two other cases. The only graphs presented are the results. One is in the lowest limit of the region of usage



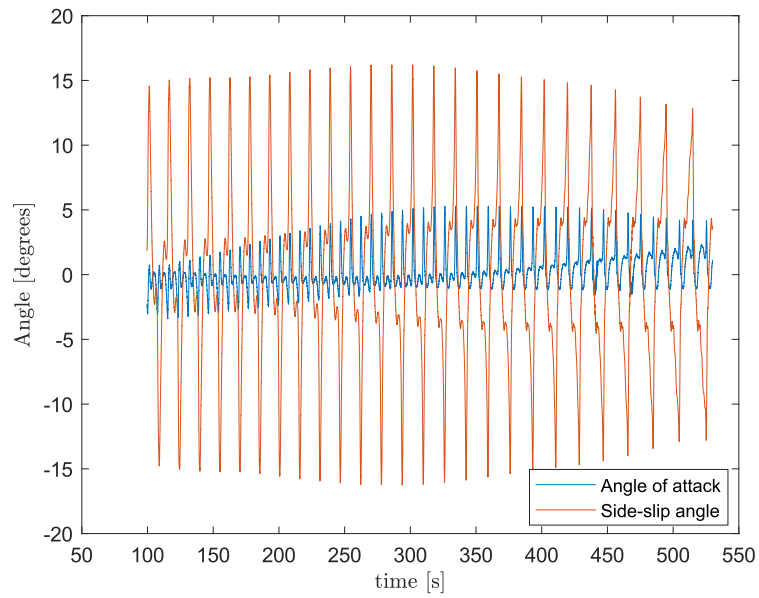
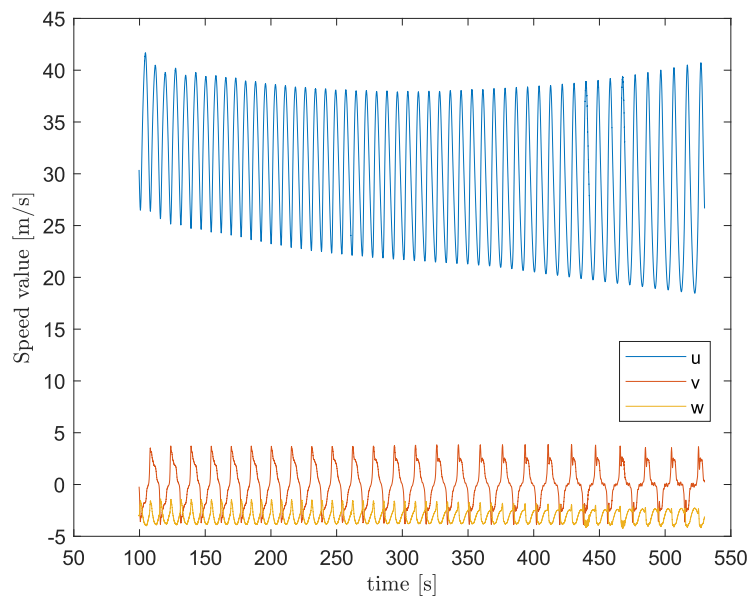
(a)



(b)

Figure 5.20: Phase 5 - generation

of the method with the values chosen in this thesis, figure

(a) α and β 

(b) body speeds

Figure 5.21: Phase 5 - speed and aerodynamic angles

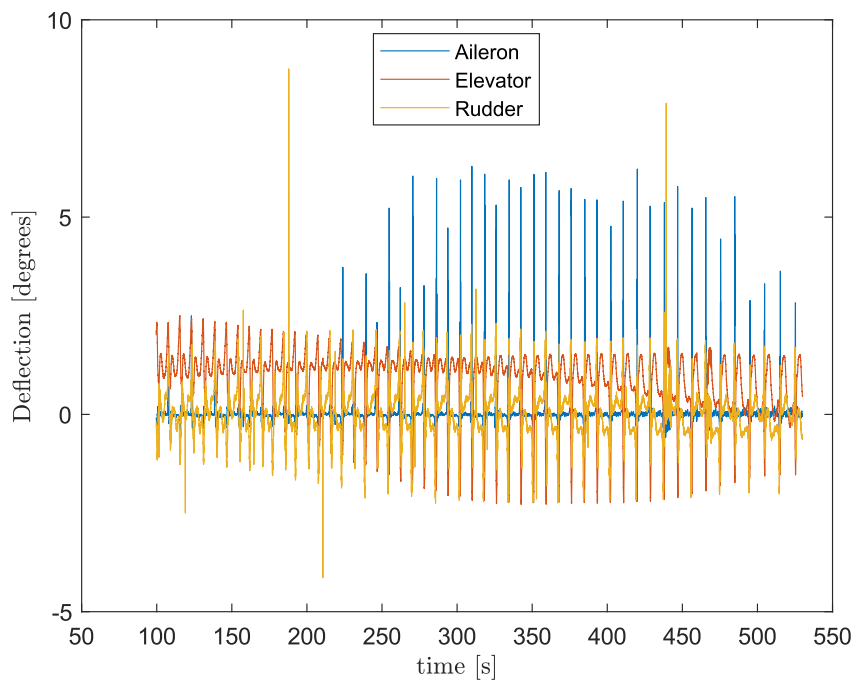
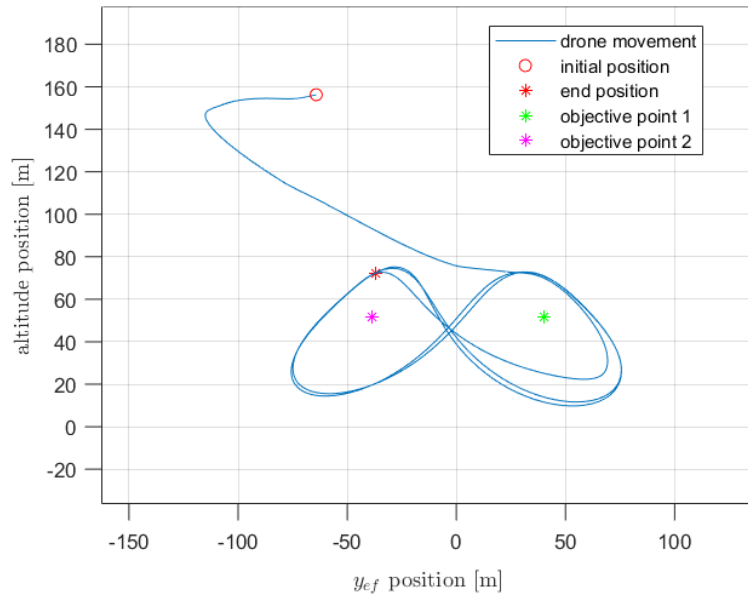
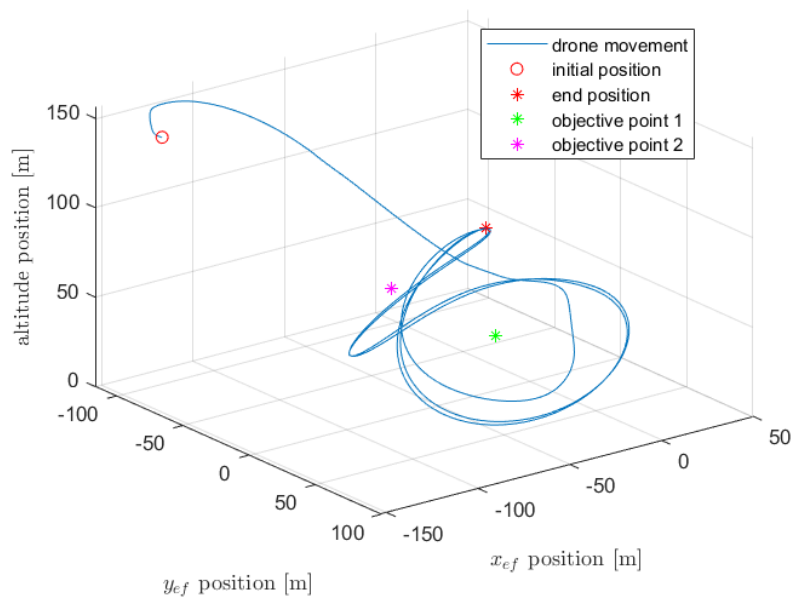


Figure 5.22: Phase 5 - control surfaces

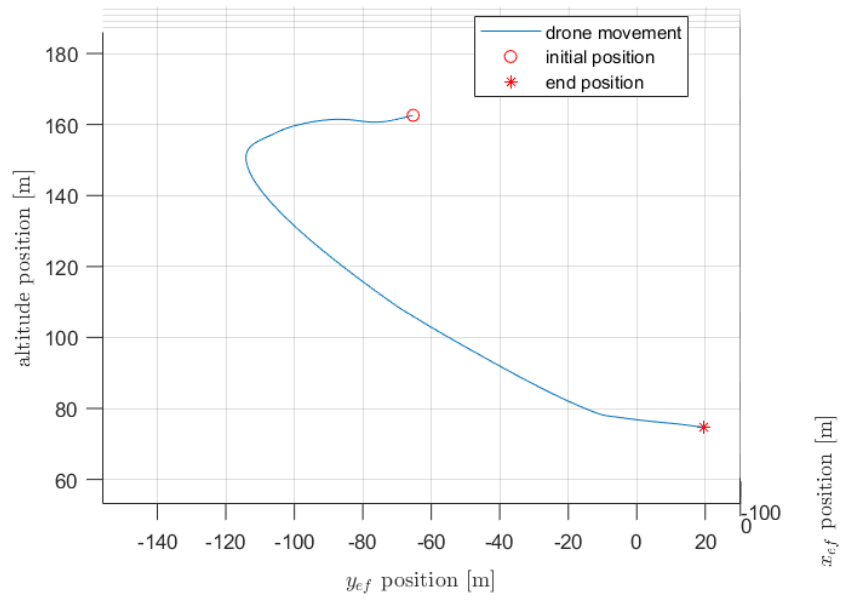


(a)

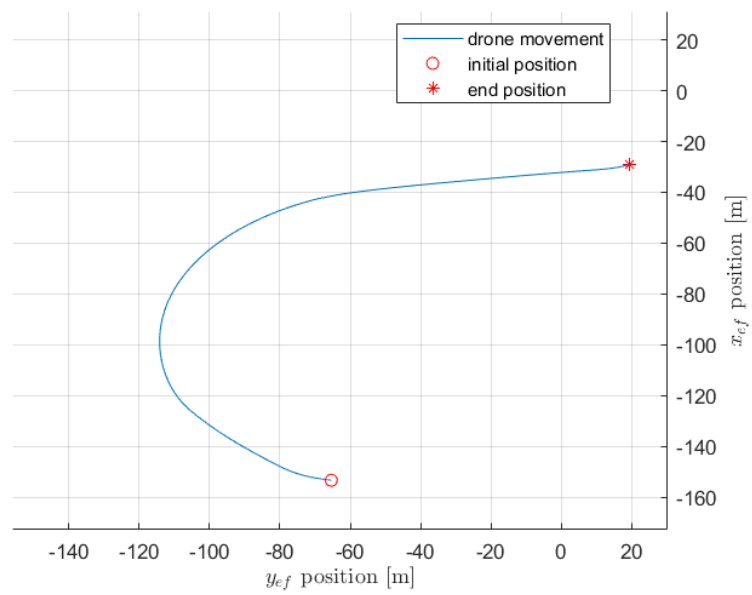


(b)

Figure 5.23: Transition back to generation



(a)



(b)

Figure 5.24: Transition back to generation

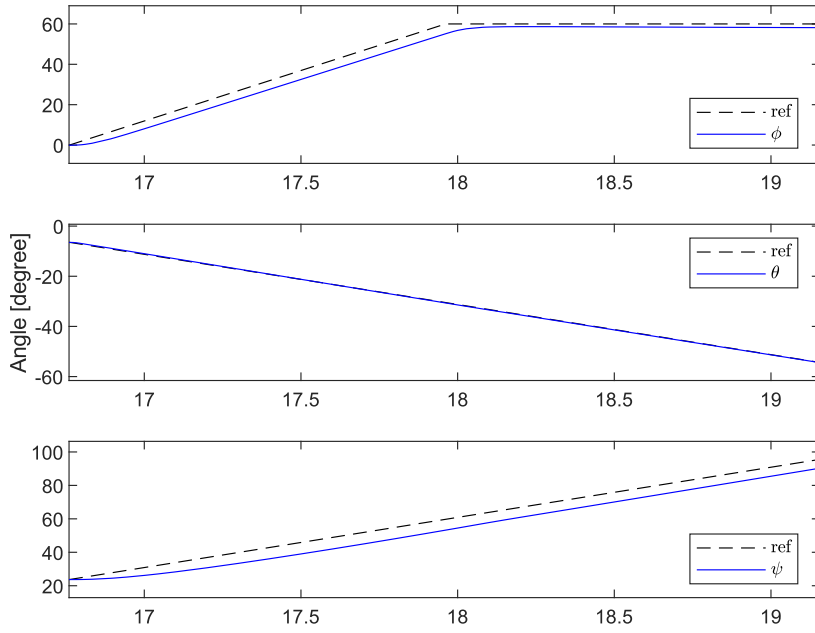


Figure 5.25: Phase 6 - part 3 - Euler angles and their references

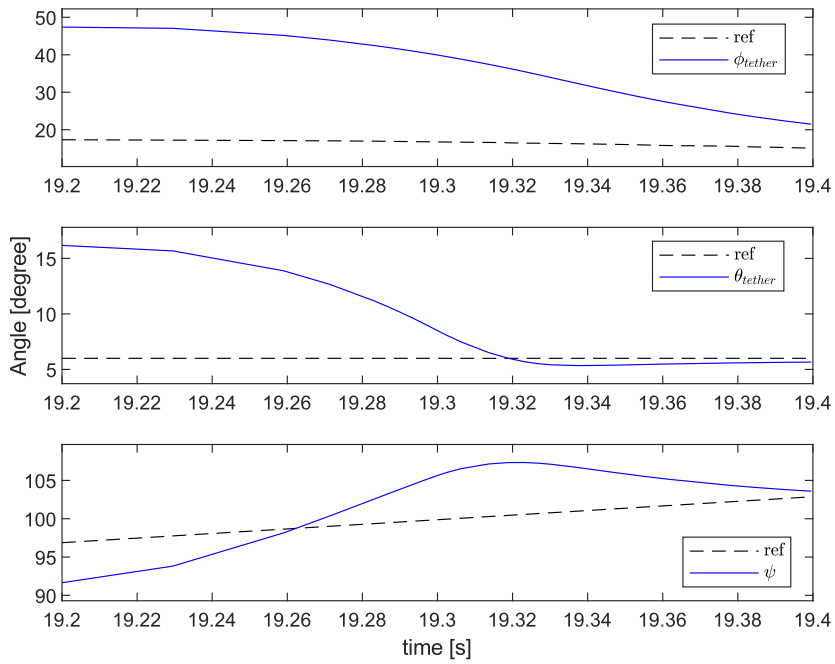
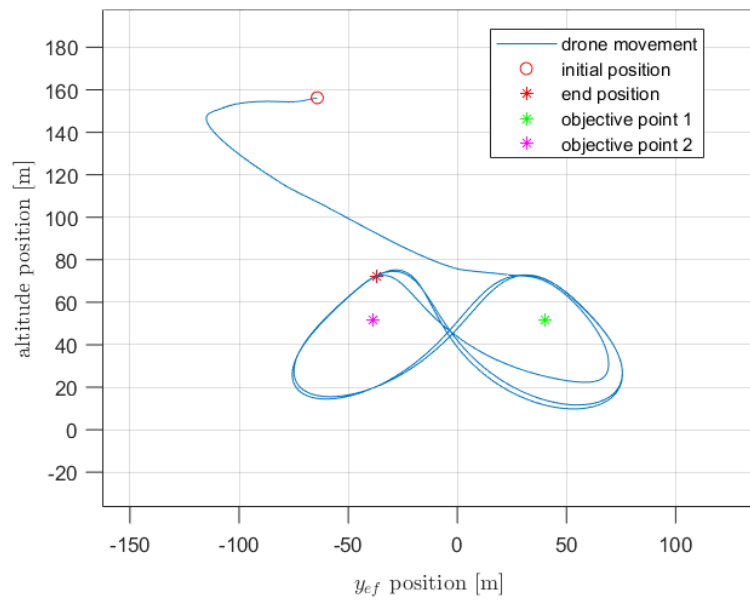
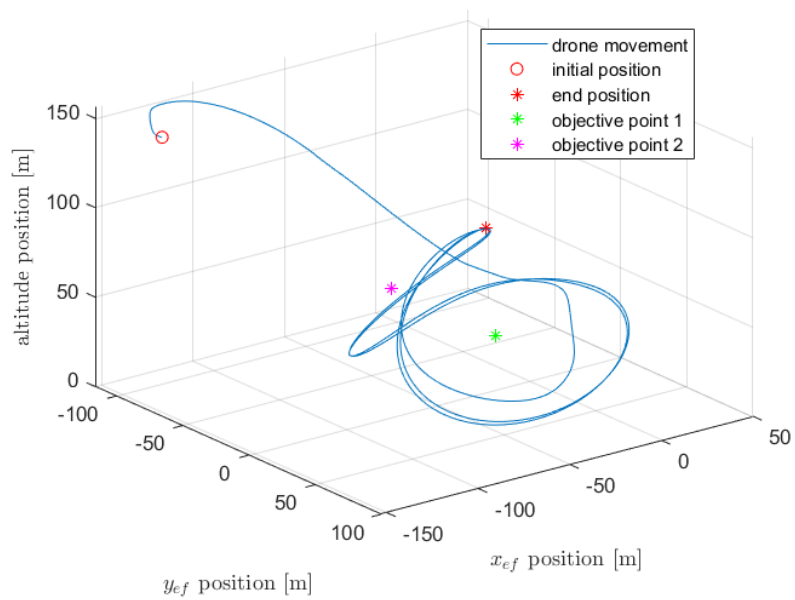


Figure 5.26: Phase 6 - part 4 - Tether angles and their references

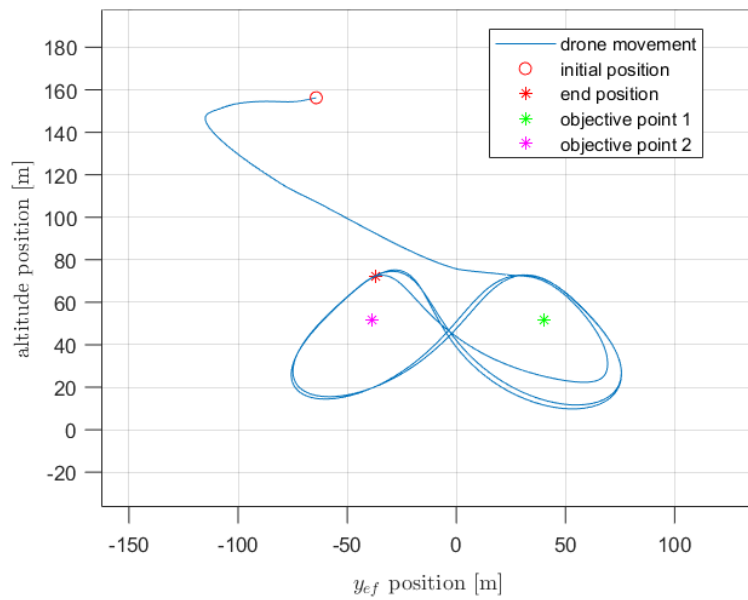


(a)

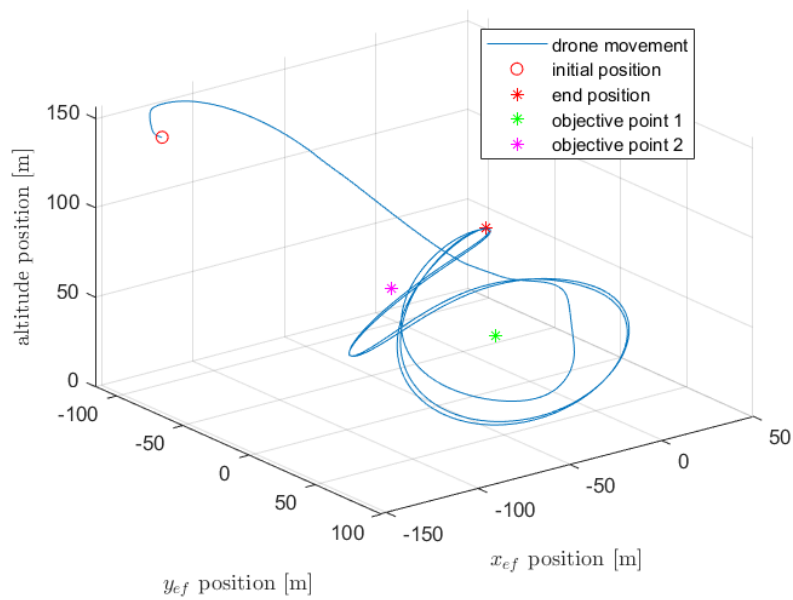


(b)

Figure 5.27: Transition back to generation - second case



(a)



(b)

Figure 5.28: Transition back to generation - third case

6 | Conclusions and future developments

To conclude this work, it is possible to see that the methodology proposed enables the possibility of a safe and correct transition by tuning very little parameters. Once the drone has finished Phase 5, with any type of controlled chosen, the methodology gives some simple rules for control design of Phase 6. As the guidelines are set on the references for the upper level references and for the state machine, there is total freedom with the decision on how to shape the inner layers of the cascade control. This is a great advantage in terms of flexibility.

It is also important to mention which are those parameters again. The first one is the altitude of the Target point. The second one is the dive distance. the third one is the rate of change for ψ_{ref} . The final one is the distance in x_{ef} from the Target point to change to Phase 3. This four parameters produced clear variations in the shape of the resulting path, thus affecting the feasibility of any transition strategy. As it was possible to define how is the effect of each of them, it is also simpler to change and adapt the resulting path to any requirements.

The future developments that may push this methodology forward are related to how to optimize the value of the parameters. Given a certain type of glider, it should be possible to find a set of parameters that produce an optimal transition from different perspectives. One of them is the optimal set of values for the less consumption of energy in control actions. Other possibility is the optimal set of values that permits a transition without the requirement of having to go through Phase 4. Another future development comes from the test and validation of the method in non-ideal wind conditions, in the present work there is assumed that the average wind speed doesn't change with time, there is no turbulence and no gusts. The inclusion of any or all of them will lead to an even better method, less necessary tunings, before putting it into practice.

Bibliography

- [1] S. AS. Stim300. <https://www.sensor.com/products/inertial-measurement-units/stim300/>, 2022.
- [2] BBC, 2021. URL <https://www.bbc.com/news/science-environment-58130705>.
- [3] A. Berra. Optimal control of pumping airborne wind energy systems without wind speed feedback. Master's thesis, Politecnico di Milano, 2019-2020.
- [4] G. Cillari, F. Fantozzi, and A. Franco. Passive solar solutions for buildings: Criteria and guidelines for a synergistic design. *Applied Sciences*, 11, 2021.
- [5] W. E. Council and P. S. Institute. World energy scenarios, composing energy futures to 2050. Technical report, World Energy Council, 2013.
- [6] Enerdata, 2021. URL <https://www.enerdata.net/publications/reports-presentations/world-energy-trends.html>.
- [7] L. Fagiano and M. Milanese. Airborne wind energy: An overview. In *2012 American Control Conference (ACC)*, pages 3132–3143, 2012. doi: 10.1109/ACC.2012.6314801.
- [8] G. C. Goodwin, S. F. Graebe, and M. E. Salgado. *CONTROL SYSTEM DESIGN*. Pearson, 2000.
- [9] P. Kasinathan, P. Sanjeevikumar, F. Blaabjerg, V. K. Ramachandramurthy, U. Govindarajan, R. Arul, and P. Varunraj. Conceptual framework of antecedents to trends on permanent magnet synchronous generators for wind energy conversion system. *Energies*, 04 2019.
- [10] T. Mohammed and L. Fagiano. Quad-rotor fixed-wing hybrid uav fault-tolerant control for safety-critical application. 8 2020.
- [11] N. R. D. C. (NRDC), 2018. URL <https://www.nrdc.org/stories/renewable-energy-clean-facts#sec-types>.
- [12] S. Rapp, R. Schmehl, E. Oland, and T. Haas. Cascaded pumping cycle control

- for rigid wing airborne wind energy systems. *Journal of Guidance, Control, and Dynamics*, 42:1–18, 06 2019. doi: 10.2514/1.G004246.
- [13] D. Todeschini, L. Fagiano, C. Micheli, and A. Cattano. Control of a rigid wing pumping airborne wind energy system in all operational phases. *Elsevier*, 06 2020.
- [14] G. Tumble, 2019. URL <https://greentumble.com/the-different-types-of-solar-energy/>.
- [15] E. Union, 2021. URL https://ec.europa.eu/info/strategy/priorities-2019-2024/european-green-deal/delivering-european-green-deal_en.
- [16] G. van der Lee Rope Factory, 2022. URL <https://www.gvanderlee.com/products/dyneema-sk78-high-modulus-polyethylene>.

List of Algorithms

- 4.1 Angular speed references' saturation logic 42
- 4.2 Signal selector logic 49
- 5.1 Target points modification logic 78
- 5.2 Objective selector logic 79

List of Figures

1.1	Human effect on climate	2
1.2	Wind turbine scheme	5
1.3	Wind turbine development through years [9]	5
1.4	AWE systems working closely thanks to different altitudes for each of them. [7]	6
1.5	Comparison of AWE's and wind turbines' CF for different locations [7]	8
1.6	Schematic system representation	9
1.7	AWE systems schemes	9
2.1	5 kW prototype of Kitemill AS	12
2.2	Sphere coordinates	15
3.1	Drone's motor numeratio	23
4.1	Phase 0	29
4.2	Phase 1	30
4.3	Phase 2	31
4.4	Phase 3	32
4.5	Phase 4	34
4.6	Phase 5	35
4.7	Phase 6	37
4.8	Complete hovering control block diagram	38
4.9	Schematic block diagram of the Taut Tether Control subsystem	39
4.10	Schematic block diagram of the Loose Tether Control subsystem	40
4.11	Schematic block diagram of the Position controller	40
4.12	Schematic block diagram of the Inner layer for airplane mode	43
4.13	Schematic block diagram of the Outer layer for airplane mode	50
4.14	Angular error during Gliding	51
5.1	Reference tracking with a step reference in P, Q and R	57
5.2	Reference tracking with a step reference in P, Q and R	58

5.3	Reference tracking with a step reference in the Euler angles	60
5.4	Reference tracking with a ramp reference in the Euler angles	61
5.5	Reference tracking with a step reference in \dot{x}_{ef} and \dot{y}_{ef}	63
5.6	Reference tracking with a ramp reference in \dot{x}_{ef} and \dot{y}_{ef}	64
5.7	Reference tracking with a step reference in x_{ef} and y_{ef}	67
5.8	Reference tracking with a ramp reference in x_{ef} and y_{ef}	68
5.9	Airplane mode - reference tracking with a step reference to the Euler angles	70
5.10	Airplane mode - Phase 6 - reference tracking with a step reference to the Euler angles	72
5.11	Target points' position update	78
5.12	Phase 6 - Effect of change in the Target point's altitude	82
5.13	Phase 6 - Effect of change in $\psi(t)$ reference rate of change	83
5.14	Phase 6 - Effect of change in the dive distance	84
5.15	Phase 1 and 2 - move to the edge of the sphere	86
5.16	Phase 1 and 2 - motors' speed	87
5.17	Phase 3 and 4 - climbing and stabilization	88
5.18	Phase 3 and 4 - speed and aerodynamic angles	89
5.19	Phase 3 and 4 - control surfaces	90
5.20	Phase 5 - generation	91
5.21	Phase 5 - speed and aerodynamic angles	92
5.22	Phase 5 - control surfaces	93
5.23	Transition back to generation	94
5.24	Transition back to generation	95
5.25	Phase 6 - part 3 - Euler angles and their references	96
5.26	Phase 6 - part 4 - Tether angles and their references	96
5.27	Transition back to generation - second case	97
5.28	Transition back to generation - third case	98

List of Tables

2.1	drone's earth frame: symbolic description	15
2.2	drone's earth frame: symbolic description	16
2.3	drone's states: symbolic description	16
3.1	Representative values for the State machine	19
4.1	Parameters used in the State machine	28
5.1	Hovering controllers' proposed poles for their synthesis	54
5.2	Relation between altitude difference and $\phi(t)$ saturation value	80
5.3	Representative values for the State machine	84

List of Acronyms

Variable	Description
AWE	airborne wind energy
bf	Body Frame
CF	Capacity Factor
ef	Earth Frame
GLG	ground generator
IPCC	Intergovernmental Panel on Climate Change
LQR	Linear Quadratic Regulator
NED	North-East-Down Frame
OBG	on-board generator
VTOL	vertical take off and landing
T	Complementary sensitivity funcion

List of Symbols

Variable	Description	SI unit
α	angle of attack	rad
β	side-slip angle	rad
δ_a	deflection of the ailerons	rad
δ_e	deflection of the elevator	rad
δ_r	deflection of the rudder	rad
$\theta(t)$	rotation around y axis, called pitch	rad
θ_{sphere}	complementary to the Polar angle	rad
$\theta_{stg6-line}$	linear $\theta(t)$ reference for the sixth Phase	rad
θ_{tether}	rotation around E_{sphere}	rad
ρ	air density	kg/m ³
ρ_{tether}	tether density	kg/m ³
$\phi(t)$	rotation around x axis, called roll	rad
ϕ_{sphere}	azimuthal angle	rad
$\phi_{stg6-line}$	linear $\phi(t)$ reference for the sixth Phase	rad
ϕ_{tether}	rotation around N_{sphere}	rad
$\psi(t)$	rotation around z axis, called yaw	rad
ψ_{error}	tracking error on $\psi(t)$	rad
ψ_{tether}	rotation around D_{sphere}	rad
$\psi_{stg6-line}$	linear $\psi(t)$ reference for the sixth Phase	rad
C_D	dimensionless drag coefficient	
C_L	dimensionless lift coefficient	
C_{LQ}	variation of C_L due to Q	
C_Y	dimensionless side force coefficient	
C_{YP}	variation of C_Y due to P	
C_{YR}	variation of C_Y due to R	
C_{lP}	variation of C_l due to P	
C_{lR}	variation of C_l due to R	

C_m	dimensionless pitching moment coefficient	
C_{mQ}	variation of C_m due to Q	
C_n	dimensionless rolling moment coefficient	
C_{nP}	variation of C_n due to P	
C_{nR}	variation of C_n due to R	
C_q	dimensionless yawing moment force coefficient	
d	distance of the drone from the Target point chosen	m
D	drag force	N
F_{T_x}	motors' force in x	N
F_{T_y}	motors' force in y	N
F_{T_z}	motors' force in z	N
J_i	drone's moment of inertia, $i=xx,xy,yy,yz,zz,xz$	$kg\ m^2$)
K_{tether}	tether's elastic coefficient	N/m
L	lift force	N
P	rate of change of the roll angle	rad/s
Q	rate of change of the pitch angle	rad/s
Q_i	moment of i_{th} motor	Nm
R	rate of change of the yaw angle	rad/s
S	wing area	m^2
T_i	force of i_{th} motor	N
V_a	unperturbed air velocity	m/s
V_{drone}	Velocity of the drone	m/s
$V_{freestream}$	unperturbed air velocity	m/s
Y	side force	N
b	wing span	m
\bar{c}	average wing's chord	m
c_i	drone's attitude dynamic coefficients, $i = 3,4,7,9$	$1/(kg\ m^2)$
c_i	drone's attitude dynamic coefficients, $i = 1,2,5,6,8$	$1/(kg\ m^2)$
g_x	gravity in x	m/s^2
g_y	gravity in y	m/s^2
g_z	gravity in z	m/s^2
l	rolling moment	Nm
l_R	motors' rolling moment	Nm
m	pitching moment	Nm
m_R	motors' pitching moment	Nm
n	yawing moment	Nm
n_R	motors' yawing moment	Nm

q	quaternion representation of the attitude	
q_{bar}	dynamic pressure	
q_i	quaternion elements, $i = 1,2,3,4$	
u	velocity in the x direction	m/s
v	velocity in the y direction	m/s
w	velocity in the z direction	m/s
x	drone's longitudinal axis	m
x_{def}	North axis, starting at the drone	m
x_{ef}	North axis, starting at the generator	m
y	axis to the drone's side	m
y_{def}	East axis, starting at the drone	m
y_{ef}	East axis, starting at the generator	m
z	position perpendicular to the plane formed by the drone	m
z_{def}	down axis, starting at the drone	m
z_{ef}	down axis, starting at the generator	m

Acknowledgements

First, I would like to thank my family. Even while living one ocean apart, they have supported me in every way possible.

Second, I would like to thank to my friends. The ones back in Argentina and in other parts of the world have given me their support and love all this time, it has been very important to me. The ones that are or were living my daily experiences with me in here made this trip easier, more enjoyable and memorable.

Third, I want to thank my girlfriend. She has been there for me in the moments when I hated and when I loved this thesis, or my different courses, and she has given me a lot of support. Fourth, to Lorenzo Fagiano for proposing this amazing topic to me. I am very grateful for his patience and him being understanding when everything didn't see to work at all. Also for his guidance in this path and him being available for me to discuss the progress.

